Alma Mater Studiorum – Università di Bologna

DOTTORATO DI RICERCA IN

Scienze Farmacologiche e Tossicologiche, dello Sviluppo e del Movimento Umano

Ciclo XXX

Settore Concorsuale: 05/G1

Settore Scientifico Disciplinare: BIO/14

Identification and *in vitro* preclinical study of natural compounds and derivatives as inducers of immunogenic cell death

Presentata da: Dott.ssa Elena Catanzaro

Coordinatore Dottorato   **Supervisore**

Chia.ma Prof.ssa   **Chia.ma Prof.ssa**
Patrizia Hrelia   **Carmela Fimognari**

Esame finale anno 2018

Table of Content

Abstract

A number of studies in the past decade consistently indicates that effectiveness of a variety of anti-cancer treatments, initially meant to directly inhibit tumor cell survival and proliferation, is actually based on immune system activation [1, 2]. Defined cytotoxic or genotoxic agents promote the generation of anticancer immune responses, potentially leading to tumor eradication, by inducing in malignant cells immunogenic cell death (ICD) [3]. The immunogenic characteristics of ICD are due to the mobilization of the so-called damage-associated molecular patterns (DAMPs), like calreticulin and heat shock proteins (HSPs) exposure on the cell surface or ATP and high-mobility group box 1 (HMGB1) release in the extracellular matrix [4]. Inside the cell, these molecules have mostly non-immunological functions, while when released on the extracellular environment or exposed on the cell surface, they act as both danger signals and adjuvant for the innate immune system [4].

The ability of different synthetic chemotherapeutic drugs to induce ICD has been characterized in detail [5]. In contrast, there is a paucity of data regarding natural products of potential clinical relevance [6]. A variety of natural anticancer compounds have been successfully characterized [7, 8]. However, their immunogenic potential has not been analyzed in comparable detail [9].

In the following essay, the latest cancer research developments and their relationship with the immune system are explored, as well as the definition and characterization of ICD and the use of natural products in cancer research. The thesis is then divided into three distinct chapters, each covering one natural or semisynthetic product investigated for its ability to induce ICD in different cancer models. In particular, I provided a comprehensive preclinical,

in vitro study of cell death mechanisms and immunologic characteristics of two botanical drugs, *Withania somnifera* (WS) and *Hemidesmus indicus* (HI), and one isothiocyanate (ITC) derivative synthesized *ad hoc* in order to reach the ER, MG28. MG28 didn't give the expected results and the study was interrupted, while both botanical drugs resulted able to trigger the main *in vitro* hallmarks of ICD. The most promising agent was HI. I demonstrated its ability to trigger oxidative and endoplasmic reticulum stress, two crucial events for the exploitation of ICD immunogenicity, then I proved its proficiency to positive modulate the expression and mobilization of characteristic DAMPs, including calreticulin, HSP70, ATP, and HMGB1 [5]. Prompted by these observations, I addressed HI's ability to promote the activation of immature dendritic cells (iDC) and explored its immunomodulatory ability. Data consistently indicate that HI-treated tumor cell supernatants are able to promote the transition from an immature to a mature state of *in vitro* generated professional antigen-presenting cell (APC).

On the whole, the evidence reported in this thesis shows and confirms the remarkable potential of natural products in the oncological area and highlights their ability to induce ICD.

List of abbreviations

2H4MBAC127	2- hydroxy-4-methoxybenzoic acid
2H4MBAL	2- hydroxy-4-methoxybenzaldehyde
3H4MBAL	3-hydroxy-4-methoxybenzaldehyde
AIP1	Actin-interacting protein 1
APC	Antigen presenting cells
ASK1	Apoptosis signal-regulating kinase 1
ATF6	Activating transcription factor 6
Bcl-2	B-cell lymphoma 2
Bip	Binding immunoglobulin protein
BITC	Benzyl isothiocyanate
CCCP	Carbonyl cyanide m-chlorophenyl hydrazone ()
CHOP	C/EBP homologous protein
CLR	Calreticulin
DAMP	Damage-associated molecoular patterns
DC	Dendritic cell
DCFDA	2',7'-Dichlorofluorescin diacetate
DCFDA	2',7'-Dichlorofluorescin diacetate
DHR	Dihydrorhodamine
DHR	Dihydrorhodamine
eIF2α	Eukaryotic initiation factor 2 alfa
ER	Endoplasmic reticulum
FCB	Flow Cytometry buffer
FDA	Food and Drug Administration
FHA	Fast Halo Assay
GRP78	Endoplasmic reticulum luminal glucose-regulated protein 78
GSH	Glutathione
HI	Hemidesmus indicus
HI	Hemidesmus indicus
HID	Hemidesmus indicus decoction
HMBA	2-hydroxy 4-methoxy benzoic acid
HMGB1	High mobility group box 1
HSP70	Heat shock protein 70
HSP90	Heat Shock protein 90
Hyp	Hypericin
ICD	Immunigenic cell death
iDC	Immature DC
IRE1	Inositol-requiring protein 1
ITC	Isothiocyanates
JNK	c-Jun N-terminal kinase
LOD	Limit Of Detection
LOQ	Limit Of Quantification
MAP	Mitogen-activated protein
MAPKKK	Mitogen-activated protein kinase kinase kinase
MEF	Mouse embryonic fibroblast
MFI	Mean fluorescence intensity
MLKL	Mixed lineage kinase domain-like protein
MOMP	Mitochondria outer membrane permeabilization
MUH	4-Methylumbelliferyl heptanoate
NAC	n-acetyl cysteine
Nrf2	Nuclear factor (erythroid-derived-2)-like 2
NSF	Nuclear diffusion factor
p- eIF2α	Phosphorylated eukaryotic initiation factor 2 alfa
p-PERK	Phosphorylated PKR-like endoplasmic reticulum kinase
PAMP	Pathogen-associated molecular pattern
PARP	Poli ADP-riboso polymerase
PBMC	Total peripheral blood mononuclear cells
PEITC	Phenethyl isothiocyanate
PERK	PKR-like endoplasmic reticulum kinase
PRR	Pattern recognition receptors

RCD	Regulated cell death
RFP	Red fluorescent protein
RIPK1	Receptor-interacting serine/threonine-protein kinase 1
RIPK3	Receptor-interacting serine/threonine-protein kinase 3
SFN	Sulforaphane
TAA	Tumor associated antigen
TLR	Toll like receptors
TNF	Tumor necrosis factor
TRAF2	Tumor necrosis factor receptor-associated factor 2
TUDCA	Sodium tauroursodeoxycholate
UPR	Unfolded protein response
WDA	Witanolide A
WDB	Witanolide B
WFA	Witaferin A
WS	Withania somnifera
WSDE	Withania somnifera DSMO extract
XBP1	X-box binding protein 1

I. Introduction

Cancer is the second leading cause of death among non-communicable diseases worldwide [10]. Carcinogenesis is a multifactorial and a multistep process. Sequential acquisition of specific mutations in key genes (oncogenes) is the cause of the ruthless transformation from normal to tumor cells. Thus, tumor cells acquire peculiar common abilities that reflect DNA mutations and enable cancer cells to survive, proliferate and differentiate. The *hallmarks of cancer* consist of: proliferative signaling sustain, growth suppressors evasion, cell death resistance, replicative immortality, angiogenesis, invasion and metastasis activation, energy metabolism reprogramming, and immune evasion (Figure 1.1) [11].

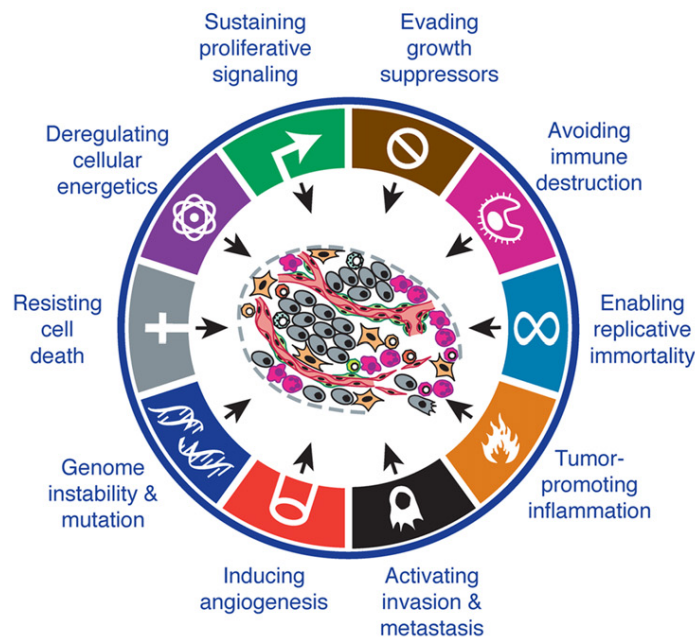Figure 1.1 The *hallmarks of cancer* proposed by Douglas Hanahan and Robert A. Weinberg© [11].

As a consequence of the remarkable progress in the knowledge of cancer biology, effective antitumor strategies have been developed. It's now been almost 80 years since a patient afflicted by cancer was successfully treated with a chemotherapeutic agent (nitrogen mustards) for the first time [12]. Since

then, cancer research has come a long way and was able to find cures for Hodgkin disease, childhood acute lymphoblastic leukemia (the 1960s) and testicular cancer (the 1970s), as well as discovering methods to manage many other types of cancer [13]. However, cancer is still a huge burden on populations worldwide. Even at present, an average of 4600 new patients are being diagnosed with cancer on a daily basis in the United States of America and about 1650 of them won't survive [14]. Colorectal cancer is the third most common cancer diagnosed among the entire population and American Cancer Society expected to be the second cause of death among all type of cancer in 2017 in the USA, second only to lung cancer, hypothesizing 50260 victims (Figure 1.2 A and B). It has been demonstrated that incidence rates increase with age for the majority of tumors [10]. This notion is intuitive since it basically reveals cell DNA damages gathered over time. At the same time, it can suggest that different groups of population can be affected in a different way from different types of tumor, depending on the age. Pursuing this assumption, it turns out that colorectal cancer is still a burden for the older population (Figure 1.2 D), but it doesn't affect children from 0 to 14 years old [10]. In this part of the population the biggest burden is represented by leukemia, which is responsible for the 35% of deaths among all type of cancers [10] (Figure 1.2 C). Thus, both colorectal and leukemia neoplasms affect two sensitive part of the population and whether mortality trend is descending in both cases [10], any exhaustive cure has not been discovered yet and the limit of currently chemotherapy is still causing too many victims.

Resistance to cancer therapies and immunoevasive characteristics of tumor cells are two of the major problems that preclude the success of antitumor strategies [15]. For a long time, research has focused on exploring new approaches that implied a complete tumor eradication coupled with increased sensitivity to chemotherapy or the immunological identification by

the immune system of low immunogenic tumors cells [16]. Thus, a therapeutic approach that combines these two stratagems would determine long-term success of anticancer therapies. In this context, immunogenic cell death (ICD), which is a regulated form of cell death capable of exerting immune stimulation, represents the link between tumor demise and recruitment of the immune system.

On the other hand, it has been reported that in the past few years nature has become the most productive source of drug leads in the pharmaceutical field, with more than 100 new natural products currently being studied in clinical trials. Particularly, it represents a very interesting and prosperous source of compounds with antitumor potential, emphasized by the fact that cancer is the major recipient among all pathologies for the use of these drugs [17] .
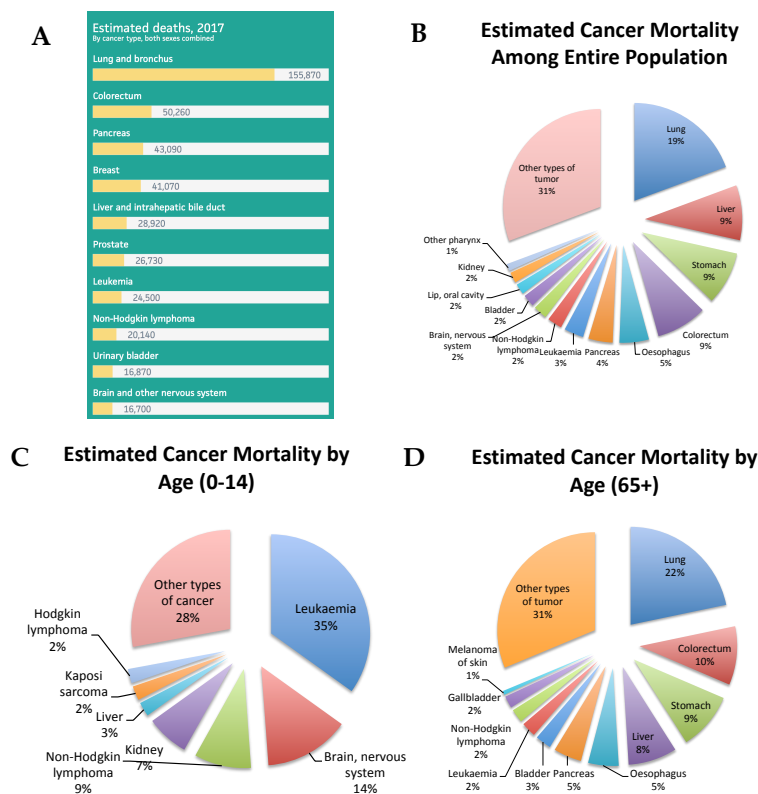
Figure 1.2 Estimated deaths for 2017, by cancer type, both sexes combined-Copyright © 2017 American Cancer Society (A), estimated percentage of cancer death all ages (B) 0-14 years old (C) 65+ years old (D), both sex combined [10].

I.I   Cancer and Immune System

Ideally, the immune system should be able to identify and eradicate cancer cell precursors, avoiding the development of relevant tumors in the first place [15]. However, one of the hallmarks of tumors is exactly the ability to escape immunosurveillance. Immunosuppressive microenvironment or other common characteristics that participate in carcinogenesis, like the presence of hypoxic area, can be indirect causes of this phenomenon. In addition, cancer cells themselves have many weapons to their disposal. During each phase of the tumorigenic process, an intense crosstalk between cancer cells and intrinsic (cell to cell) or extrinsic (cell to host immune system) elements make them achieve the capability of neglecting the host's immune system. Initially, tumors elicit an –albeit transient- immune response, that is insufficient to nip carcinogenesis in the bud. Later on, tumor cells face immunoselection. This means that the established pre-malignant lesions consist of the highest mutagenic cell fraction that was able to escape the surveillance of the immune system as a result of its intrinsic nature or, again, due to the ineffective immune response that in turn was caused by the induction of tumor-antigen specific immune tolerance [15]. Then, after the full-blown tumor is formed, immunosubversion — the active suppression of immune response — could annihilate both innate and adaptive immune responses [15].

Thus, overtaking the immunoevasive phenotype of tumor cells to increase their immunogenic potential represents a very promising strategy for effective cancer treatment [18]. In particular, this strategy embraces the purpose of eradicating all neoplastic lesions and preventing any possible relapse through the acquisition of an adaptive immune memory against tumor cells. Many interesting immune-therapies engage a direct stimulation of autologous or innate immune cells or retrieve T cells effector activity. Such

therapies are, for example, dendritic cells (DCs)-based vaccines, immune checkpoint blockers and adoptive T-cells transfer. However, an autologous stimulation of DCs, where the demising tumor cells themselves exert the imprinting to the adaptive immune system, in an "endogenous vaccine"-like effect, could be more efficient in long term cancer eradication. In this context, ICD is the antitumor strategy that provides the implant for this kind of immunity.

In this regard, in order to understand how dying cells can trigger ICD, it is necessary to take a step back and understand how the immune system relates to the surrounding *stimuli*. For a long time, the immune system was described through the self/non-self model. Briefly, all molecules that come into contact with the immune system of a certain organism were categorized depending on whether they belong to that organism or not. To clarify, the organism's own cells and cellular antigens (self-antigens) were included in the self-category, while pathogens, viruses, bacteria and anything which had an extraneous origin to the organism and possessed non self-antigens was considered non-self (Figure 1.3). According to this model, self and non-self *stimuli* respectively inhibited or triggered the immune response through the interaction with the pattern recognition receptors (PRRs) that are expressed on immune cells [19, 20]. The "non-self" category is in turn subcategorized and includes "microbial-like non-self", "missing self" or "induced or altered self". In the case of microbial invasion, the activation of PRRs lies on the pathogen-associated molecular patterns (PAMPs) that are biological components of the invaders, such as the lipopolysaccharide of gram-negative bacteria or the DNA/RNA-based genome of viruses. The "missing self" refers to the loss or downregulation of outer membrane molecules, such as the "don't eat me" signal CD47, while the "altered self" indicates the detection of abnormalities such as the transformation that normal cells incur after viral infections [20]. So,

according to the self/non-self theory, only these three categories are able to trigger the PRRs and to prompt the immune response. However, the limitations of this theory become apparent when the immunogenicity of dying cells is envisaged. Indeed, the self/non-self theory considers both necrosis and apoptosis silent or tolerogenic processes. According to this theory, phagocytes remove apoptotic cells without eliciting any immune response in a way that could also lead to tolerogenicity. Following the same rationale, the necrosis-driven inflammation favors tissue repair processes instead of immunity, even if currently it's accepted that tissue repair is largely mediated by the immune system [20]. Moreover, the concept of Tumor-Associated Antigens (TAA) is not coherent with this schematic explanation of immune system. In fact, immune system recognizes TAA, but they cannot be considered either non-self, missing self or altered self [21]. To explain these discrepancies, the self/non-self model was molded into the danger model of immunity. In this scenario the immunological recognition does not rely on the discrimination between self and non-self entities but, regardless from the source, it distinguishes safe or dangerous *stimuli* [19, 22]. These dangerous entities alert the immune system through the emission of danger signals and alarmins that can be released, for example, by dying cells and are called damage-associated molecular patterns (DAMPs). DAMPs resemble to endogenous PAMPs and share with them the PRRs [19]. Indeed, the danger model embraces a larger spectrum of molecules that can be considered dangerous and can activate an immune response. For example, starting from pathogens arriving to wound or necrotic tissue, from diseased cells to cells undergoing non-physiological death, they all are immunogenic entities [19]. This new model of immunity also explains how self-cells in sterile conditions are able to stimulate an immune response if properly stimulated, and paved the way for the elaboration of ICD concept.
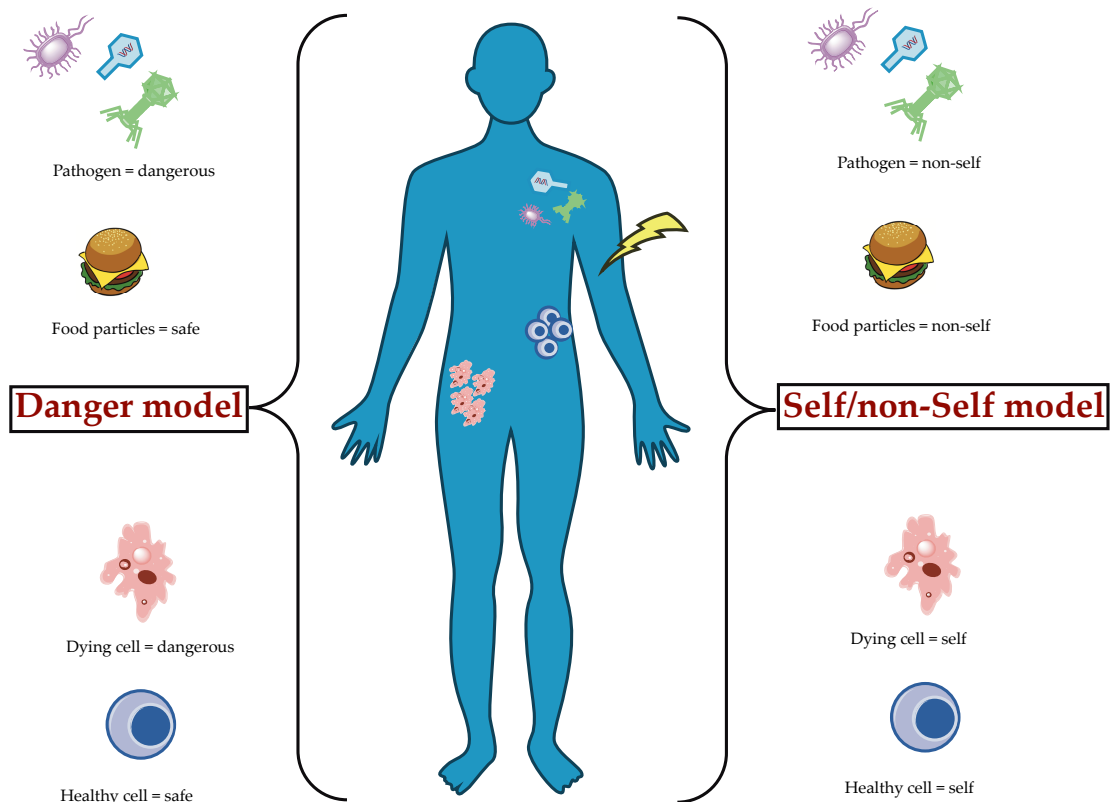
Figure 1.3 Schematic representation of Self-nonself theory *versus* Danger theory

Another very common pitfall parallel to the self/non-self model of immunity was to strictly categorize cell death routes into two closed classes: a not regulated, pathologic and inflammatory cell death (necrosis), and a form of regulated, physiological, not immunogenic or tolerogenic ones (apoptosis). This outdated and wrong concept prevailed for a long time, but now it's clear that these sharp-cut differences do not exist. On the contrary, cells can decease after the activation of a genetically programmed molecular pathway in a necrotic morphological way and, at the same time, apoptotic cells are able to activate an antigen immune response [23]. More specifically, according to the immunological effect and the contingent activation of TAA-targeted immunity, three distinct profiles of cancer cell death can be triggered depending on the prompting antitumor agent [21, 24]: tolerogenic, immunogenic and

inflammatory cell death. As the name suggests, tolerogenic cell death is the physiological or homeostatic kind of cell demise that produces the active suppression of the immunity through the deliverance of anti-inflammatory factors [21]. At the other extreme, ICD is a non-homeostatic kind of cell death [25], which produces proinflammatory cytokines and chemokines as a result of DAMPs release and that culminates in the immunostimulatory phagocytosis of apoptotic corpses [26]. Inflammatory cell death occurs when indistinct immune responses induced by a plethora of tolerogenic and immunogenic signals are elicited and culminate in acute reactions [27].

Thus, apoptosis can be either tolerogenic or immunogenic whether is physiological or triggered by ICD inducers, respectively [21]; necroptosis can be both immunogenic and inflammatory [27] and non- programmed necrosis is considered strictly inflammatory [28].

I.II   Immunogenic Cell Death as Anticancer Strategy

The concept of ICD was proposed for the first time after the danger model of immunity was developed and it was clear that regulated forms of cell death (RCDs) (*i.e.* apoptosis, necroptosis, etc) could be immunogenic instead of immunological silent or tolerogenic, depending on the initiating *stimuli* [25]. So far, several chemotherapeutic agents — both physical and chemical — were identified as *bona fide* ICD inducers. Doxorubicin, oxalilplatin and the hypericin-based photodynamic therapy (Hyp-PDT) are all examples of ICD promoters. It's impossible to find similarities among them in their mechanism of action or molecular structure but apparently they all induce ICD, acting through a different interpretation of the same pathway. Two crucial events are essential to trigger immunogenic apoptosis: endoplasmic reticulum (ER) and oxidative stress.

ER is a fundamental organelle for eukaryotic cells. It regulates lipid biosynthesis, calcium ion (Ca^{2+}) storage, and synthesis, modification and folding of proteins that are designed to be released or incorporated into the plasma membranes [29].

Three major sensors — PKR-like ER kinase (PERK), inositol-requiring protein 1 (IRE1) and activation of transcription factor 6 (ATF6) — constitute the unfolded protein response (UPR) and are in charge for ensuring that homeostatic conditions are maintained. Normally, they are coupled with binding immunoglobulin protein/ ER luminal glucose-regulated protein 78 (Bip/GRP78) to form an inhibitory complex that unties in condition of stress. In this situation Bip gains the function of chaperon with rescue activities in order to restore ER homeostasis and at the same time make the three sensors free to activate the UPR. If stress conditions are not severe, the UPR is able to reestablish cellular integrity: PERK phosphorylates its main downstream protein eukaryotic initiation factor 2 alpha (eIF2α), which in turn slows down protein synthesis and reduces the load of incoming naïve proteins. At the same time, it stimulates Ca^{2+} preservation while IRE1 and ATF6 allow transcription of x-box binding protein 1 (XBP1), which ensures the prevention of the aggregation of unfolded proteins. This fast response enables the cells to restore homeostasis. However, if stress is prolonged or too severe, the balance is tipped toward pro-death signals. In this case, different pathways can trigger apoptosis. IRE1-tumor necrosis factor (TNF) receptor-associated factor 2 (TRAF2)-c-Jun N-terminal kinase (JNK) pathway could elicit apoptosis through the interaction with the mitogen-activated protein (MAP) kinase kinase kinase (MAPKKK), apoptosis signal-regulating kinase 1 (ASK1) and its activator actin-interacting protein 1 (AIP1), or through the involvement of the proapoptotic B-cell lymphoma 2 (Bcl-2) family members that in turn amplify IRE1 signal [30]. In addition, PERK is able to upregulate C/EBP

homologous protein (CHOP) which in turn downregulates the anti-apoptotic protein Bcl-2 and activates the transcription of ER-Oxidase 1α, which is an apoptosis effector [30]. So far, it has been demonstrated that while all UPR sensors are activated during ICD, only the activation of PERK is mandatory to elicit immunogenicity [31].

ICD-inducing agents elicit a form of ER and oxidative stress that activate a danger pathway which involves the mobilization of the ICD mediators, the so-called DAMPs. As above mentioned, DAMPs are endogenous molecules that acquire immunostimulant properties when exposed on the outer cellular membrane or released in the extracellular matrix, in a defined spatial-temporal manner that differs on which agent/*stimulus* started the process. When exposed or liberated to the cellular matrix by damaged or dying cells, DAMPs bind PRRs directly on the surface of immune cells, such as different types of toll like receptors (TLR's), creating a bond between the demising cancer cells and the immune system [31]. In other words, they turn in "eat me" or "find me" signals for antigen presenting cells (APC), like DCs, macrophages, certain T-cells, or natural killer (NK) cells. Moreover, they foster DCs maturation and the activation, elaboration and presentation of the TAA to immature lymphocytes T. In this way, the host immune system established the first contact with the specific TAA and a subsequent stimulation of TAA-specific T-cell-mediated immune responses would result into the eradication of the remaining cancer cells together with an immunological memory [4]. In this way, the adaptive immunity is triggered and the treatment of the tumor resulted in an endogenous vaccine-like effect (Figure 1.4). Furthermore, DAMPs sustain the opsonization of dying cancer cells and foster the activation of inflammatory processes dependent on the inflammatory transcription factors in immune cells and the inflammasome [32].
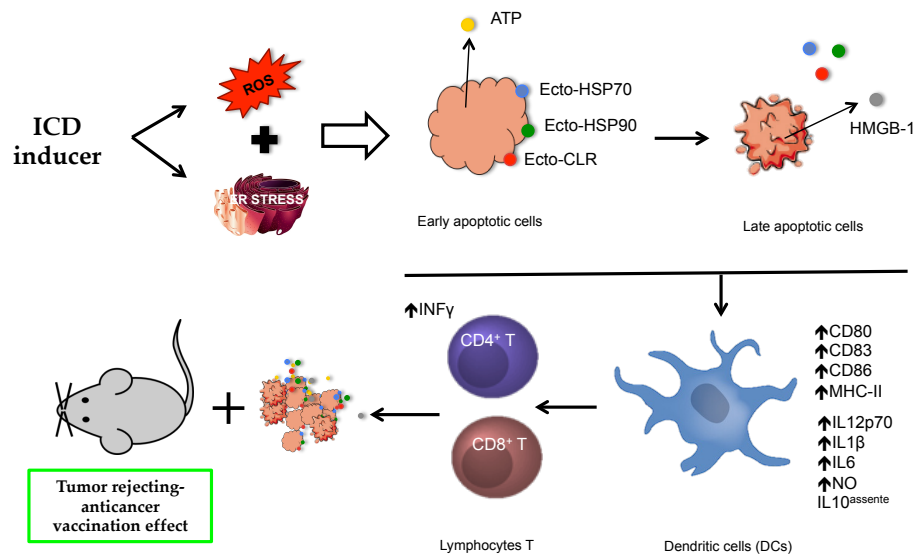
Figure 1.4 Schematic representation of the immunogenic cell death (ICD) pathway.

I.III   Anticancer Therapy triggers ICD through different Regulated Forms of Cancer Death

The concept of ICD is usually used as synonym for immunogenic apoptosis. However, other pathways may potentially lead to the immunogenic stimulation.

Among all RCDs, apoptosis is the most renowned and is mediated by effector caspases. Three main pathways are able to initiate this process. The extrinsic or receptor-mediated via, which foresees the activation of death receptors on the outer cell surface that leads to the activation of caspase 8 [33]; the intrinsic or mitochondrial pathway, which releases cytochrome c and allows the activation of the effector caspases 3 and 7 [33]; the ER pathway that was examined in detail in the last paragraph, which foresees the activation of executor caspases 3, 6 and 7 [30]. Morphologically and functionally, apoptosis is characterized by a loss of plasma membrane symmetry, exposure of

15

phosphatidylserine on the outer leaflet of the plasma membrane during the early stages, chromatin condensation, intranucleus DNA cleavage and cytoplasmic membrane blebbing, while keeping cellular integrity. All these events prevent cells from losing all their content like during necrosis [34]. Once immunogenic apoptosis is triggered, DAMPs trafficking involves all the apoptotic phases, from the very early to late stages. For example, during the early phases of apoptosis, the ER chaperone calreticulin (CLR), heat shock protein (HSP)-70/90 are exposed on the outer surface of the cells, recognized by the CD91 receptors and act as *eat-me* signals inducing the engulfment of dying cancer cells [35, 36]. ATP can be released actively or passively during the pre-apoptotic or early- to mid-apoptotic phases respectively, and could represent either a potent short-range *find-me* signal for attracting monocytes or as a proinflammatory molecule by binding the P_2Y_2 purino-receptors, or the P2X7 receptor on innate immune cells [32]. During the late phase of apoptosis the most important DAMP is the high mobility group box 1 (HMGB1). When it is released, it binds TLR2 and TLR4 on DCs, stimulating production of proinflammatory cytokines and assisting in the proper antigen presentation [37].

Necrosis, on the other hand, is a non-regulated form of cell death, in which cell membranes become permeable during the early phases of the process and release all the cytoplasmic material and induce an inflammatory response. However, it's not completely true that this uncontrolled pouring of cytoplasmic material is able to trigger a complete immune response. Certainly, the same DAMPs mobilized during apoptotic immunogenic cell death are released in the extracellular matrix, but the lack of spatial-temporal arrangement of this process could decrease its immunogenic potential. Additionally, during necrosis many other substances are infused outside the cells and quench the immunogenic potential of the emitted DAMPs [23].

16

This means that the mere disassembly of plasma membrane and the flow of the cytoplasmic content into the microenvironment are not sufficient to induce ICD. This statement is supported by different *in vitro* and *in vivo* experiments. *In vitro* experiments showed that mouse cancer cells undergoing necrosis via boiling or freeze–thawing cycles do not activate DCs [38], nor are tumor necrotic cells able to stimulate protective immune response after repeated inoculations of syngeneic mice [39]. Accordingly, TC-1 cells undergoing accidental necrosis do not efficiently vaccinate syngeneic C57BL/6 against a successive inoculation of living cells of the same type [40], as opposed to cells undergoing through the regulated form of necrosis, *i.e.* necroptosis [40].

Necroptosis is a caspase-independent form of RCD. It is initiated by death receptors ligands' activation, which in turn activates the kinase activity of receptor-interacting serine/threonine-protein kinase 1 (RIPK1), which mediates the RIPK3 and mixed lineage kinase domain-like protein (MLKL) activation, the downstream mediators of necroptosis. The morphological changes during necroptosis correspond to those of necrosis, thus its pro-inflammatory activity is still significant. However, unlike necrosis, a pattern in DAMPs mobilization has been discovered. Necroptotic TC-1 and EL4 cells show ecto-CLR, ATP secretion and HMGB1 release only in absence of RIPK3 and MLKL knock-out conditions [40], which means that DAMPs pattern is triggered only when the necroptotic machinery is working. Moreover, recently it has been attested that at least part of the immunogenicity triggered by the *bona fide* ICD inducer mitoxantron relies in its capability to trigger necroptosis. In fact, necroptotic TC-1 cells treated with mitoxantron elicited protective immunity in C57BL/6 only in the presence of active RIPK3 and MLKL. This behavior has been linked to the inability to secrete ATP and release HMGB1 when necroptosis doesn't subsist [40]. What's more, unlike wild-type, RIP3 and MLKL null TC-1 cells growing on C57BL/6 mice are less sensitive to the

direct antitumor effect of mitoxantron and after the treatment the microenvironment is less rich in CD11c+-CD86+ APCs and CD8+ T cells [40]. Surprisingly, the mechanisms that underline the immunogenicity of ICD seem to be different if this process is triggered by necroptosis or apoptosis. A very recent study showed that necroptotic cell death promoted ICD in CT26 cells in an UPR-unrelated way, infusing the idea that necroptotic ICD could be a complete distinctive form of apoptotic immunogenic death [39].

More, autophagy has recently been added as additional engine which drives the immunogenicity of ICD. [41]. Properly, autophagy is a defense mechanism triggered in response to a different kind of stress, such as a lack of nutrients or energy, bacterial infections or damaged intracellular organelles. It is a multistep self-degradation process, where cytoplasmic material is sequestered into phospholipidic membranes to form autophagosomes. These vesicles are then fused with lysosomes and degraded by lysosomal hydrolases with the aim of gaining energy from these anabolic reactions. Kroemer's group noticed that during drug-induced autophagy, cells were able to release ATP and demonstrated that the autophagic process is also required, but not sufficient, to optimally spark pharmacologically induced immunogenicity [25]. In fact, inhibiting autophagy by blocking different nodes of the autophagic machinery leads dying cells to significantly impair ATP release that *in vivo* translates into a lesser enrollment of DCs, macrophages and monocytes and lacking antitumor immune responses and therapeutic failure [42]. Indeed, coupling autophagy inhibitors to the ATP degradation enzyme inhibitor ectonucleotidase restored normal ATP levels and the related immunogenicity [42]. It's worth mentioning that many tumors are characterized by defects in the autophagic process and that may reveal at least one way through which tumors escape from immunosurveillance [41].

Other forms of RCD, such as ferroptosis, seem capable to trigger ICD

[31], however, the limited literature data available on this topic makes an extensive survey impossible at this time.

Currently, almost no anticancer drug elicits its antitumor potential through the activation of only one cell death mechanism, and these observations give promising indications about a synergistic strategy, which could involve the associations of different variants of ICD to induce a more efficient immune response. But attention must be kept when consistent necrosis fosters other RCDs.

For simplification purposes from this point on, every time ICD will be mentioned it will refer to the apoptotic form, unless specified differently.

I.IV   Type I and II Inducers of ICD

As mentioned above, the two compelling events necessary to elicit ICD are ER and oxidative stress. Each ICD inducer elicits ER stress in a different way and this translates into different DAMPs trafficking in terms of spatio-temporal release during the death process, composition patterns and/or entity [29]. Accordingly, the way ROS levels and ER stress are related mirrors the different immunogenic outcome. On this basis, two broad groups of ICD inducers have been identified: type I and type II.

Type I inducers comprehend all those compounds which the main proapoptotic "on target" effect doesn't involve ER, thus provoking ICD-related immunogenicity via "off target" ER stress. ER stress can be induced by mitochondrial ROS, as it happens in the case of cardiac glycosides and wogonin [4, 43-45]. In this case, ROS are transferred from the mitochondria to the ER through the mitochondria-associated ER membranes (MAMs) [46] and there they exert the stress. Doxorubicin and mitoxantrone are two other type-I-ICD inducers. Their mechanism of action requires the interaction with lipid

membrane, thus with ER lipid membrane too, which results in ROS-related lipid peroxidation and consequent ER stress [4, 43, 44, 47]. Another subfamily of ICD type I inducers acts through direct or indirect unfolded protein overload, which only causes ROS production in a second phase. Shikonin and bortezomib fall into this category [4, 25].

Type II inducers, on the contrary, induce immunogenic apoptosis orchestrating danger and apoptotic signaling on the same "on target" ROS-based ER stress. In this way, oxidative stress that originates in the ER can be amplified to the mitochondria and the lipid membrane in an opposite direction as mentioned above. Currently, the only chemotherapeutic agent able to elicit ICD in a type I manner is the Hyp-PDT. Hyp localizes in the ER and when activated with the proper wavelength evokes a strong ROS production that also activates the UPR response [46, 48].

Of note, other treatments outside the strict chemotherapeutic category, such as oncolytic viruses (*e.g.*, Newcastle disease virus) [49, 50] and platinum II–N-heterocyclic carbene complexes [51], have been identified as type I ICD inducers.

Due to the greater amount and promptness of the mobilization of DAMPs induced by type II agents, it's clear that the quality of ER stress elicited generates a better immunological profile than type I [4]. Furthermore, type I and II differ in the role of PERK. In type I inducers, it regulates the canonical UPR pathway via eIF2α, while in type II it regulates the expansion of the secretory pathway in an unknown way. But not enough is known to unravel key mechanisms underlying these differences.

Usually, every ICD inducer is characterized by its own pattern of DAMPs, in terms of quality (type of DAMPs and how they are mobilized), quantity and release/exposure kinetic depending on the ER stress provoked [29]. Furthermore, besides DAMPs emission, cancer cells themselves can

stimulate the immune system if triggered by ICD inducers. In this case, dying cells typically trigger the host's defense response in the same manner as pathogens or viral infection trigger the so-called "altered-self mimicry" [31]. For instance, cells dying through ICD can mediate the chemokine (C–X–C motif) ligand 1 (CXCL1), chemokine (C–C motif) ligand 2 (CCL2) and CXCL10 release, which directly attracts neutrophils in a way that reminds the response of bacterial or viral infections. Through respiratory burst, the neutrophils will then direct anticancer cytotoxicity against the remaining cancer cells [52].

I.V   ICD and Drug Discovery

As above reiterated, ICD inducers do not have a structure-activity relationship or common biochemical features, but they definitely follow some patterns that are still unknown. Indeed, the incapability to prompt enough amount of stress underlying the mobilization of DAMPs or the mere inability to promote the mobilization of a single DAMP is enough to compromise all the immunogenicity of the treatment [23]. The most fitting example of this issue refers to the ICD inducer oxaliplatin and the immunogenic null cisplatin. They both are DNA alkylating agents but only oxaliplatin targets the UPR and promotes CLR exposure to the outer membrane of damaged or dying cells [53]. By consequence, unlike oxaliplatin-treated cells, cisplatin-treated mouse cancer cells are not able to vaccinate syngeneic hosts. Only the combined treatment with an ER stressor, such as thapsigargin or tunicamycin, is able to restore the immunogenicity of cisplatin [53].

Even trickier is the example of cardiac glycosides which *in vitro* induce CLR exposure, ATP secretion and HMGB1 release, but are not able to create an immunological memory in mice via antigen-specific response [54]. This behavior suggests that new and more significant DAMPs have yet to be identified, and confirms that so far the prediction of the immunogenicity of

a cell death cannot rely solely on the DAMPs' analysis. These discrepancies underline the importance of vaccination assays, but at the same time raise the issue of translational experiments on human cancer models, since vaccination is not an option. While waiting for humanized mice to give a syngeneic model of human tumorigenesis, valid alternatives are *in vitro* study on DC maturation [23].

To conclude, if possible, tumor heterogeneity and the not fully understood mechanism of action of ICD inducers make the process of drug discovery even harder.

II. Natural Products in Cancer Therapy

From ancient times, plants have been used as a source of remedies for the most diverse pathologies, and even today they keep on representing the richest library of drug leads for the discovery of new medicines. They play a pivotal role in anticancer therapy and they usually show a more favorable profile than newly synthesized chemical compounds, in terms of bioavailability and low toxicity [55]. The relevance of natural compounds in cancer research is confirmed by statistics. Between 1999 and 2008, 36% of the first-in-class small molecules approved by the US Food and Drug Administration (FDA) for cancer treatment were natural products or natural product derivatives [56]. Moreover, from 2004 to 2014, 28 of 70 antitumor drugs originating from natural products have been approved, while the others were in phase 1 (14), 2 (19) or 3 (9) of clinical trials at the end of 2014, respectively [55] underlying the proficiency of these products in the field of cancer treatment.

Natural products can be categorized in single molecules (phytochemicals) or botanical drugs. FDA defines botanical drugs as "products that consist of vegetable materials, which may include plant materials, algae, macroscopic fungi, or combinations thereof, intended for a use in the diagnosis, cure, mitigation, treatment or prevention of disease in humans" [57]. They contain a combination of potential active compounds that together exert the biologic activity. Intuitively, the complex composition of botanical drugs mirrors their capability to affect more than one biological pathway, which in turn results in a wider global activity. Actually, *in vitro* and animal studies documented that both phytochemicals and botanical drugs share the significant pleiotropic mechanism of action that makes them able to simultaneously target

23

multiple hallmarks of diseases, thus increasing the chances to beat complex pathologies such as cancer [58].

On the other hand, as a consequence of their complex intrinsic nature, botanical drugs offer more challenges than purified phytochemicals in terms of drug development process. In fact, even if safety and toxicity are usually not crucial problems since botanical drugs have frequently been used in traditional medicine and they're commonly available as dietary supplements, batch-to-batch differences in composition could affect the biological effects. Indeed, the weather, seasonal variations and geographical location are some of the elements that could affect the intrinsic composition of the growing plant. Thus, to guarantee quality, botanical drugs routine analyses are more complex than those necessary for high-purified drugs (phytochemicals or synthetic molecules indiscriminately) [59]. Quality controls concern all the phases of botanical drug production. For instance, before the harvesting, raw materials in the field are checked and both chromatographic analyses and biological assays are necessary for the quantification of the components and the control of pharmacological consistency [59]. In this context, a useful habit could be to assess the exact chemical composition of botanical drugs, in order to draw a comprehensive "fingerprint" of these substances. Then, marker compounds would be used to rapidly and unambiguously check batch consistency.

To date, the FDA approved two botanical drugs as prescription medicines for the market: Veregen, a water extract of green tea leaves obtained from *Camelia sinensis* and used to topically treat external genital and perianal warts, and Crofelemer (also known as Fulyzaq or Mytesi), obtained from the latex of the South American tree *Croton lechleri*, indicated for the oral symptomatic treatment of HIV/AIDS-related diarrhea on patient going through antiretroviral therapy. Still, no cancer treatment has been approved, but the number of submissions is rapidly escalating and it won't be long until

it will happen.

CHAPTER 1. *Withania Somnifera*

1.1. Introduction

Name: Withania somnifera - Ashwagandha

Family: Solanaceae

Genus: Withania

Species: Whitania somnifera (L.) Dunal

Geographical origin: India, South Africa, Eastern Asia, Mediterranean region

Withania somnifera (WS), better known as Ashwagandha or Indian winter cherry for the characteristic shape of its fruits, is a plant used in Ayurvedic medicine from ancient time. Before the intense cultivation in India, it was frequent spread in the dry and warmest Mediterranean areas, like Italy (Sicily and Sardinia), in the tropical regions of Africa and South Africa, Cape Verde island, Arabia and, of course, Middle East areas, like India, Sri Lanka and China [60].

WS is an evergreen, erect shrub that can achieve 150 cm in height. The petiolate leafs are ovate or elliptic-ovate, acute to obtuse at the apex and oblique at the base, covered by grey *tomentum* (pubescence). Large and small leafs alternate on the vegetative shoots in a way that floral branches are opposed to the large leafs. The axil embraces cluster of cymose of 4-25 pale

monoceous flowers [61]. Flowers blossom during spring, they are sessile and form axillar clusters. The white-yellow corolla is composed by lanceolate lobes while the calyx expand around the reddish fruit. Fruits are small orange-red berry-shaped and carry abundant seeds [62]. Roots are long about 15 cm and have an average diameter of 12 mm. They are cylindrical, light yellow-brownish, and taper down at the lower extremity [61].

In Ayurvedic medicine WS is used for a whole variety of disorders and pathologies. It has aphrodisiac, diuretic, narcotic and sedative properties, as the name implies. It is used as tonic-adaptogen and stimulant to increase vitality and longevity, characteristics that allowed WS earning the name "Indian ginseng" [63]. It demonstrated anti-Parkinson and anti-Alzheimer disease potential, and is considered a remedy for anxiety and depression [63]. It has anti-inflammatory, immune-modulating, anti-stress properties, and a well-documented antitumor potential, showing both antineoplastic and cancer chemopreventive activities [63]. More, it is able to sensitize tumor cells to radiation or chemotherapy, thus decreasing the most common side effects of conventional anticancer therapies when used in combination. An exhaustive body of literature supports these statements with many *in vitro* and animal studies [63].

Leaf, seed or root extracts have been tested to prove WS pleiotropic pharmacologic activities. For instance, aqueous leaf extract exhibited antiproliferative activity in osteogenic sarcoma and breast cancer cell lines [64], while the aqueous ethanolic root extract slowed down tumor growth and increased survival in albino mice affected by Dalton's ascites leukemia [65]. As expected, WS antitumor mechanism of action is most likely multifactorial. It induces apoptosis, and shows both pro- and antioxidant activity (root extract) in different tumor models [66, 67]; it regulates cell cycle (methanolic root

extract) [68], inhibits angiogenesis (hydroalcoholic root extract) [69], and enhances the immune system in different animal models stimulating, among others, NK cells activity, macrophage count and chemotaxis (methanolic and hydroalcoholic root extracts) [62, 70, 71].

The lack of standardization in the preparation of the extract makes impossible a univocal characterization. However the pharmacological activity of the root is attributed to different alkaloids and steroidal lactones that in different amount are found in all WS extracts. The most characterizing elements are withanolides (family of steroids having an ergostane skeleton), withaferins (steroidal lactone) and sitoindosides (saponins) [63]. Witaferin A (WFA) is the most studied among all these compounds and demonstrated antineoplastic potential when used as a single agent. *In vivo*, it inhibited cell growth and increased surviving in prostate, medullary thyroid, soft tissue sarcoma, cervical, uvean melanoma, mesothelioma, pancreatic, and both human and mice breast tumor types [72]. As for WS extracts, WFA's core mechanisms of action concern apoptosis induction, inhibition of angiogenesis and proteasome inhibition [72].

The promising overview here provided and, in particular, the renown anticancer and immunomodulating properties showed by different WS extracts made it a perfect candidate to evaluate its capability to induce ICD.

1.2. Aim of the study

During the first year of my PhD, my research aimed at a characterization of the pharmacotoxicological profile of a DMSO root extract of WS (WSDE) on acute T lymphocyte leukemia cells (Jurkat). I investigated WSDE antitumor potential in terms of cytotoxicity – IC_{50} (inhibitory concentration causing cell toxicity by 50% following one cell-cycle exposure) – apoptosis and

proliferation. Then, I evaluated the capability of the same extract to induce ER and oxidative stress, in order to pave the way for the investigation of WSDE ability to induce ICD. To exploit the latter task, I assessed the ability of WSDE to mobilize the most significant DAMPs that are CLR, HSP70, HSP90 and ATP. The genotoxic potential was investigated in order to collect preliminary indications about the risk-benefit profile of WSDE.

1.3. Results and Discussion

Literature data show an enormous amount of different extracts obtained from the root of WS, all having interesting antitumor potential. We decided to test two extracts obtained with two different solvents: DMSO or a hydro-ethanolic solution (1:1). Both are polar solvents and both are able to dissolve either polar or non-polar substances, but in a different way since DMSO is an aprotic solvent, while the ethanol mixture is able to share hydrogen bonds. Thus, a very different biological activity was not expected. Cytotoxic activity of both extract has been tested on Jurkat cells and no significant differences emerged in their action (data not shown), implying that the active molecule extracted from the root of WS were almost the same using the two solvents. Taking into account the recognized easier dissolution of WFA in DMSO than in protic solvents, WSDE was selected for the study [73].

1.3.1. WE Contains Withaferin A (WFA), Whitanolide A (WDA), and Trace of Withanolide B (WDB)

The most renowned markers of WS were detected and quantified through HPLC analysis. WSDE was enriched mostly in WFA (113.65 µg/mL) followed by WDA (39.42 µg/mL). WDB and Withanone were both in quantities under the limit of quantification (Table 1). This result is not surprising, since

WFA is the prevailing bioactive molecule found in different WS extracts [72, 74, 75].

Since the aim of this research was the understanding of the antitumor activity of the extract in its entirety, from later on the more stringent activities of WSDE will be compared to the activity of the single phytomarker revealed through HPLC and to the combination of them at the same concentration found in the extract. This analysis would allow understanding whether these molecules all together exploit the biologic activity.

Table 1. Quantification of WFA and WDA

Compound	Amount (μg/mL)	LOD	LOQ	Amount (mg/g of dried extract)	Recovery %
WFA	113.65±2.84	6.54±0.11	19.81±0.63	5.68±0.14	96.85±1.98
WDA	39.42±1.44	1.64±0.07	4.96±0.26	1.97±0.07	110.57±2.11
withanolide B	tr	2.03±0.34	6.36±0.65	/	/
withanone	/	1.99±0.29	15.95±1.18	/	/

LOD: limit of detection, LOQ: limit of quantification, tr=trace

1.3.2. WE Induces Apoptosis and Alters Cell-Cycle Residence

WSDE induces a concentration-dependent reduction of cell viability in Jurkat cells. After 24 h of treatments with 1.60 or 3.20 mg/mL, the percentage of viable cells reached 64.4 and 16.6, respectively (Figure 1.1). The resulting IC_{50} was 2.3 mg/mL. Concentrations close to the IC_{50} were chosen for the following experiments. Of note, the rationale of the assay used to measure cell viability was the distinction of the two populations (viable and dead) on the basis of cellular membrane permeability. Thus, an overestimation of the percentage of viable cells is unavoidable since it includes both viable and early apoptotic

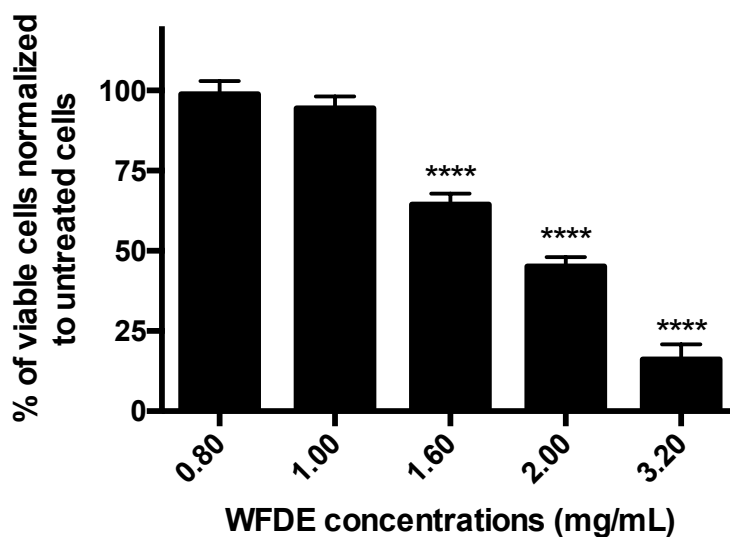cells, both characterized by membrane integrity.

Figure 1.1 Percentage of viable Jurkat normalized to the untreated cells, after 24 h treatment with increasing concentration of the DMSO root extract of WSDE.

Therefore, to discriminate whether the cytotoxic effect of WSDE on Jurkat cells was the result of a RCD, induction of apoptosis was investigated. After 6 h of treatment at 0.40 and 0.80 mg/mL, WSDE increased the fraction of apoptotic cells compared to untreated cells of about 3.4 and 4.1 times, respectively. After 24 h treatment apoptosis was even more pronounced, and statistically significant starting from 0.40 mg/mL, where 33.1% of apoptotic events was observed *versus* 3.1% of untreated cells (Figure 1.2 A and 1.6 B). From 0.80 mg/mL treatment, the number of permeabilized cells (*i.e.* necrotic, necroptotic or late apoptotic cells) increased in a significant way (11.6% *versus* 1.7% of untreated cells) (Figure 1.2 A and 1.6 B). At the highest tested concentration of WSDE (1.60 mg/mL), both apoptotic and "necrotic" events markedly increased, but the percentage of apoptotic cells was significantly higher than that of permeabilized cells (53.2% *versus* 28.2%, respectively) (Figure 1.2 A). Besides, we treated Jurkat with WFA, WDA or their association, at the same concentration found in the extract at 0.20, 0.40 and 0.80 mg/mL. An increase in the percentage of apoptotic cells occurred only for WFA-treated

cells, at all the concentrations tested (Figure 1.2 B). Furthermore, the proapoptotic effect of the association WFA plus WDA was very similar to that of WFA (Figure 1.2B), suggesting the inactivity of WDA at the tested concentrations. Nonetheless, the effect of WSDE was significantly higher than that observed for WFA or the association WFA plus WDA, which bolster the assumption that WSDE cytotoxic and proapoptotic activity stands on the synergistic activity on WFA and others, not yet identified, phytomarkers (Figure 2.2 C).
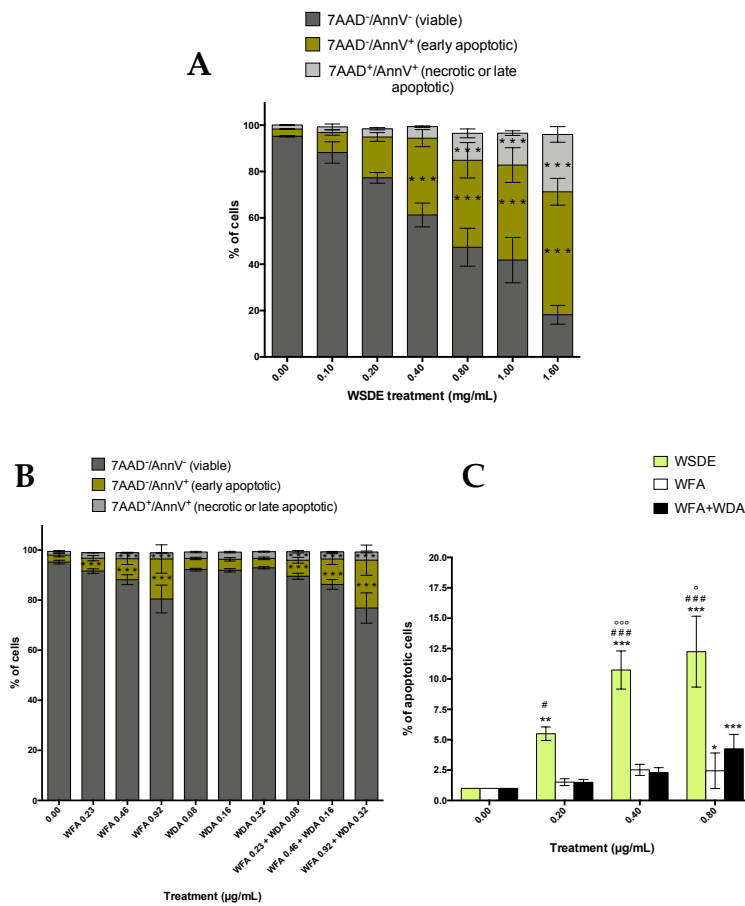
Figure 1.2 Percentage of Percentage of viable (7AAD$^-$/AnnV$^-$), early apoptotic (7AAD$^-$/AnnV$^+$), and late apoptotic or secondary necrotic (7AAD$^+$/AnnV$^+$) after 24 h treatment of Jurkat cells with increasing concentrations of WSDE (A), WFA, WDA or WFA plus WDA (B). Fold increase in the percentage of apoptotic cells after treatment with different concentrations of WSDE, WFA, or WFA plus WDA (C). *, #, ° $P < 0.05$, ** $P < 0.01$, ***, ###, °°° $P < 0.001$ *versus* untreated cells.

In the ensuing experiments, the cytostatic effect of WSDE has been investigated. Jurkat cells were treated for 24 h with increasing concentration of WSDE and provoked a blockage in G2/M phase that was significant starting from 0.10 mg/mL (39.6% *versus* 22.4% of untreated cells), complemented by a decrease in cells in phase G0/G1 (45.7% *versus* 63.0% of untreated cells) (Figure 1.3). WSDE showed the same tendency up to 0.40 mg/mL, where we revealed an increase in cells in G2/M phase (30.3%) and a decrease in cells in G0/G1 phase (50.1%), while at the highest concentrations tested, the cell-cycle distribution turns back to that of untreated cells (Figure 1.3).
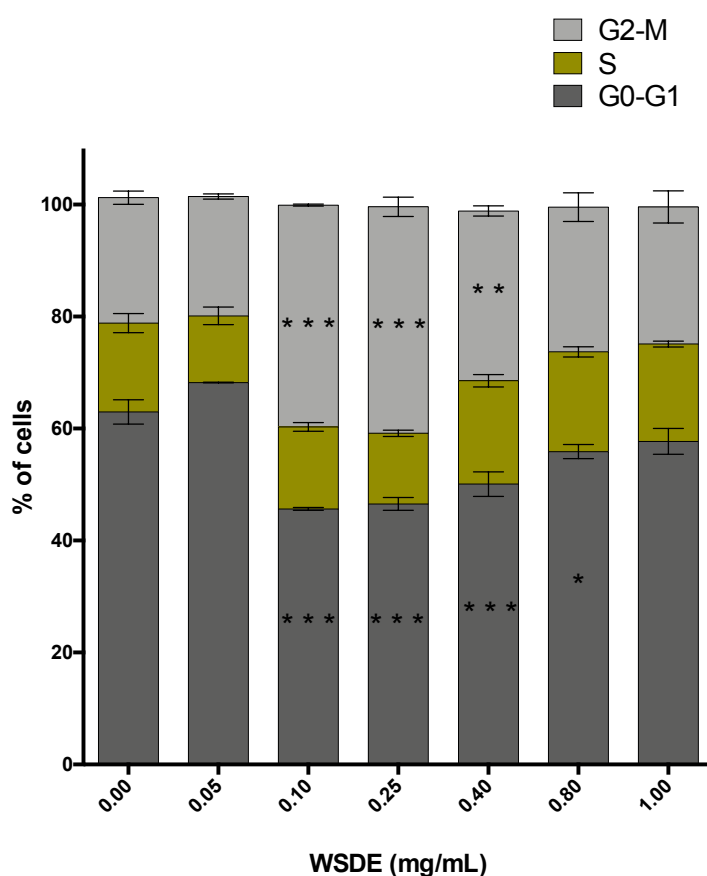

Figure 1.3 Cell-cycle distribution following 24 h treatment of Jurkat with increasing concentrations of WSDE. * $p < 0.05$; ** $p < 0.01$; *** $p < 0.001$ *versus* untreated cells.

Taken together, the proapoptotic and cytostatic effects are consistent

with the characteristics of different withanolides and a methanolic crude leaf extract tested in different leukemia cell lines [76]. However, the mentioned methanolic leaf extract was much potent than WSDE in terms of IC_{50}. This is not surprising, since the two extracts differ for the part of the plant used (root *versus* leaf) and more, the methanolic leaf extract was subjected to a sequential solvent extraction, which progressively concentrated the active components of WS leaves. Conversely, taken together, our results indicating that WSDE interferes with at least two of the hallmarks of cancer (resisting cell death and sustaining proliferative signaling) have to be highlighted.

1.3.3. WSDE Increases Intracellular Ca^{2+} ($_i[Ca^{2+}]$)

Numerous studies conveyed that calcium ionophores exhibit proapoptotic activity [77] and that a controlled intracellular $[Ca^{2+}]$ ($_i[Ca^{2+}]$) increase, prompted by milder insults, stimulate cell death through apoptosis [78]. Moreover, the release of $[Ca^{2+}]$ from the ER to the cytosol could be the consequence of ER stress and the resultant apoptosis an effect of it [78]. Since WSDE revealed marked proapoptotic ability, its faculty to modulate $_i[Ca^{2+}]$ was explored. As well as for apoptosis, WSDE increased $_i[Ca^{2+}]$ levels in a concentration-dependent way, starting from 6 h treatment and significantly at 0.40 mg/mL [837.5 mean fluorescence intensity (MFI) *versus* 410.5 MFI of untreated cells] (Figure 1.4). After 24 h a significant increase in $_i[Ca^{2+}]$ at all tested concentrations was registered and a fold increase of 3.7 times (1530 *versus* 399.7 MFI of untreated cells) was obtained for the highest tested concentration (1.60 mg/mL) (Figure 1.4). Dead cells were analyzed separately as unique cluster.

The demonstration that MSDE-treated Jurkat cells sustain a cytosolic $[Ca^{2+}]$ increase confirms the involvement of this cation in MSDE antileukemic

activity and gives a hint to move forward with the evaluation of the extract's ability to trigger ER stress.
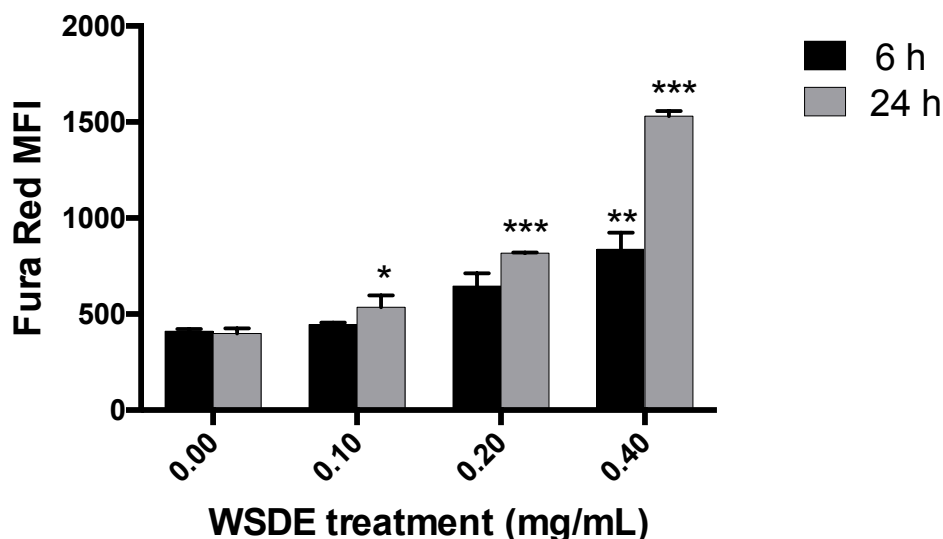
Figure 1.4 Fraction of viable cells with increased $_i[Ca^{2+}]$ following 6 and 24 h exposure to increasing concentrations of WSDE. * P < 0.05; ** P < 0.01;*** P < 0.001 *versus* untreated cells.

1.3.4. WSDE Induces Oxidative and ER Stress

In order to keep on unraveling WSDE mechanism of action and at the same time understand if it could be a suitable candidate for ICD studies, both oxidative and ER stress were investigated in WSDE-treated Jurkat.

After 1, 3, 6, 18 and 24 h treatment with increasing concentrations of WSDE, ROS levels were recorded. The modulation of ROS started after 3 h of Jurkat incubation with the extract, but the highest levels were recorded after 6 h treatments (Figure 2.5 A). At 6 h, 0.80 and 1.60 mg/mL of extract led to ROS levels similar or even higher than those promoted by a mildly toxic dose of H_2O_2 (0.1 mM for 15 minutes), used as positive control. After longer treatment, ROS escalation reached a plateau (data not shown). These data indicate that WSDE rapidly prompts a pro-oxidative status in intoxicated cells. Similar

35

results were obtained by Malik [79], who highlighted a significant ROS rise after 1 to 3 h of exposure to only WFA [80].

To understand the origin of ROS increased levels, Jurkat cells were treated with WSDE in combination with the non-selective ROS quencher N-acetylcysteine (NAC), the copper chelating agent ortho-phenantroline or the inhibitor of mitochondrial electron transport at NADH-ubiquinone oxidoreductase rotenone. NAC prevented almost all ROS production since the ROS levels delivered through the co-treatment NAC-WSDE were comparable to those of untreated cells (Figure 1.5 B). Hydroxyl ions looked the main radical species involved in WSDE-mediated oxidative stress. Indeed, the co-treatment of Jurkat cells with the extract plus ortho-phenantroline for 6 h prevented almost all ROS production (Figure 1.5 B) to the same extent of the effect produced by NAC in the same experimental conditions. Ortho-phenantroline, in fact, is an inhibitor of Fenton reaction that is the main way through which H_2O_2 is transformed in hydroxyl ions. Of note, the results obtained with ortho-phenantroline confirm and avoid any doubt about the protection conferred by NAC to WSDA-treated cells, since this molecule was pointed as direct WFA quencher, implying that the protective role of NAC could be the consequence of the dismantle of WFA, instead of ROS demise. [72]. Conversely, rotenone didn't exert any protective effect on WSDE-mediated oxidative stress suggesting that mitochondrial complex I is not involved in this WSDA-mediated ROS production and that further studies will be needed to individuate the exact site where WSDE mediates ROS production.
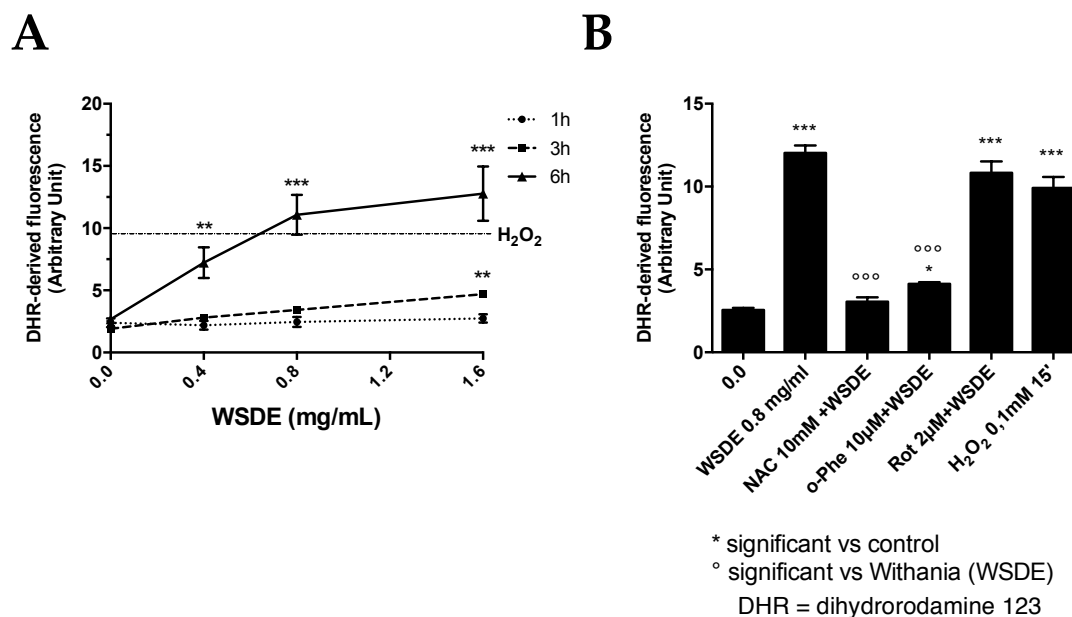
A

B

* significant vs control
° significant vs Withania (WSDE)
DHR = dihydrorodamine 123

Figure 1.5 ROS levels in WSDE-treated cells. (A) Jurkat exposed to increasing concentrations of WSDE for 1, 3 or 6 h. Cells treated with H_2O_2 0.1 mM for 15 minutes represent the positive control (dotted line parallel to x-axis). (B) Cells were treated for 6 h with WSDE 0.80 mg/mL in the absence or presence of o-phenanthroline (o-Phe, 10 µM), rotenone (Rot, 2 µM) or N-acetylcysteine (NAC, 10 mM). Cells treated with H_2O_2 0.1 mM for 15 minutes represent the positive control. * $P < 0.05$, ** $P < 0.01$ and ***,°°° $P < 0.001$.

Since ROSs look crucial in WSDE bioactivity and oxidative stress is one critical event promoting ICD, their role in WSDE-mediated apoptosis was evaluated. Jurkat cells have been treated with the extract plus NAC for 24 h. A significant decrease in the WSDE-induced apoptosis was observed (Figure 1.6 A and B). The apoptotic events were significantly reduced from 33.1% after 0.40 mg/mL of WSDE to 9.4% after WSDE plus NAC and from about 38.5% after 0.80 mg/mL of WSDE to 10.71% after WSDE plus NAC (Figure 1.6 A and B). These data clearly point out the involvement of oxidative stress in WSDE antileukemic potential.

Beside ROS production, the other pivotal event eliciting ICD is ER stress. To evaluate WSDE capacity to induce ER stress we used an indirect method. We pre- and co-treated Jurkat cells with the ER stress inhibitor sodium tauroursodeoxycholate (TUDCA) [81]. Attenuation of ER stress by TUDCA

protected Jurkat cells from WSDE-induced apoptosis (Figure 1.6 A and B). The apoptotic population was lessened in a lesser extent than NAC, but still significantly (from 33.1% 0.40 mg/mL of WSDE to 17.36% after WSDE plus TUDCA and from 38.5% after 0.80 mg/mL of WSDE to 23.28% after WSDE plus TUDCA) (Figure 1.6 A and B). Moreover, the combination of TUDCA and NAC significantly blunted WSDE-induced apoptosis showing how these two events, together, lead to apoptosis. These results are not surprising since WFA itself showed already the ability to trigger ER stress through eIF-2α (PERK main effector) activation and CHOP-mediated apoptosis in renal carcinoma Caki cells [82].

Taken together, these data demonstrated that oxidative and ER stress are the engine that drives WSDE-mediated apoptosis and represent a perfect foundation for the following ICD studies.
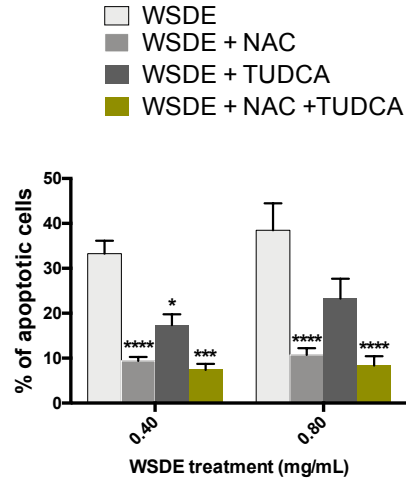
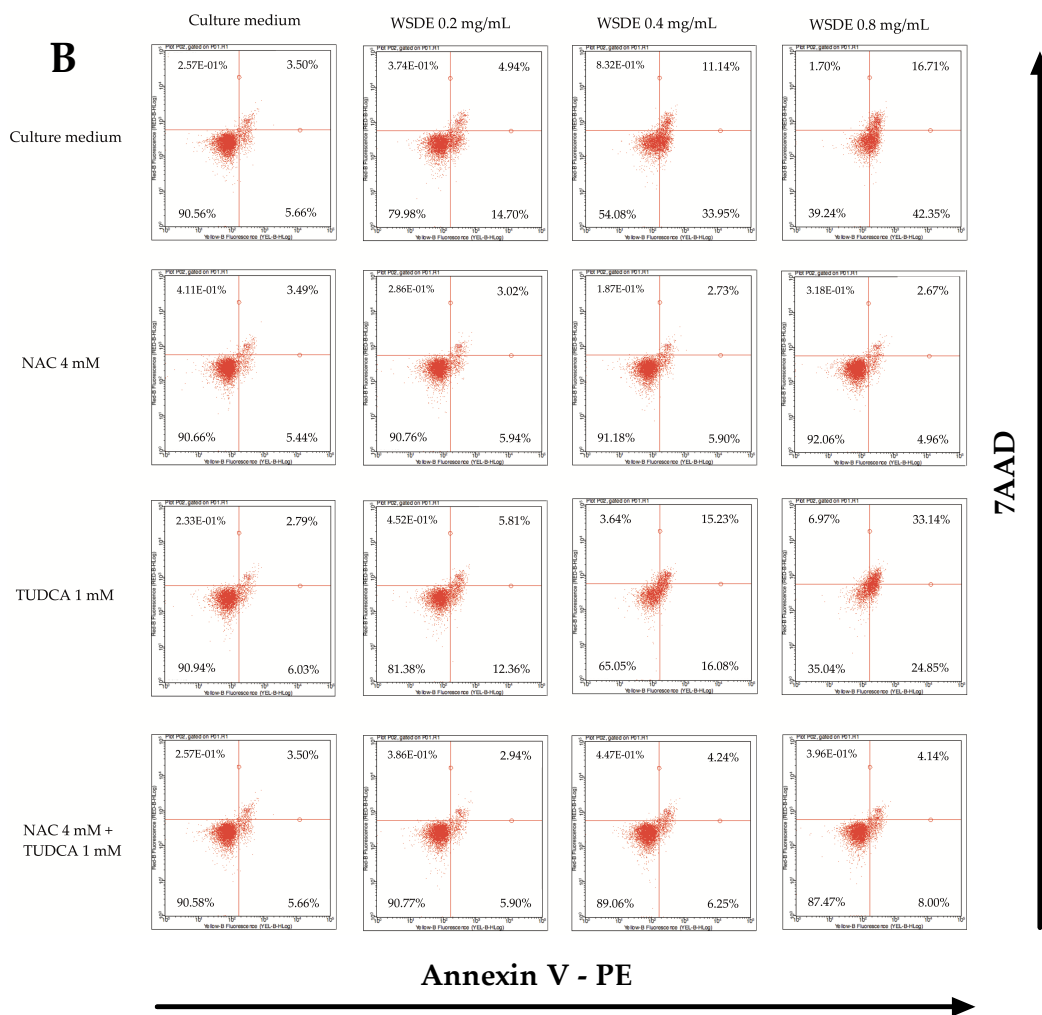Figure 1.6 Apoptotic events after 24 h of Jurkat treatment with WSDE in the absence and presence of NAC, TUDCA or NAC and TUDCA (A). * P < 0.05; *** P < 0.001; **** P < 0.0001 *versus* WSDE; representative dot plots of annexinV-PE/7AAD viability dye cell death assay of Jurkat cells 24 h after treatment with increasing concentration of WSDE, in the absence and presence of NAC, TUDCA or NAC and TUDCA (B).

1.3.5. WSDE Induces DAMPs Trafficking

To evaluate the ability of WSDE to induce ICD *in vitro*, the mobilization of the most representative and immunogenic DAMPs has been explored. The externalization of CLR, HSP70 and HSP90 on the outer leaf of the membrane and the ATP release were investigated after the treatment of Jurkat cells with WSDE.

Although the analyzed DAMPs are usually mobilized during the early phases of apoptosis, none of them has been affected by WSDE after 6 h of treatment (data not shown). On the contrary, 24 h of incubation of Jurkat cells entailed the translocation on the extracellular membrane of CLR, (MFI of 8.39 at 0.2 mg/mL and 8.72 at 0.4 mg/mL *versus* 6.83 of untreated cells) (Figure 1.8 A), HSP70 0.2 mg/mL (57.92 MFI *versus* 42.17 of untreated cells) (Figure 1.8 B) and HSP90 0.2 mg/mL (151.09 MFI *versus* 58.45 of untreated cells) (Figure 1.8 C). At 0.4 mg/mL, the expression of both HSP70 and HSP90 increased up to 85.22 and 144.14, respectively (Figure 1.8 B and C, respectively). A significant increase in ATP levels has been recorded at both tested concentrations (2- and 2.45-fold increase compared to untreated cells, respectively) (Figure 1.8 G).

ICD induction was also investigated after Jurkat cell treatment with WDA and WFA, used at the concentration detected in the WSDE at 0.40 mg/mL, alone or in combination for 24 h. No treatment caused any statistically significant DAMP's trafficking (Figure 1.8 D-F), suggesting that the intrinsic complexity of the extract in its entirety is the trigger that make ICD possible.
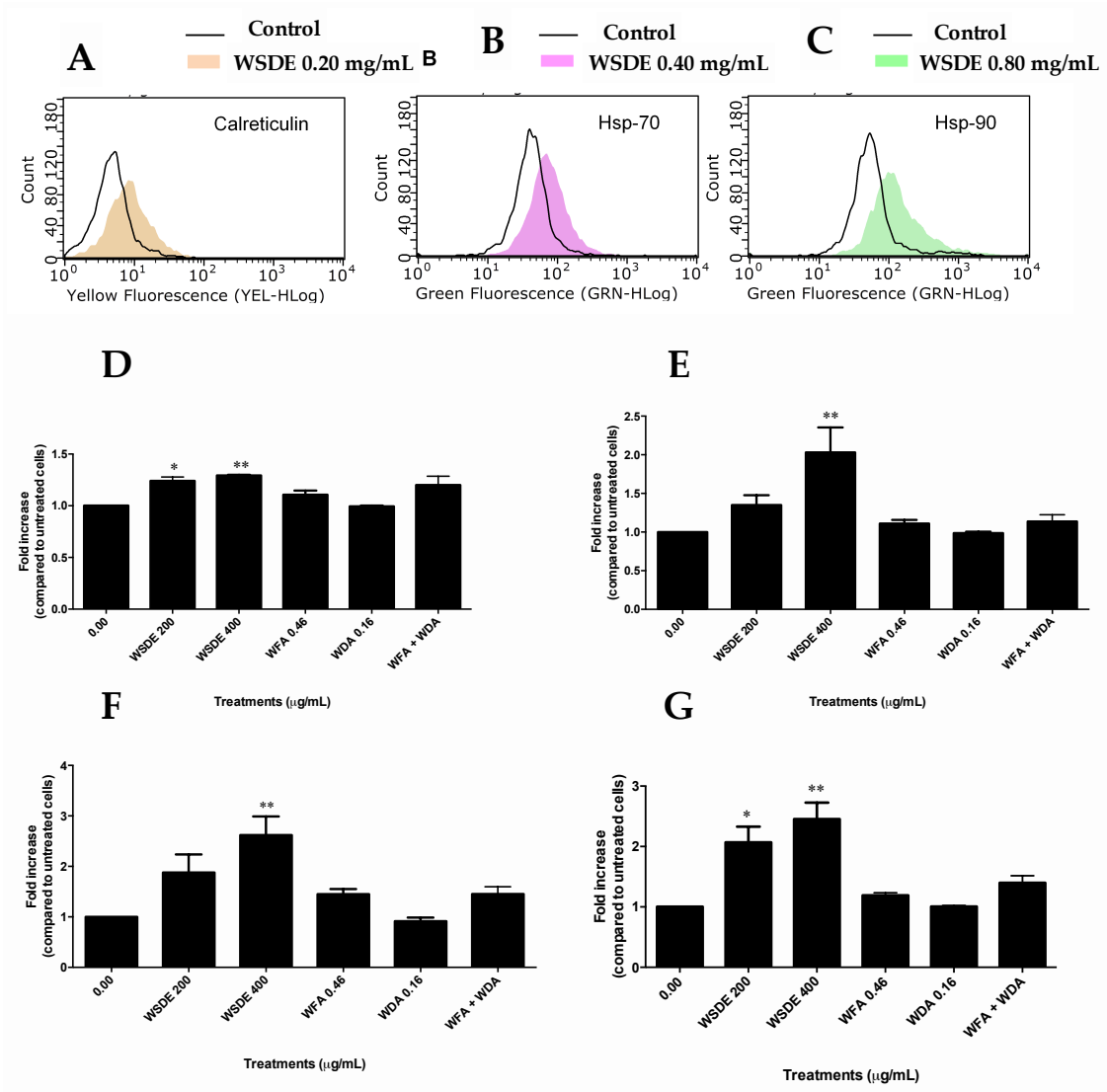
Figure 1.8 Fluorescence hystograms of immunolabeled calreticulin (A), HSP70 (B) and HSP90 (C) and modulation of the expression of calreticulin (D), HSP70 (E), HSP90 (F) and of ATP release (G) after treatment with WE, WFA, WDA or WFA plus WDA. Histograms are representatives of three independent experiments. * $P < 0.05$, and ** $P < 0.01$ *versus* untreated cells.

1.3.6. WSDE Induces DNA Damage

To explore more deeply the promising pharmacological profile of WSDE, we took the first step to assess its toxicological profile through the evaluation of the genotoxic potential. Jurkat cells were treated with increasing

concentration of WSDE for 6 h, and then histone H2A.x phosphorylation was analyzed. H2A.X phosphorylation at Ser 139 represents a sensitive marker for DNA single strand damage [83]. WSDE induced a dose-dependent increase in H2A.X phosphorylation, which was 8 times higher than untreated cells at the highest tested concentration (0.80 mg/mL). This increase was similar to the phosphorylation induced by etoposide 10 μM, used as positive control (Figure 1.9). However, even if γ-H2A.x is an index of the ability of a compound to interact with DNA, the lesion recorded is pre-mutational, thus reparable *per se*. Further studies will be necessary to determine if the damage is repaired or fixed, estimating the actual mutagenic potential of WSDE. In contrast with our data, plenty of studies showed WFA chemopreventive activity. For instance, it was demonstrated its ability to provide protection against the 7,12-dimethylbenz(a)anthracene-induced genotoxicity [84, 85]. The different genotoxic profile of WSDE and WFA could be explained by the so-called "matrix effects". Indeed, it could happen that genotoxic studies on complex products of natural origin are performed on single phytochemicals rather than on the product in its complexity. The matrix effect can cause an incomplete release of a key constituent from the vegetal carrier or modulate its bioavailability. This means that the use of toxicity data concerning the pure phytochemical are unsuitable for assessing the risk derived from the use of the same phytochemical within the complex vegetal matrix [86].
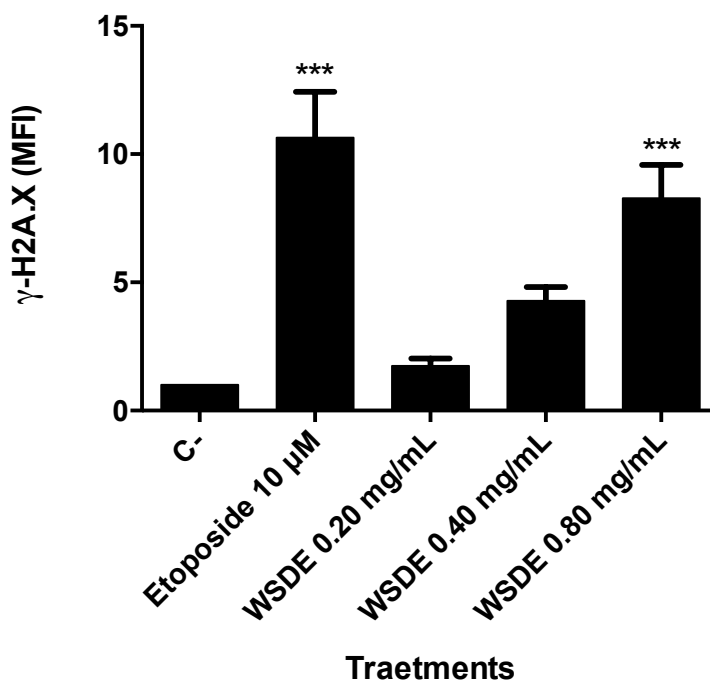
Figure 1.9 Relative expression of phosphorylated H2A.X (γ-H2A.X) induced by WSDE in Jurkat cells after 6 h of treatment. Etoposide (10 μM) was used as positive control. *** P < 0.001 *versus* untreated cells.

1.4. Conclusions

My first year of PhD ended with the characterization of the pharmacotoxicological profile of WSDE. I demonstrated the WSDE antitumor potential, which was exerted through a cytostatic activity and a ROS- and, to a lesser extent, ER-mediated apoptosis. I proved that, most likely, the actual reactive specie, to which the apoptotic effect is ascribed, is the hydroxyl radical, but I was not able to exactly localize oxidative stress inside the cell, whether data suggest an alternative region than mitochondria. Indeed, it would be easy to speculate that ROS could localize in the ER, since cytosolic [Ca^{2+}] levels are increased after the treatment of Jurkat cells with WSDE and at the same time ER stress was registered. This conjecture would also agree with the demonstrated capability of WSDE to mobilize DAMP's trafficking in Jurkat

cells. The most promising element is that all four DAMPs have been activated by WSDE treatment after 24 h of treatments and that, as explained above, the immunogenicity of a dying cell is directly proportional to the intensity of DAMPs' emission. Of note, DAMPs mobilization has been registered for the sum of apoptotic and necrotic cells, without any distinction, since at the time of the execution of the experiments, the debate about the capability of necrotic cells to induce ICD was ongoing. Since *in vivo* vaccination is not possible in human models, translational studies on mouse models could help to estimate the real immunogenic properties of WSDE. However, these latter considerations do not change the very promising profile of the analyzed extract that still represents an interesting candidate for further ICD studies.

To conclude, it's worthy to remind that WS extracts and WS's phytomarkers are currently available as dietary supplements to treat different disorders, including naturopathic care for infertility [87], anxiety [88], and osteoarthritis [89]. Hence, genotoxicity should be carefully taken into account for an accurate evaluation of the risk-benefit profile. It is important to emphasize once again that the H2A.X phosphorylation test used in our study detects premutational and thus reparable DNA lesions. For this reason, further experiments are needed to define the frank mutagenic effect of the lesions caused by WSDE and to directly relate the DNA damage to the potential mutagenic effect.

1.5. Material And Methods

1.5.1. Extract preparation

WE roots were collected during summer (balsamic period) and authenticated by Dr. Paolo Scartezzini, Maharishi Ayurveda Product Ltd., Noida, India. The quality control was performed by Vedic Herbs s.r.l. (Caldiero, VR, Italy), which gifted us with a sample of root powder

(voucher #12/11). The extract was prepared by resuspending 10 g of *Withania* root powder with 100 mL of DMSO or ethanol. The suspension was vortexed for 15 minutes at room temperature and centrifuged at 4000 rpm for 5 minutes to discard any insoluble part. The experiments and the HPLC analysis were performed using the DMSO stock solution of 100 mg/mL.

1.5.2. HPLC Analysis and Validation

WSDE extract was subjected to RP-HPLC-DAD analysis to identify and quantify the main phytomarkers. The reference compounds WFA, WDA, WDB, and withanone were purchased from Extrasynthese, Lyon, France. WFA and WDA were used as external standards to set up and calculate appropriate calibration curves. The analyses were performed using a Jasco modular HPLC (model PU 2089, Jasco Corporation) coupled to a diode array apparatus (MD 2010 Plus) linked to an injection valve with a 20 µL sampler loop. The column used was a Kinetex XB-C18 (5 µm, 15 cmx0.46 cm) with a flow rate of 0.6 mL/minutes. The analyses were performed at 25 °C with mobile phase and gradient chosen according to literature [90]. Following chromatogram recording, sample peaks were identified by comparing their ultraviolet (UV) spectra and retention time with those of the pure standards. Dedicated Jasco software (PDA version 1.5, Jasco Corporation, 2004) was used to calculate peak area by integration. The individual stock solutions of each phytomarkers were prepared in ethanol or acetonitrile. The calibration curves of the considered compounds were prepared within different range: 500–50 µg/mL for WFA, and 100–10 µg/mL for WDA. Each calibration solution was injected into HPLC in triplicate. The calibration graphs were obtained by the regression analysis of the peak area of the analytes *versus* the related concentrations. The analysis of the extract was performed under the same experimental conditions. The obtained calibration graphs allowed the determination of the concentration of

the phytomarkers inside the extract.

LOD and LOQ were calculated following the approach based on the standard deviation of the response and the slope for WFA and WDA, on signal and noise ratio for WDB and withanone, as presented in the "Note for guidance on validation of analytical procedures: text and methodology", European Medicine Agency ICH Topic Q2 (R1). The accuracy was reported as percent of recovery and was estimated by adding known amount of analyte in the studied sample.

1.5.3. Cell Cultures and Treatments

Acute human T-lymphocytes leukemia cells (Jurkat) were provided from LGC standards. Cells were grown in suspension in Roswell Park Memorial Institute (RPMI) 1640 supplemented with 10% heat-inactivated bovine serum, 1% penicillin/streptomycin solution, and 1% L-glutamine solution (all obtained from Biochrom, Merck Millipore). Cells were incubated at 37 ℃ with 5% CO_2. To maintain exponential growth, the cultures were diluted to never exceed the maximum suggested density of $3x10^6$ cells/mL.

Jurkat cells at $1.5x10^6$ cells/mL density were treated with increasing concentrations of WSDE (0.0–1.6 mg/mL) for 1, 3, 6 or 24 h, according to the experimental requirements, or with WFA, WDA or WFA plus WDA for 24 h. WFA and WDA were tested at the concentrations found in the WSDE extract at 0.2, 0.4 and 0.8 mg/mL: 0.23–0.92 μg/mL for WFA; 0.08–0.32 μg/mL for WDA. Etoposide 10 μM and hydrogen peroxide 0.1 mM were used as positive controls. For oxidative and ER stress-related experiments, Jurkat cells were pretreated with TUDCA 1 mM (Sigma Aldrich), NAC 4 mM or TUDCA and NAC for 1 h and then co-incubated with increasing concentrations of WSDE.

1.5.4. Analysis Of Cell Viability And Induction Of Apoptosis

To determine cell viability of Jurkat cells, Guava ViaCount Reagent (Merck Millipore) was used according to manufacturer's instructions. Briefly, cells were appropriately diluted with the reagent containing 7-amino-actinomycin D (7-AAD) and incubated at room temperature in the dark for 5 minutes before detection with flow cytometer. Furthermore, to discriminate between necrotic and apoptotic events, Guava Nexin Reagent (Merck Millipore) was used. Through the use of 7-AAD and annexin V-phycoerythrin, the assay allows the discrimination of apoptotic and necrotic events. Cells were incubated with the reagent for 20 min at room temperature in the dark and then analyzed *via* flow cytometry. IC_{50} was calculated by interpolation from non-linear regression and log of concentration–response curve. Concentrations close to IC_{50} were used in the subsequent experiments.

1.5.5. Cell-Cycle Analysis

After treatment with WSDE for 24 h, cells were fixed with 70% ice-cold ethanol and, after washing, suspended in 200 μL of Guava Cell Cycle Reagent (Merck Millipore), containing propidium iodide. At the end of incubation at room temperature for 30 minutes in the dark, samples were analyzed *via* flow cytometry.

1.5.6. Measurement of $[Ca2+]_i$

After WSDE treatment for 6 or 24 h, $[Ca^{2+}]_i$ was analyzed by using Fura RedTM, AM (Thermo Fisher Scientific), according to manufacturer's instructions. Briefly, after treatment, cells were incubated with the dye that freely permeates the cytoplasmic membrane but, once inside the cells, is hydrolyzed by the intracellular esterases and trapped into the cells. The fluorescence of this molecule is enhanced once it binds Ca^{2+}. The use of the

lowest concentration of Fura Red is recommended. Following this experimental phase, the concentration of 1 μM was adopted. To detect intracellular calcium levels, Jurkat cells were incubated at 37 °C for 30 minutes in PBS without calcium and magnesium. This buffer condition allows detecting the intracellular calcium stores and excluding the secondary increase in [Ca2+]$_i$ due to Ca^{2+} entry [91]. Moreover, the removal of external Ca^{2+} reduces the non-specific fluctuations in [Ca^{2+}]$_i$ normally observed during the first 20–30 s of sample acquisition *via* flow cytometry. Results are expressed as MFI.

1.5.7. Detection of ROS Levels

ROS levels were determined after 1, 3, 6, 18 or 24 h of WSDE extract, alone or after a pretreatment with NAC 4 mM treatment by using the probe DHR 10 μM [92] or 2′,7′-dichlorofluorescin diacetate (DCFDA), which was added during the last 20 minutes of incubation. Hydrogen peroxide was used as positive control. After three washing in PBS, cellular fluorescence was imaged using a Leica DMLB/DFC300F fluorescence microscope (Leica Microsystems) equipped with an Olympus ColorviewIIIu CCD camera (Polyphoto). Fluorescence images (100 cells *per* sample from randomly selected fields) were digitally acquired and processed for fluorescence determination at the single cell level on a personal computer using the public domain program, Image J. Mean fluorescence values were determined by averaging the fluorescence of at least 100 cells/treatment condition/experiment.

1.5.8. Analysis of Calreticulin, HSP70 And HSP90 Expression, and ATP Release

After 6 or 24 h of treatment, cells were washed and incubated with phycoerythrin-labeled calreticulin antibody (1:100, Abcam). To analyze HSP70 and HSP90 expression, cells were incubated with an anti-HSP70 or anti-HSP90

antibody (1:100, Abcam, for both antibodies) and, after washing, incubated with fluorescein isothyocianate-labeled secondary antibody (1:100, Sigma, Merck Millipore) MFI was detected *via* flow cytometry and compared to the untreated cells.

The kit ATPLiteTM 1step (Perkin Elmer, Waltham, MA, USA) was used for the detection of ATP extracellular concentration. Jurkat cells were seeded and treated with WSDE in Hank's Balanced Salt Solution (HBSS) or complete medium for 6 and 24 h, respectively. At the end of incubation, supernatants were collected and treated with 100 μL of ATPLite 1step reagent containing luciferase and D-luciferin. After shaking for 2 minutes at 700 rpm using the orbital microplate shaker 711/+ (Asal srl), luminescence of the samples was measured in a 96-well black plate using the microplate reader Victor X3 (Perkin Elmer).

1.5.9. DNA Damage Analysis

Phosphorylation of histone γ-H2A.X was used as marker of WSDE genotoxic potential. After 6 h of treatment with WSDE, cells were fixed, permeabilized and incubated for 30 minutes in the dark at room temperature with an anti- γ-H2A.X-Alexa Fluor® antibody (Merck Millipore). Etoposide 10 μM was used as positive control. Samples were analyzed via flow cytometry.

1.5.10. Flow Cytometry

EasyCyte 5HT (Merck Millipore) were used to perform all flow cytometric analyses, with the exception of the measurements of $[Ca2+]i$ performed by using a FACSCanto II (BD Bioscience, Franklin Lakes, NJ, USA). For each sample, at least 10000 events were evaluated.

1.5.11. Statistical Analysis

All results are expressed as mean ± SEM of at least three independent experiments. Differences between treatments were assessed by t test or one-way ANOVA and Dunnet or Bonferroni was used as post-tests. All statistical analyses were performed using GraphPad InStat 5.0 or 6.0 version (GraphPad Prism, San Diego, CA, USA, 2007). $P < 0.05$ was considered significant.

CHAPTER 2. MG28

2.1. Introduction

Isothiocyanates (ITCs) are very reactive sulfur-containing compounds (Figure 2.1). This ITC chemical moiety is stabilized by resonance in a way that sulfur and nitrogen attract all the electrons. In this way the electrophilic central carbon is the perfect target for nucleophilic compounds, such as thiols, amino groups, and hydroxide ions [93], all chemical groups eventually occurring in many proteins or intracellular structures.

$$R - N = C = S$$

Figure 2.1 Chemical structure of an isothiocyanate

Brassicaceae (Cruciferae) family, which includes Brussels sprouts, broccoli, cauliflowers or kale cabbages, is the richest source of ITCs, in nature. ITCs are molecules stored in the plants in the form of precursors, the glucosinolates. Myrosinases catalyze the hydrolysis of glucosinolates into ITCs. These enzymes are kept close to glucosinolates, but in separated compartments and allow the conversion of glucosinolates only when plant's tissues are ruptured and the two entities come into contact, as after insect attacks, chewing, chopping or cooking preparation. If this is not enough, in mammals, myrosinases springing from the gastrointestinal tract bacteria complete the conversion [93].

Many studies related the food intake of *brassicaceae*, against different types of cancer [94]. These effects are imputable to their content of ITCs. Some ITCs, such as sulforaphane (SFN), phenethyl isothiocyanate (PEITC), and

benzyl isothiocyanate (BITC), are highly efficient chemopreventive and antitumor agents [95]. ITCs' antitumor potential relies on their ability to induce apoptosis, cell-cycle arrest, angiogenesis and histone deacetylation inhibition, and modulating many other pathways [93]. Moreover, oxidative stress is often the key of their mechanism of action. For instance, PEITC provoked apoptosis of myeloblastic (ML-1) and promyelocyte leukemia (HL-60) cells through glutathione (GSH) depletion and the consequent increase of oxidative stress, while SFN caused ROS-mediated apoptosis in U937 promonocytic leukemia cells [96], glioblastoma cells, [97], and in PC-3 and DU145 human prostate cancer cells [98].

Despite the promising characteristics of ITCs, their aptitude to exert ICD has never been investigated.

Bearing in mind 1) that the two crucial events that trigger ICD are oxidative and ER stress, and 2) the interesting antitumor potential and reactivity of the chemical ITCs moiety, and 3) that type II ICD inducers are able to exert a more efficient immunogenic response than type I [48], we designed an ITC derivative which could reach directly the ER and trigger ROS-mediated apoptosis together with ER stress. Dott. Andrea Milelli from the University of Bologna, Department for Life Quality Studies, synthesized and provided us with MG28. MG28 is a molecule composed by a renowned ER carrier [99] bonded to the ITC moiety through an aliphatic chain (Figure 2.2). The carrier is a fluorinated hydrophobic rhodol analogue that has intrinsic green fluorescence.
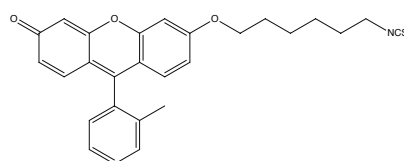
Figure 2.2 Chemical structure of MG28

2.2. Aim of the study

During the second year of PhD, my research aimed at drawing the pharmacological profile of MG28 with a particular focus on those characteristics that make it a candidate for ICD studies. The project took place in two phases. During the first phase, preliminary studies were carried out to assess the antitumor potential of MG28 in terms of cytotoxicity, apoptosis studies and oxidative profile on a human cell line of leukemia (Jurkat), while in the second phase the results obtained has been translated on a murine cell line of colon cancer (CT26) in order to pave the way for potential *in vivo* studies in syngeneic mice. The latter part of my research was held at the Cell Research and Therapy Laboratory of Cellular Medicine, Department of Cellular and Molecular Medicine of the Catholic University of Leuven, under the supervision of Prof. Agostinis and Dr. Abhishek Garg.

2.3. Results and Discussion

2.3.1. MG28 has Intrinsic Fluorescence

In order to draft MG28 profile, its fluorescence *spectrum* was recorded (Figure 2.3). At any wavelength it was excited, the maximum emission was reached at 518 nm. However, MG28 emission covers a broad range of wavelengths, which prominently limited the use of all those techniques that involves the use of fluorescent probes, such as flowcytometry or microscopy studies.
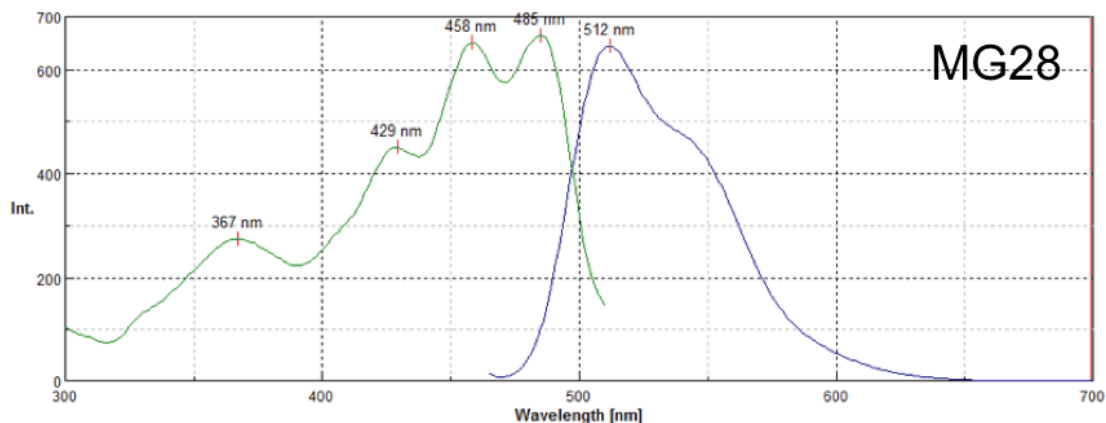
Figure 2.3 Excitation (green line) and emission (blue line) spectrum of an MG28 solution 1.33 μM in methanol prepared from a stock solution 4.00 mM in DMSO.

2.3.2. MG28 Reaches the ER

To make sure that MG28 reached the ER, localization studies were made. Since the thin layer of cytoplasm of Jurkat cells made the subcellular localization of MG28 problematic, this model was replaced using the same cell line utilized by Hakamata et al. in the paper where the ER carrier *per se* was described: HeLa cells [99]. HeLa cells were transfected with the red fluorescent protein (RFP) version of the ER resident CLR and treated with a low concentration of MG28. After 6 h of treatment, cells were fixed and analyzed (Figure 2.4). The right image of Figure 3.4 shows the merged version of the green fluorescence of MG28 and the red one of RFP and confirms the localization at ER. However the green fluorescence of MG28 is diffused within the cell, suggesting the non-specific localization of the studied ITC derivative. The high reactivity of the ITC moiety could be responsible for the dissemination of the molecule. In fact, the amino groups or thiols of proteins and molecules inside the cell could attract the electrophilic carbon of the ITC, and hamper MG28 localization in the ER.
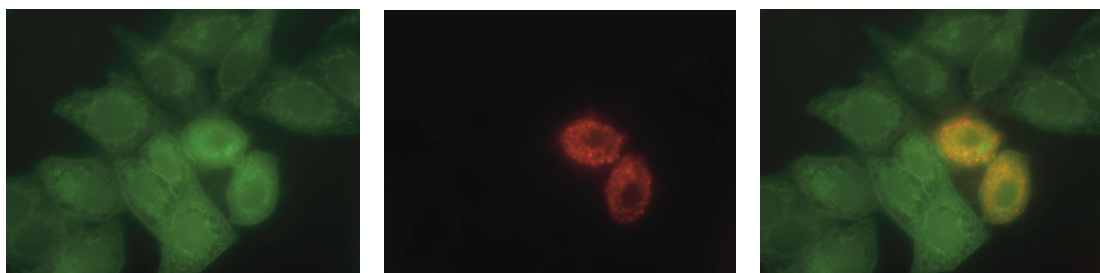
Figure 2.4 Microscopic analysis of HeLa cells transfected with red fluorescent protein (RFP)-calreticulin (ER localization) and treated with subtoxic concentration of MG28. Representative co-localization experiment: the fluorescence images for MG28 (left) and RFP (middle) were taken and merged (right). The merged image shows MG28 localization at ER in a non-specific way.

2.3.3. MG28 is Cytotoxic for Both Jurkat and CT26 cell lines

After 24 h treatment, MG28 induced a concentration-dependent decrease in cell viability in both human and murine cell lines. On Jurkat cells, MG28 cytotoxic activity was significant starting from 2 μM (86.9% of viable cell). At 4 μM the cell viability was 65.5% and reached 13.6% at 16 μM (Figure 2.5 A). The IC_{50} obtained from these results was 5.85 μM. The IC_{50} obtained testing MG28 on CT26 cells was 7.80 μM. In the latter case the effect of MG28 treatments started to be significant at 5.0 μM concentration (16,71% of dead cells). The percentage of dead cells was 40.68 and 31.30 at 7.5 and 10 μM, respectively (Figure 2.5 B). Since the two cell lines differ from tumor type and host, the slight difference between the two IC_{50} is coherent and acceptable. Concentrations around the respective IC_{50} were chosen for the further experiments.

Additionally, to exclude that the cytotoxicity of MG28 was driven by the ER carrier instead of the ITC moiety, Jurkat cells were treated with the only carrier, MG27 (Figure 2.6 A). The carrier didn't exert any significant decrease

in cell viability until 32 μM treatment (Figure 2.6 B), highlighting the crucial role of the ITC in the MG28 antitumor activity.

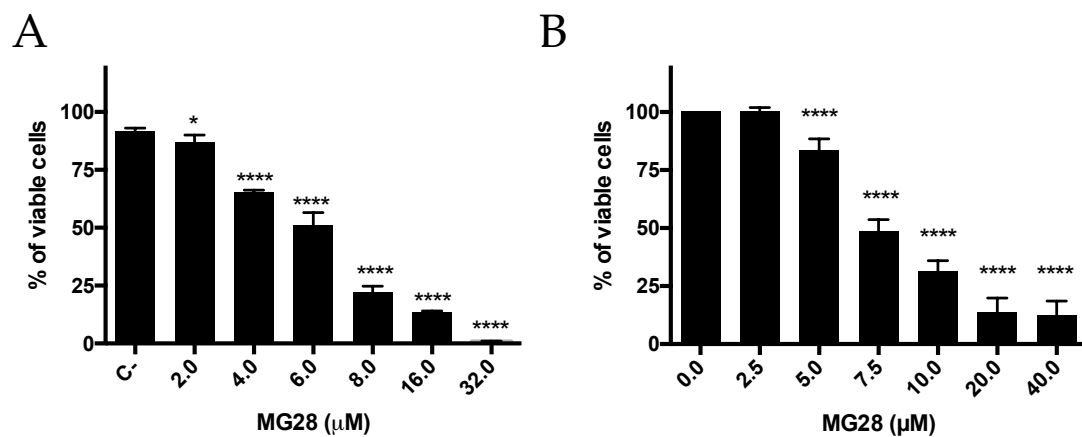Figure 2.5 Percentage of viable Jurkat (A) or CT26 (B) cells after 24 h treatment with increasing concentration of MG28. *$P < 0.05$; ****$P < 0.0001$.
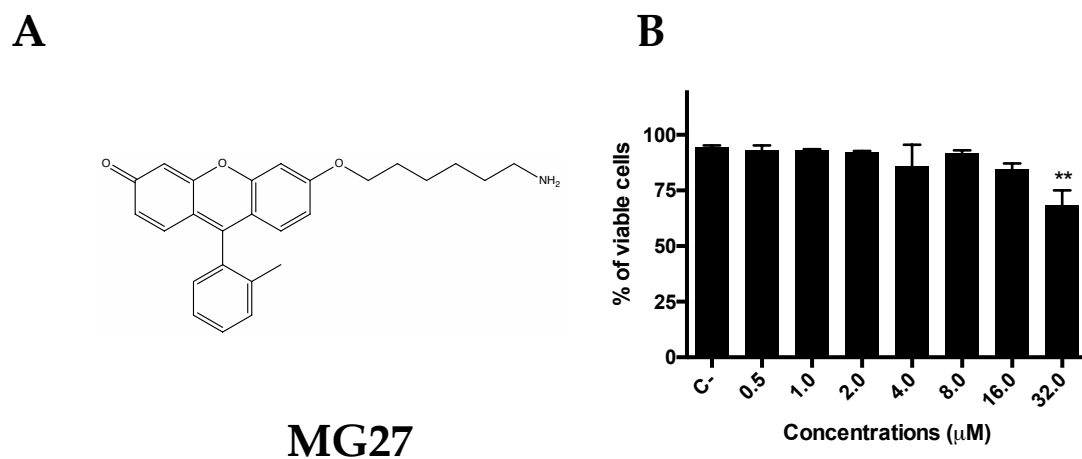

Figure 2.6 MG27 chemical structure (A); Percentage of viable Jurkat cells after 24 h treatment with increasing concentration of MG27 (B). **$P < 0.01$.

2.3.4. MG28 Induces Apoptosis Through both Intrinsic and Extrinsic Pathway in Jurkat Cells

To dissect the mechanism of action of MG28, apoptosis studies have been performed. Twenty-four h of treatments at 6 and 8 μM resulted in 13.81 and 56.33% of apoptotic Jurkat cells, respectively (Figure 2.7 A). Moreover, MG28 6 μM stimulated caspase-3 activity 6.89 times more than untreated cells (Figura 2.7 B), confirming the involvement of apoptosis in MG28 antitumor potential. At this point we analyzed which apoptotic pathway was involved in the proapoptotic potential of MG28. Cell-surface death receptors activate the extrinsic pathway of apoptosis. Upon activation they cluster and form the death-inducing-signaling complex that in turn provokes the cleavage (*i.e* activation) of procaspases 8, 10 or both, which stimulate the effector caspase 3. The intrinsic pathway depends on the mitochondria and involves the mitochondria outer membrane permeabilization (MOMP). MOMP provokes the release of proteins into the cytoplasm. Among these proteins, cytochrome c is crucial to assemble the apoptosome, the structure that in turn activates caspase 9. Then, caspase 9 triggers the effector caspases 3 and 7 that lead to apoptosis [100]. Therefore, MG28's ability to modulate caspase 8 activity and alter mitochondrial potential was evaluated. At 6 μM, MG28 increased 2.22 times the activity of caspase 8 compared to untreated cells (Figure 2.7 C) and decreased the mitochondrial potential of 32.96% of cells *versus* 5.32% of the untreated cells (Figure 2.7 D). Thus, MG28 triggers both apoptotic pathways. This evidence is very interesting since, very often, chemotherapeutic drugs elicit apoptosis through the only intrinsic pathway [101]. Thus, on one hand the double activation could bring to a more efficient apoptotic induction and on the other hand it could restore sensitivity in resistant tumors, in the case of mutation and blockage of one of the two pathways [101].
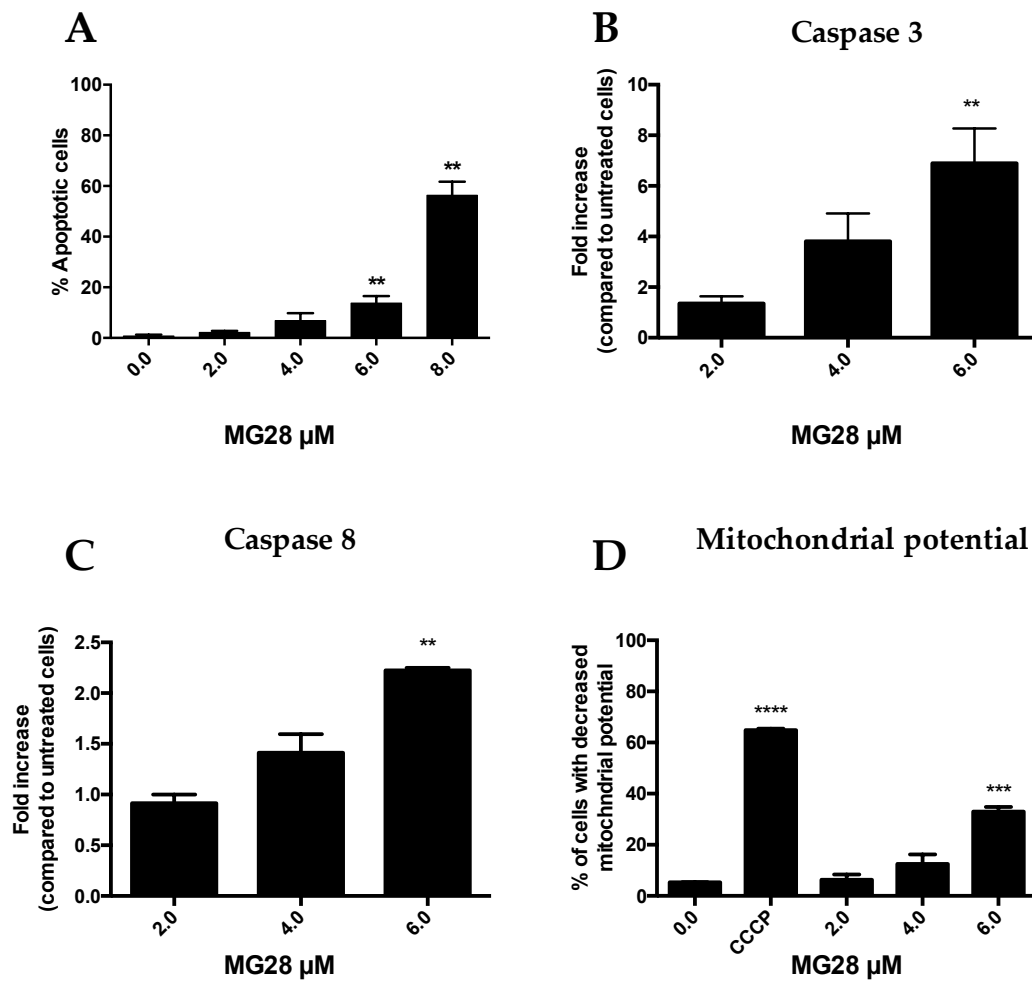
Figure 2.7 Percentage of apoptotic Jurkat cells after 24 h treatment with increasing concentration of MG28. Apoptosis was assessed by Fast Halo assay (A) Caspase 3 (B) and Caspase 8 (C) activity was evaluated and compared to untreated cells after Jurkat treatment with increasing concentration of MG28 through colorimetric assay. Fraction of Jurkat cells with decreased mitochondrial potential after MG28 treatment assayed through flow cytometry analysis after incubation with the fluorescsnt dye cyanine dye DiIC1(5) (D). ** $P < 0.01$; *** $P < 0.001$; **** $P < 0.0001$.

2.3.5. MG28 Does not Trigger Apoptosis nor ER Stress in CT26

Mixed results were obtained for the apoptotic potential of MG28 on CT26 cells. To first understand if this form of RCD was involved in MG28

mechanism of action, we decided to block the activity of the apoptosis mediators, caspases. Thus, we pretreated and co-incubated MG28-treated CT26 cells with the pan caspase inhibitor Zvad-fmk. After 24 h of 7.5 and 15 μM, the blockage of apoptosis resulted in an increase in cell viability of 1.69 and 4.19 times, respectively, compared to only MG28-treated cells (data not shown). However, the protective effect of Zvad-fmk didn't completely restore cell viability, implying a secondary mechanism of action involved in MG28 *modus operandi*. To confirm these data, apoptosis was directly assessed through flow cytometry analysis, operating the Annexin V/dead cells assay. Briefly, one characteristic event of early apoptotic cells is the early translocation of phosphatidylserine (PS) from the inner to the outer side of the plasma membrane and its exposure to the external cellular environment. *In vivo*, PS acts as a marker of recognition for macrophages, while *in vitro* represents a useful marker of apoptosis. Annexin V is a Ca^{2+}-dependent phospholipid-binding protein with high affinity for PS. Annexin V labeled with a fluorophore identifies apoptotic cells by binding to PS exposed on the outer leaflet. Then, adding a viability dye, which discriminates viable and dead cells on the basis of membrane permeability, makes the discrimination among four different cellular populations: viable (Annexin V negative/viability dye negative), early apoptotic (Annexin V positive/viability dye negative), late apoptotic, secondary necrotic or necroptotic (Annexin V positive/viability dye positive) or primary necrotic (Annexin V negative/viability dye positive) cells [102-104]. Flow cytometry analysis showed that after 24 h MG28 induced necrosis (Figure 2.8 A), with no early apoptosis detected. In particular, data suggested that primary necrosis is the main pathway through which MG28 exerts cytotoxicity.

Since these results were in contrast with previous data, we expolred if, at least in part, apoptosis was involved in MG28 antitumor potential on CT26.

Thus, during the following steps MG28's ability to induce caspase 3 and its substrate poli ADP-riboso polimerase (PARP) cleavage was assessed [105]. A slight and non-significant increase of cleaved PARP was recorded after 24 h treatment of CT26 (Figure 2.8 B), while no caspase 3 activation was detected (Figure 2.8 B).

These data, taken together, suggest that MG28 antitumor potential on CT26 does not rely on apoptosis. The protective effect of caspases inhibition, plus the slight activation of PARP can together indicate that apoptosis is one event eventually implied in MG28 activity, whereas its entity is not enough to be measured by the annexin V assay, nor to provoke a detectable amount of cleaved caspase 3.
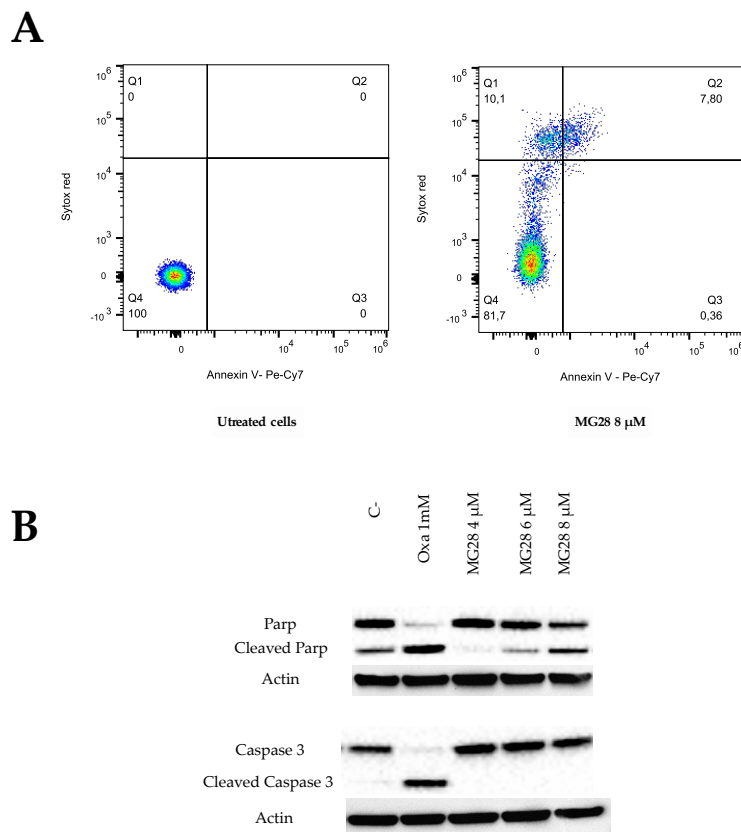
Figure 2.8 Representative dot plots of annexinV-PE-Cy7/Sytox Red Dead Cell Stain cell death assay of CT26 cells 24 h after treatment with MG28 8 μM (A). Representative blots of at least three independent experiments analysis for PARP and caspase 3 (total and cleaved) protein levels in MG28-treated CT26 cells, oxaliplatin was used as positive control (B).

Since the aim of the study was to assess MG28's ability to trigger ICD and ICD doesn't rely exclusively on apoptosis, its ability to trigger Perk-mediated ER stress was investigated. A PERK knockout CT26 cell line was used. We tested MG28 cytotoxic activity on the PERK-knockout cell line and compared the effects obtained on the wild type cells. No difference was recorded (data not shown), suggesting that the antitumor potential of MG28 on the murine cell line does not involve PERK-mediated ER stress.

The very moderate activity of MG28 on CT26 cells provides input into the study of MG28 on Jurkat cells.

Furthermore, the different antitumor potential of M28 on Jurkat and CT26 cells cannot be considered completely surprising. More than once, drugs, which have proven to be effective on human models, were not active when tested on mice, and *vice versa* [106]. The differences between human or animal activity to a same drug can be attributed to the different evolutionary and developmental intrinsic biology that in turn translates, for instance, into dissimilarities in gene regulation and expression or epigenetics discrepancies. Moreover, the two cellular models represent two different types of neoplasms (leukemia and colon cancer), and specific cancer-related mutations can significantly alter the response to drugs [107].

2.3.6. Oxidative Profile of MG28 on Jurkat Cells

The study progressed with the evaluation of MG28's ability to prompt oxidative stress in Jurkat cells. Since emission *spectra* of DCFDA or DHR, the two most common probes used to assess intracellular ROS levels, overlap with the emission of MG28, oxidative stress was evaluated through an indirect way. Based on the major role of glutathione (GSH) as crucial cellular antioxidant, its content after MG28 treatments was recorded. After 1 and 3 h, all tested

61

concentrations induced a decrease in GSH levels compared to untreated cells. However, following the initial drop, GSH content increased in a time-dependent manner (Figure 2.9 A). After 6 h at 2 μM and 24 h for all the other tested concentrations, GSH content exceeded the one recorded for untreated cells. The initial lower intracellular levels of GSH could be the consequence of increased ROS levels or the direct interaction between the ITC moiety and the thiol group of GSH, which in turn would be depleted. Indeed, the conjugation with GSH is the main mechanism through which ITCs are removed from cells [108]. For example, in HL60 and ML1 leukemia cells, PEITC formed GSH *S*-(*N*-phenethylthiocarbamoyl)-GSH that was then exported from cells [109]. Thus, to understand the role of GSH in MG28 cytotoxicity and how the low GSH levels recorded after MG28 treatment are linked to ROS, we evaluated MG28 cytotoxic potential on Jurkat cells after pretreatments with the antioxidant and GSH precursor NAC, or with the GSH synthesis inhibitor buthionine sulfoximine (BSO). Of note, we avoided the simultaneous treatment of Jurkat cell with NAC and MG28 to prevent the direct interaction and subsequent quenching of MG28. Interestingly, NAC pretreatment didn't affect MG28 activity, while it recovered Jurkat viability when treated with H_2O_2, used as positive control (data not shown). On the contrary, BSO pretreatment provoked a more cytotoxic effect on Jurkat cells than MG28 alone (Figure 2.9 B). Taken together, these results demonstrated that the antitumor potential of MG28 does not rely on oxidative stress, since the ROS quencher NAC didn't exert any protection, but demonstrated the pivotal role of GSH. Indeed, depletion of GSH significantly entails MG28 cytotoxicity. Taken into consideration both the effect of NAC and BSO, the most probable hypothesis is that GSH directly binds MG28 in order to favor its externalization. This would explain the initial decrease in free GSH after MG28 treatment and the higher toxicity when GSH is absent. Moreover, the subsequent increase in GSH

content could be the effect of the stimulation of the nuclear factor (erythroid-derived-2)-like 2 (Nrf2). Nrf2 is a transcription factor playing a major role in controlling oxidative status through the modulation of the expression of many antioxidant proteins, such as GSH. Indeed, the same GSH trend induced by MG28 was observed in SFN-treated mouse embryonic fibroblasts (MEFs). There, following a GSH initial acute depletion (4 h of exposure to SFN), after 18 h GSH increased in a Nrf2-dependent way [110].
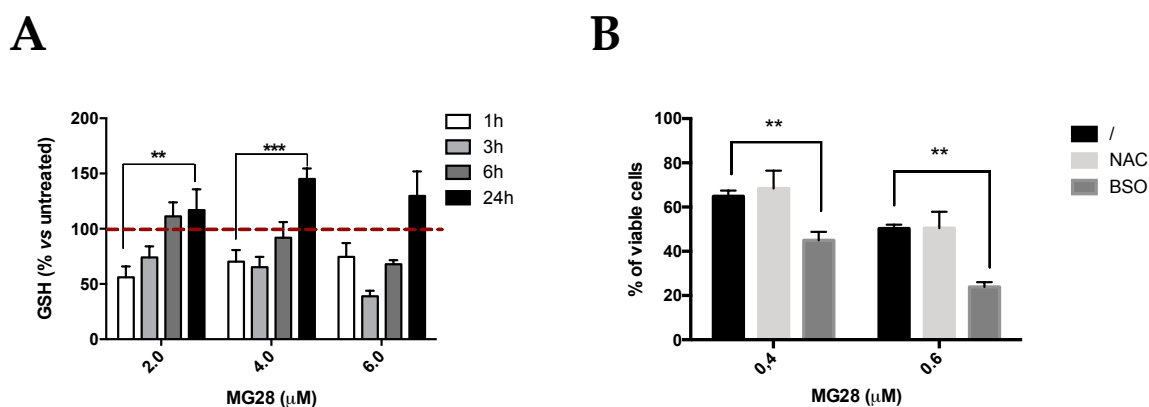
Figure 2.9 GSH content expressed as percentage compared to untreated cells, after 1, 3, 6 or 24 h treatments (A); percentage of viable cells of MG28-treated Jurkat cells alone or after 24 h pretreatment with NAC 5mM or BSO 0.2 mM (B). ** $P < 0.01$; *** $P < 0.001$.

On the whole, our results taken together draw an interesting picture of the antileukemic activity of MG28. However the lack of the ability to trigger oxidative stress does not allow to keep on investigating its ICD potential.

2.4.   Conclusions

MG28 is an ITC derivative constituted by an ER carrier linked to the active side through an aliphatic chain. It was synthesized *ad hoc* with the precise aim to bring an active chemical moiety to the ER, and to concurrently elicit oxidative and ER stress. In this way a type II of ICD inducer would have been created. So far only Hyp-PDT is *a bona fide* type II ICD inducer and

still the most reliant and effective immunogenic anticancer therapy promoter.

Firstly we ensured that MG28 would reach the ER, and thanks to its green intrinsic fluorescence it was not hard to find it out. It does reach the ER, but its localization is not selective and it clearly diffuses all over the cell.

We tested MG28 antitumor activity on two different cell lines, a human leukemia cell line (Jurkat) and a murine colon cancer cell line (CT26). The latter model was chosen to pave the way to *in vivo* syngeneic studies. However, in this cell line MG28 did not exert the expected effects. It induced a cytotoxic activity attributable more to necrosis than to apoptosis and did not produce PERK-mediated ER stress. Thus, the research focused on the leukemia model. In this case, the pharmacologic profile of MG28 was very promising. It induced apoptosis at μM range concentrations, triggering both intrinsic and extrinsic pathways, thus doubling the probability of success in apoptosis-resistant cancer cells. However, the oxidative profile of MG28 did not deserved further studies to assess its ability to trigger ICD. Indeed, its mechanism of action did not rely on ROS production, since the pretreatment with the ROS quencher NAC did not affect its antitumor potential. On the contrary, our data suggested that long-term treatments increase GSH intracellular contents, probably through Nrf2 activation.

Even if we expected different results, the inability of MG28 to trigger oxidative stress and its conjugation and quenching with the cysteine sulfhydryl group of GSH is a possibility. The chemopreventive properties of ITCs actually reside on the induction of phase II enzymes [111]. For example SFN, probably the most studied ITC, has the dualistic nature of chemopreventive promoter, thus showing antioxidant properties, and antitumor agent using ROS increased level as the engine which drives its activity [95], depending on the dose.

In conclusion, the antileukemic profile of MG28 is very interesting and

should be deeply unravel. However it does not endow the characteristics needed to trigger ICD and for this reason this project was suspended.

2.5. Material and Methods

2.5.1. Synthetic Compounds

MG27 and MG28 were provided by Dr. Andrea Milelli from the University of Bologna, Department for Life Quality Studies. MG28 is composed by an active ITC moiety linked to a renowned ER carrier through an aliphatic chain (Figure 2.2). MG27 represents the non-active part of MG28.

2.5.2. Cell Cultures and Treatments

Jurkat, CT26 and PERK$^{-/-}$ CT26 were cultured in RPMI 1640 (Sigma), while HeLa in Eagle's Minimum Essential Medium (EMEM). All media were completed with 1 mmol/L glutamine, penicillin–streptomycin (Sigma) and 10% FBS at 37 °C under 5% CO_2. Jurkat cells were obtained from the ATCC and always seeded at 1.5×10^6 cells/mL of complete medium. They were treated with MG27 (0 – 32 μM) or MG28 (0 – 32 μM) for the indicated time. With a density of $0.010 \times 10^6/0.33$ cm^2 of well surface, HeLa, CT26 or CT26 PERK$^{-/-}$ were seeded and treated with MG28 (0 – 40 μM) for the indicated time.

2.5.3. Localization Study

HeLa cells were transfected with CellLight® ER-RFP (Thermo Fisher Scientific) following manufacture's instruction. Then, cells were treated with MG28 1 μM for 6 h, fixed with paraformaldehyde 4% for 10 minutes, washed and observed by an Olympus FV1000 fluorescent microscope. The analysis was performed through the Image J software.

2.5.4. Analysis of Cell Viability

Cell viability was assessed after 24 h treatments. For Jurkat cells, analysis of cell death was performed with Trypan blue Exclusion Assay as described in Buytaert *et al* [112]. To assess MG28 oxidative profile, cells were pretreated for 24 h with NAC (Sigma Aldrich) 5 mM (GSH 150% *vs* Control) or BSO (Sigma Aldrich) 0.2 mM (GSH 20% *versus* Control).

Alternatively, to determine the amount of CT26 and PERK$^{-/-}$ CT26 cell death, intracellular alkaline esterase activity was measured through the 4-Methylumbelliferyl heptanoate (MUH) assay (SIGMA), according to manufacturer's instructions. Briefly, after 24 h treatment in 96-well plate, colon cancer cells were incubated with 0.01 mg/mL MUH in PBS for 20 minutes at 37°C. The fluorescence was measured with Flex Station (Molecular Devices) with excitation 355 nm, emission 460 nm and cut off value 455 nm. For caspases inhibition, cancer cells were preincubated for 2 h with zVAD-fmk (Bachem, 50 μM). Incubation with zVAD-fmk continued throughout the treatments.

2.5.5. Analysis of Apoptosis

To allow the detection of apoptosis in Jurkat cells, DNA double strand breaks (DSBs) were assessed through the Fast Halo Assay (FHA), carried out at non-denaturing pH conditions. Briefly, after the 24 h treatments, Jurkat cells were resuspended at 4.0×10^4/mL in ice-cold PBS containing 5 mM EDTA: 25 μL of this cell suspension was diluted with an equal volume of 1% low melting agarose in PBS and immediately sandwiched between an agarose-coated slide and a coverslip. After complete gelling on ice, the coverslips were removed and the slides were immersed in a lysis solution (0.15 M NaOH, 0.1 M NaH$_2$PO$_4$, 1 mM EDTA, Triton ×100 1% v/v, pH 10.1) for 10 minutes, incubated for further 15 minutes in PBS (pH 7.4) containing 0.1 mg/mL RNase (bovine

pancreas Type 1A); ethidium bromide was directly added to this solution during the last 5 minutes of incubation. The slides were then washed and destained for 5 minutes in distilled water and analyzed The ethidium bromide-labelled DNA was visualized using a Leica DMLB/DFC300F fluorescence microscope (Leica Microsystems) equipped with an Olympus Colorview IIIU CCD camera (Olympus Italia Srl) and the resulting images were digitally recorded on a PC and processed with an image analysis software (Scion Image, Scion Corporation). The amount of fragmented DNA diffusing out of the nuclear cage, *i.e.* the extent of strand scission, was quantified by calculating the nuclear diffusion factor (NSF), which represents the ratio between the total area of the halo and nucleus and that of the nucleus.

For CT26, apoptosis was assessed using the annexinV-PE-Cy7 (eBioscience)/SYTOX® Red Dead Cell Stain (Invitrogen). After 24 h treatments, cells were detached with Tryple (Thermo Fisher Scientific) and collected together with the respective treated medium, in order to recover also detached cells. Each sample was washed with PBS and with Annexin V - binding buffer (10 mM Hepes pH 7.4 , 140 mM NaCl), followed by resuspension in AnnexinV-PE-Cy7 (1/20 dilution in staining buffer) and Sytox red (1:1000 diluition in Annexin V - binding buffer). After 15 minutes incubation at room temperature, cell suspension was diluted with Annexin V-binding buffer and analysed on Attune Flow Cytometer (Life Technologies).

2.5.6. Caspases 3 and 8 Activity

Proteolytic activities of caspases 3, and 8 enzymes in Jurkat cells were measured using colorimetric protease assays (Invitrogen Molecular Probes) according to the manufacturer's instructions. At the end of the 24 h incubation, cells were subjected to two freeze-thaw cycles, followed by centrifugation at 15,000 $\times g$ for 15 minutes. The protein content in the supernatants was

determined by the BCA (Pierce™ BCA Protein Assay Kit) protein assay. A total of 50 μg of protein was incubated with 5 μl of DEVD-pNA or IETD- pNA in 50 μl of reaction buffer at 37 °C for 2 h in the dark. The optical density of the reaction mixture was then quantitated at a wavelength of 405 nm using thr microplate reader Victor X3 (Perkin Elmer).

2.5.7. Mitochondrial Potential Assay

Mitochondrial membrane potential ($\Delta\psi_m$) was measured with the MitoProbe™ 1,1′,3,3,3′,3′-hexamethylindodicarbocyanine iodide (DiIC$_1$(5)) assay kit (Molecular Probes) as instructed by the manufacturer. Briefly, Jurkat were collected, washed once with PBS, and labeled with 50 nM DiIC$_1$(5) (excitation/emission, 638/658 nm) at 37 °C in the dark for 30 minutes. After been washed once in PBS, all samples were analyzed by Guava EasyCyte 5HT (Merck Millipore) flow cytometer. Carbonyl cyanide m-chlorophenyl hydrazone (CCCP) was used as positive control.

2.5.8. Western Blot

Protein extraction and immunoblot analysis were performed using a modified Laemmli sample buffer (125 mM Tris-HCl, pH 6.8 buffer containing 2% SDS and 20% glycerol) in the presence of protease and phosphatase inhibitors (Roche). Lysates were separated by SDS-PAGE under reducing conditions, transferred to a nitrocellulose or PVDF membrane, and analyzed by immunoblotting. Primary antibodies used were anti-PARP (Biomol Research Labs), anti-caspase-3 (Santa Cruz) or anti-claeaved-caspases 3 (Santa Cruz Biotechnology) and anti-actin (SIGMA). Appropriate secondary antibodies were from Thermo Fisher Scientific. Amersham ECL HRP-linked sheep anti-mouse immunoglobulin G (IgG) and donkey anti-rabbit IgG antibodies were from GE Healthcare Life Sciences. After incubation with the

appropriate secondary antibodies conjugated to horseradish peroxidase, blots were revealed using ECL western blotting substrate (Pierce), or Western Lightning plus-ECL (PerkinElmer).

2.5.9. GSH Quantification

After incubation time, cells were washed, collected and centrifuged at 1,000xg for 5 minutes and washed in PBS. The pellet was lysed in 60 μL of CelLytic M reagent (Sigma Aldrich), kept on ice and vortex for 15 minutes. Cellular debris were removed by centrifugation at 15,000xg for 15 minutes at 4°C. The protein content was quantified according to Bradford using bovine serum albumin as a standard [113]. Protein precipitation was obtained adding 25 μl of trichloroacetic acid 10% to 60 μL of supernatant. The solution was vortexed, kept on ice for 5 minutes and centrifuged at 14,000 rpm for 5 minutes at 4°C. The oxidation of GSH by the sulfhydryl reagent 5,5'-dithio-bis(2-nitrobenzoic acid) (DTNB) in Tris-HCl buffer (Tris-HCl 0.4 M, EDTA 20 mM, pH 8.9) led to formation of the yellow derivative 5'-thio-2-nitrobenzoic acid (TNB), that was measured at 412 nm [114].

2.5.10. Statistical Analysis

All results are expressed as mean ± SEM of at least three independent experiments. Differences between treatments were assessed by t test or one-way ANOVA and Dunnet or Bonferroni was used as post-tests. All statistical analyses were performed using GraphPad InStat 6.0 version (GraphPad Prism). $P < 0.05$ was considered significant.

CHAPTER 3. Hemidesmus indicus

3.1. Introduction
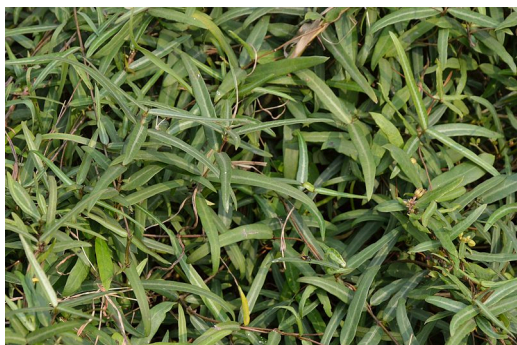
Name: Hemidesmus indicus – Indian Sarsaparilla
Family: Asclepiadacaeae
Genus: Hemidesmus
Species: *Hemidesmus indicus /Hemidesmus pubescens*
Geographical origin: India

Hemidesmus indicus var. indicus

Hemidesmus indicus var. pubescens

Hemidesmus indicus (HI) is a common weed found all over India. It naturally occurs in uncultivated soils or open scrub jungles and in all mesophytic habitat and semi dry regions of Pakistan, Sri Lanka, Moluccas, Bangladesh and Iran [115].

HI is an undershrub characterized by several wiry-thin branches with a purple-brownish cortex. Stems and branches twine anticlockwise and are elongate and narrow. The petiolate leaves are apiculate, obtuse or acute, and arrange in an opposite organization. They are dark-green on the upper leaf and paler, and eventually pubescent, on the other side. Flowers can vary from yellow to purple, depending on the specie. Five lobes form the calyx and the gamopetalous corolla is about twice bigger then the calyx. Fruits are cylindrical and divergent follicles, containing the many oblong, flat and whitish pubescent seeds [116]. Roots are reddish-brown, woody and aromatic.

HI roots store a huge mixture of biologically active compounds and represents the active part of HI. In traditional medicine, HI was assimilated in the form of root decoction. Thus in this thesis, aqueous extracts have been chosen for pharmacologic evaluations. The major constituent (91%) of HI extract is the 2-hydroxy 4-methoxy benzoic acid. But other important phytochemicals have been identified. From the highest to the lowest in amount, HI contains: saponins, tannins, alkaloids, flavonoids, phenols, coumarins and terpenoids [117]. Among the less abundant molecules found in the extract of HI, the most characterized are hemidesmins (coumarino-lignans) [118], and hemidesmosides A-C (steroidal glycosides) [119]. Of note, the two main variants of Hemidesmus, *indicus* and *pubescent*, don't differ in a significant way in terms of constituents. HI has only a higher content of phenols and free amino acids and a less content of b-sitosterol and tannins than *pubescens* [120].

Systematical studies about the pharmacological profile of HI begun more than 50 years ago, and currently many *in vitro*, *in vivo*, and *ex vivo* investigations supported and demonstrated some traditional uses of HI, such as the anti-diarrhea and anti-dysentery properties [117, 121]. Indeed, HI was widely used in traditional medicine mainly to cure diarrhea and dysentery, but was also exploited as antibiotic, ulcer and gastric protector, neutralizer of snakebites and scorpion stings, blood purifier and appetite stimulant. It was considered a remedy for a whole variety of pathologies and diseases, such as sore mouth, fever, menorrhagia, post-partum recovery, headache, inflammation and pain, venereal diseases including syphilis and gonorrhea, and erectile dysfunction [120, 122].

However, besides the folkloristic use of HI, its chemopreventive and antitumor potential has been widely investigated and established. Different HI extracts demised hepatocyte carcinoma HepG2 (aqueous and ethanolic

extracts), breast cancer MCF-7, colon cancer HT29 (methanolic extract), and leukemia Jurkat (aqueous extract) cells. Furthermore, my research group headed by Professor Fimognari performed extensive studies showing HI decoction's (HID's) antileukemic activity. They demonstrated that HID has anti-angiogenic effects and cytotoxic and cytostatic properties on promyelocytic leukemia cells, while it triggered the apoptotic mitochondrial pathway on Jurkat cells [123, 124]. Moreover, HID enhanced the antitumor potential of methotrexate, 6-thioguanine and cytarabin [123]. This ability underlines the interesting clinical potential for HID to be used as complementary drug to improve the anticancer activity of traditional chemotherapeutic agents and allow lowering their toxicity.

3.2.   Aim of the Study

The promising pharmacological profile and the deep knowledge about its antitumor potential made me choose HI as candidate for ICD studies of my last year of PhD. Thus, the aim of the study was to draw a systematic and exhaustive *in vitro* characterization of HID as ICD inducer. In the traditional medicine HI is used as a decoction. For this reason, I decided to use the human colon cancer dld1 cell line as cancer model. The study started with the evaluation of the cytotoxic and proapoptotic potential of HID on dld1 and the investigation about its ability to trigger oxidative and ER stress. Then specific ICD studies were performed and HID's ability to provoke DAMPs trafficking was assessed. As I decided to work with a human model of cancer, the understanding of HID's real immunogenic potential through vaccination experiments was not possible. To bypass this issue and directly address HID immunomodulatory potential, I evaluated the ability of the decoction to promote DCs maturation and to enhance interleukin IL1β and IL12p40 gene expression from monocytes obtained from healthy donors.

3.3. Results and Discussion

3.3.1. Characterization of HID

The main phytomarkers of HID, 2-hydroxy-4-methoxybenzaldehyde, 3-hydroxy-4-methoxybenzaldehyde and 2-hydroxy-4-methoxybenzoic acid, were identified and quantified through HPLC analysis. The difference among the batches in the phytomarker content and pharmacological activity resulted not significant (data not shown).

3.3.2. HID has Cytotoxic and Proapoptotic Potential

The study begun with the investigation of HID concentrations needed to demise more than half of the tumor population. We treated dld1 with increasing concentration of HID for 48 h to identify doses able to cause more than 50% of cell death. 0.62 mg/mL, 0.93 mg/mL and 1.55 mg/mL treatments decreased of 52.7, 62.1 and 68.8% cell viability, respectively, compared to untreated cells (Figure 3.1) and were chosen to perform all the following experiments.
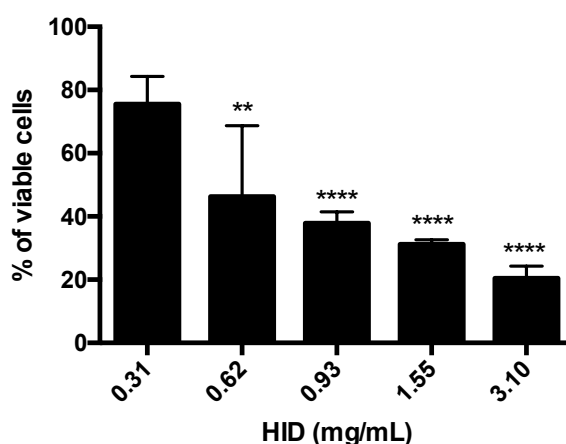
Figure 3.1 Percentage of viable dld1 cells after 48 h treatment with increasing concentration of HID. **$P < 0.01$; ****$P < 0.0001$

Then, as ICD is traditionally conceived as a particular form of apoptotic cell death, we investigated the cell death modalities that were engaged in response to HID. After 6 h, HID didn't trigger any RCD (data not shown), whereas after 24 h HID-treated dld1 revealed a dose-dependent increase in the percentage of apoptotic cells. HID elicited apoptotic cell death at all tested concentrations in a dose-dependent manner. 0.93 mg/mL treatment drove 13.8% of cells to apoptosis *versus* 3.3% of untreated cells, while HDI 1.55 mg/mL induced 24.7% of apoptosis (Figure 3.2). These data are consistent with those published on Jurkat cells by Fimognari et al. [123] except for the extent of necrotic fraction that in HDI-treated dld1 were higher. This discrepancy was probably due to the trypsinization step needed to detach dld1 before performing the apoptotic assay, step that is not required for Jurkat cells since they grow in suspension.
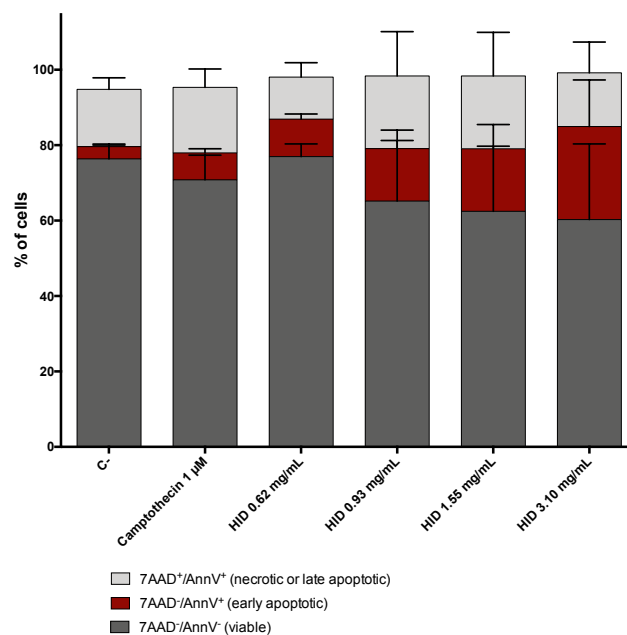
Figure 3.2 Percentage of viable (7AAD$^-$/AnnV$^-$), early apoptotic (7AAD$^-$/AnnV$^+$), and late apoptotic or secondary necrotic (7AAD$^+$/AnnV$^+$) cells after 24 h treatment of dld1 cells with increasing concentrations of HID.

3.3.3. HID Triggers ER and Oxidative Stress

Induction of ER stress was evaluated by monitoring the kinetics of key markers linked to ICD induction. I paid special attention on the PERK-eIF2α branch of the UPR that has been previously shown to govern danger signaling during ICD [125]. Thus, I evaluated the phosphorylation status of PERK and eIF2α, as a general readout of the transcriptional activation of the UPR. Of note, there is no antibody commercially available that recognizes specifically the phosphorylated state of human PERK for western blot, thus we use the molecular weight shift in SDS - PAGE as indicator of phosphorylated PERK. HID was able to trigger the activation of PERK pathway starting from 1 h and reached a peak after 3 h, while no modulation was observed after 24 h treatments (Data not shown). In particular, after 3 h at 1.55 mg/mL, HID increased phosphorylated phosphorylated PERK (p-PERK) and phosphorylated eIF2α (p- eIF2α) (Figure 3.3) of 3.14 and 3.89 times respect to untreated cells.
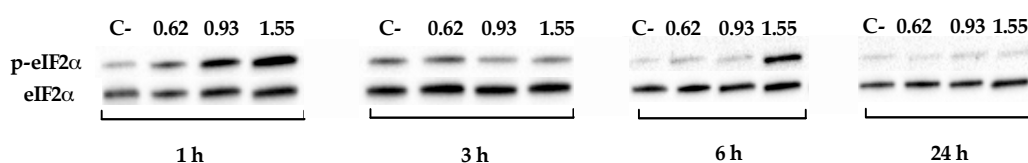
Figure 3.3 Representative blots of at least three independent experiments analysis for eIF2α and (total and phosphorylated) protein levels in dld1 cells treated with HID (mg/mL).

To directly link ER stress to the antitumor potential of HID, ER stress was prevented with specific agents before treating dld1 with HID and then recording viability. Attenuation of ER stress with both tauroursodeoxycholic acid TUDCA (general ER stress inhibitor) and AMGPERK44 (PERK-activation inhibitor) affected the cytotoxic activity of HID recorded after 24 h in a

concentration-dependent manner, that however was not enough to restore complete viability. This suggests a crucial, but not exhaustive, role of ER stress in HID mechanism of action (Figure 3.4). More, the cytoprotective effect of TUDCA did not differ from the one obtained with AMGPERK44, suggesting the complete implication of PERK branch of the UPR.
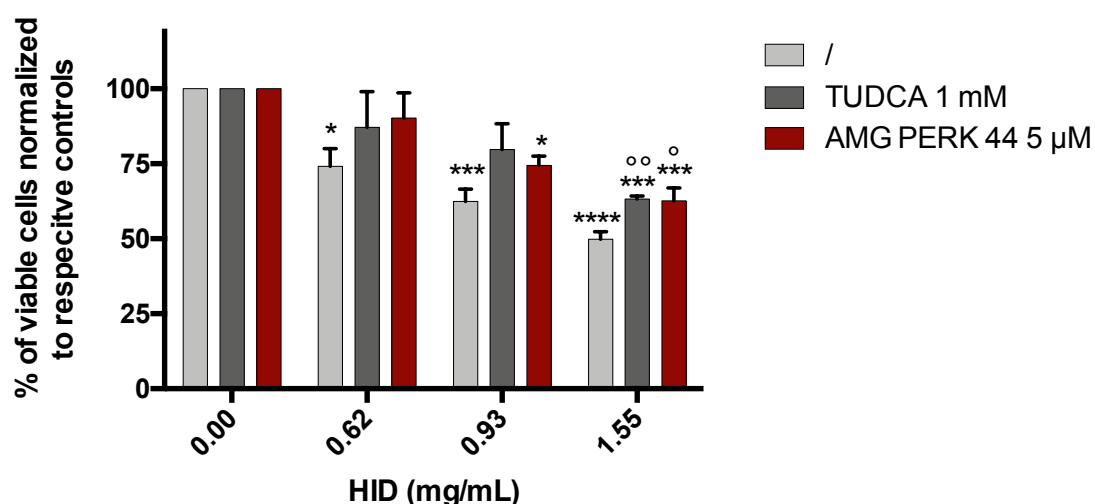
Figure 3.4 Percentage of viable cells after dld1 treatment with HID alone or in combination with TUDCA or AMGPERK44 for 24 h. * *versus* untreated cells; ° HID *versus* ER stress inhibitors, respectively TUDCA or AMG PERK 44. * or ° $P < 0.05$; °° $P < 0.01$; *** $P < 0.001$; **** $P < 0.0001$. Unpaired t test was used to calculate statistical significance of three independent experiments.

As thapsigargin demonstrates, ER stress alone is not sufficient to trigger ICD [126], thus HID's ability to provoke oxidative stress was examined. Intracellular ROS levels were recorded after 1, 3, 6 or 24 h treatment with HID 0.62, 0.93 and 1.55 mg/mL. Oxidative stress was increased starting from 1 h in a concentration-dependent manner. After 3 h at all tested concentrations, ROS levels reached the highest level recorded. 0.62, 0.93 and 1.55 mg/mL raised intracellular ROS content 5.08, 5.79 and 7.38 times, respectively, compared to untreated cells (Figure 3.5). Whether the values were still dose-dependent and

above those recorded for untreated cells, 6 and 24 h treatments showed a descending trend of ROS levels (Figure 3.5).

These data show that HID triggers ROS and ER stress following the same time tendency. This is an interesting result since ICD is a stressor-dependent kind of apoptosis, founded on ROS-based and, at least simultaneous, ER stress [43, 48, 127].
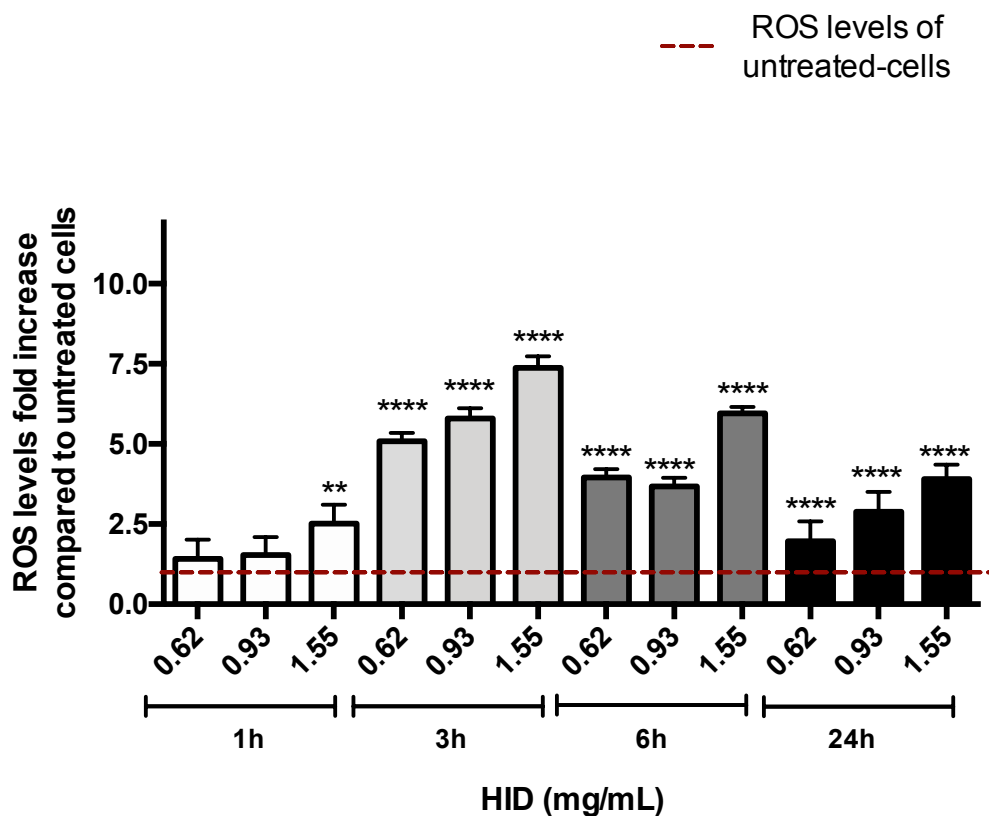
Figure 3.5 ROS fold increase in HID-treated cells for 1, 3, 6 or 24 h compared to untreated cells.

3.3.4. HID Induces DAMP's Trafficking

HID was tested in a time-course experimental setting for its ability to endorse the main *in vitro* hallmarks of ICD *i.e.* the surface exposure of CLR and HSP70 and the secretion of ATP and HMGB1.

We monitored surface exposure of CLR and HSP70 through flow cytometry in non-permeabilized cells. Expression of ecto-CLR increased

after 3 h treatments with HID 0.93 and 1.55 mg/mL, while after 6 h all tested concentrations triggered CLR mobilization. The higher ecto-CLR value was reached after 6 h of 1.55 mg/mL with a fold increase of 1.37, compared to untreated cells (Figure 3.6 A), a very similar value to that observed for mitoxantrone, a *bona fide* type I ICD inducer, in T24 cells after 4 h of incubation [48]. At 24 h post treatment, ecto-CLR was still higher than that recorded for untreated cells, but at a lesser extent than before (Figure 3.6 A). The lowest tested concentration of HID did not modulate HSP70 trafficking at any time point, while both 0.93 and 1.55 mg/mL favored its mobilization in a dose- and time-dependent fashion. After 24 h of treatment, the highest tested concentration induced the highest increase in HSP70 MFI that was 1.42 times higher than that recorded for untreated cells (Figure 3.6 B).

HID provoked ATP secretion at all tested concentrations and time point analyzed (3, 6 and 24 h). After 3 h, it induced the highest rise, increasing ATP levels in the extracellular medium of 36 and 73 times for 0.93 and 1.55 mg/mL, respectively (Figure 3.6 C). The entity of this increase reminds that of Hyp-PDT in human bladder carcinoma T24 cell line at 1 h post treatment [48]. After 48 h of HDI treatments, HMGB1 was mobilized from the cytoplasm to the extracellular matrix, as showed in (Figure 3.6 D).

Of note, after 3 h treatment, both HID-mediated ER and oxidative stress reached the highest level, and clearly initiated DAMP's trafficking.
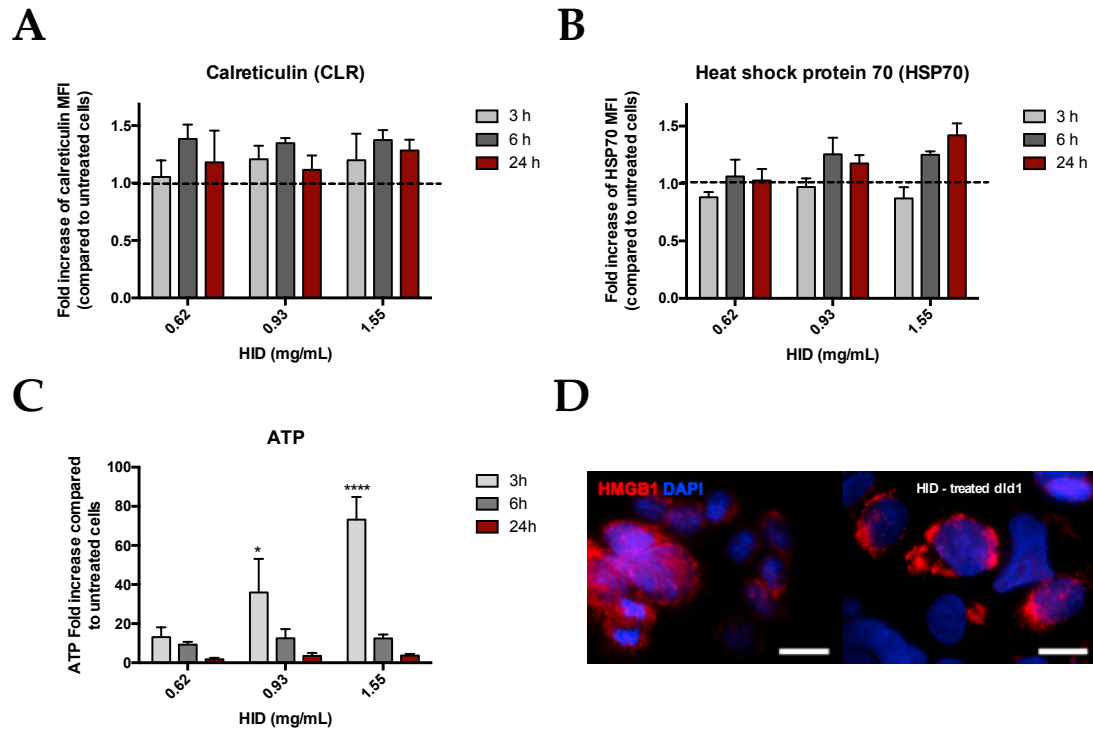
Figure 3.6 DAMPs trafficking panel: ecto-CRT (A), ecto-HSP70 (B) expression in nonpermeabilized cells after HDI-dld1 treatment at different time points; ATP secretion following HDI treatment after different time points (C); dld1 cells untreated and following 48 h treatment with HID 0.6 mg/mL were stained with anti-HMGB1 (red) and DAPI (blue) for nuclei counterstaining. Magnifications 100x, scale bar 10 μm (D). * $P < 0.05$; **** $P < 0.0001$

Even if ICD inducers do not share fixed patterns in terms of DAMP's trafficking (or common pathways have not been discovered yet), Oliver Kepp [128] and its group found a sort of spatiotemporal code through which DAMPs exert their immunological awakening. Chemotherapy agents exert a cytotoxic effect on cells that immediately elect whether cell death will be immunogenic, silent or tolerogenic [129]. Right after the damaging *stimulus*, cells activate their defensive repair mechanisms. During this phase cells are already alerted to face a potential identification and elimination of demising cells. During ICD, CRT translocation is usually the first "eat me" signal emitted, most likely balanced with following "don't eat me" signals. Ecto-CLR positioned on a membrane that still lacks of externalized phosphatidylserine is proven to

provide, at least in part, the switch to a cognate immune response by APCs instead of a silent deletion of demising cancer cells by macrophages [128]. Moreover, HSP70 is enrolled during the central response of dying cells to stress. The main role hypothesized for it is to break the tolerance of immune system acting as antigen chaperon and favoring DC-tumor cells adhesion [129-131]. Nevertheless, the mobilization of HSP70 (and other HSPs in general) arises rather late as compared to CRT and could consequently play an additional/synergistic role to CRT primary "eat me" signal favoring DCs uptake and process of the antigen. The talk between dying cells and DC (or APC in general) is complex and opposite messages can reach the immune cells [128]. This fact makes the spatiotemporal code essential for a full-triggered immune response, and explains the late release of HMGB1, that could be linked to the same iDC that incorporates antigen from dying cells thanks to CLR and HSPs. This intricate sequence represents a code that dying cells follow to counteract all signals that potentially silence the immune response [128].

Hyp-PDT causes early, pre-apoptotic induction of ecto-CRT and actives pre-apoptotic secretion of ATP in stressed cells, overlapping PERK-orchestrated pathways. These events are tailed by late apoptotic mobilization of HSP70 and HSP90 [48]. Mitoxantrone and oxalilplatin prompt pre-apoptotic ecto-CLR, early apoptotic secreted ATP, mid to late ecto-HSP70 and late apoptotic passive release of HMGBI [54, 132, 133]. Shikonin, for its part, induces early to mid apoptotic ecto-CRT and ecto-HSP70 [6, 134]. Taken together, our data perfectly describe the profile of DAMPs-trafficking triggered by an ICD inducer. They indicate that HID provokes pre-apoptotic release of ATP and exposure of CLR, early- and mid-apoptotic exposure of HSP70 and a subsequent release of HMGB1 at the late stages of dying cells.

Further studies are needed to assess which type of ICD inducer HID is.

However, except for ATP, the entity of HID- modulated DAMPs trafficking reminds that induced by mitoxantrone, presuming HID to be a type I ICD inducer. Of note, HID-driven ER stress is only mild intense. An interesting future approach would be to evaluate the ability of an ER stressor, such as tunicamycin or thapsigargin, to increase HID-mediated DAMPs trafficking that presumably would translate in a greater immunogenic potential.

Altogether, these data are interesting for many reasons. On one hand, HID is able to deploy four different DAMPs jointly, increasing the chances of a positive immunogenic outcome since the potency of the immune response depends on the complexity and intensity of the emitted DAMPs. Indeed, as above mentioned, each danger signal has a different role in the stimulation of immune system and a concurrent activation increases the chances to exert full immunogenicity. CLR is a strong "eat me" signal and mediates tumor immunogenicity [35, 48, 135, 136]; HSP70 recalls monocytes and neutrophils and fosters DC maturation and NK cell activation [47, 48, 133, 136, 137]; ATP is a "find me" signal, causes IL-1β release from DC and mediates, for instance, mitoxantrone- and oxaliplatin-induced antitumor immunity [32, 42, 48, 133]; HMGB1 acts as a potent cytokine, induces DC maturation and attracts various immune cells [47, 133, 138-141]. On the whole, those DAMPs build the biological ability to trigger ICD. On the other hand, conversely from anthracyclines, HID stimulates all DAMPs at the same concentrations (0.93 and 1.55 mg/mL), thereby incorporating the rise of these critical immunogenic signals within a single therapeutic set-up, and indicate an easier prospective of clinical use [48].

3.3.5. HID Promotes DC's Maturation and Increases ILs Expression on Human Monocytes

HID induces signature of danger signaling in colon cancer cells. Then,

we investigated the direct interactions of such treated colon cancer cells with key immune cells.

DCs are able to recognize and present antigens to different cell types such as CD4+ helper T cells, CD8+ cytotoxic T lymphocytes and B cells, hence representing the connection between innate and adaptive immune system [142]. Upon activation, DCs proceed through the maturation process during which they lose their phagocytizing ability, increase the surface expression of MHC class I and class II peptide complexes and the expression of costimulatory molecules (CD80 and CD86, among others), and secrete proinflammatory cytokines. Then, the mature DCs migrate into draining lymph nodes. All these phenotypic transformations allow DCs being in contact with naïve T cells, priming the T-cell-mediated immune response. TLRs are the best-characterized PRRs on DCs surface and promote DCs activations when the designated ligands bind them. As already mentioned, DAMPs stimulate the immune system through the interaction with DCs and TLRs [143]. For instance, ecto-CLR enables the uptake of dying cells by DCs, stimulating their engulfment [32], while HMGB1 binds TLR4 and promotes antigen processing of the phagocytic cargo [4]. HSP70 is a DCs chemoattractant and promotes their maturation via TLR4 signaling. Indeed, TLR4 activation promotes the synthesis of pro-IL-1β, the precursor of interleukin [128]. ATP is another crucial DC activator. It triggers the NLRP3 inflammasome in DCs inducing, as well, IL-1β release and the consequent priming of cytotoxic T cells [143].

We cultivated C14-derived immature DCs (iDCs) for 24 h in the 48 h-HID-treated-dld1 culture medium and measured the phenotypic maturation, (*i.e.* increased surface expression of CD80, CD83, and CD86) and functional stimulation (*i.e.* amplified production of Ilβ by DCs). LPS treatment of iDCs was used as a positive control to test the maturation potency of iDCs. HID-

treated dld1 cells induced DC-maturation, as demonstrated by the increase in all clusters of differentiation analyzed (Figure 3.7 A).

Then, we quantified IL-1β secretion in the conditioned media used in the DC maturation analysis experiments. The expression of IL1β and IL12p40 genes were both enhanced. Remarkably, those treatments resulted in the modulation of cytokine gene expression and phenotypic profiles of iDC similar to that induced by LPS and demonstrated the functional activations of DCs (Figure 3.7 B and C).

To make sure that the immunostimulant profile of HID-treated dying dld1 would not be mistaken for a direct immunostimulant effect of HID, we investigated the antigenic potential of HID to be recognized by T cells. Total peripheral blood mononuclear cells (PBMCs) from healthy donors were cultured in presence of increasing concentrations of HID. Lymphoproliferative response was analyzed by ^{3}H-thymidine incorporation on day 7. Data from 4 different experiments with cells from healthy donors indicate that HID did not *per se* induce T-cell proliferation (Figure 3.7 D), giving one more evidence of HID's ability to induce ICD.
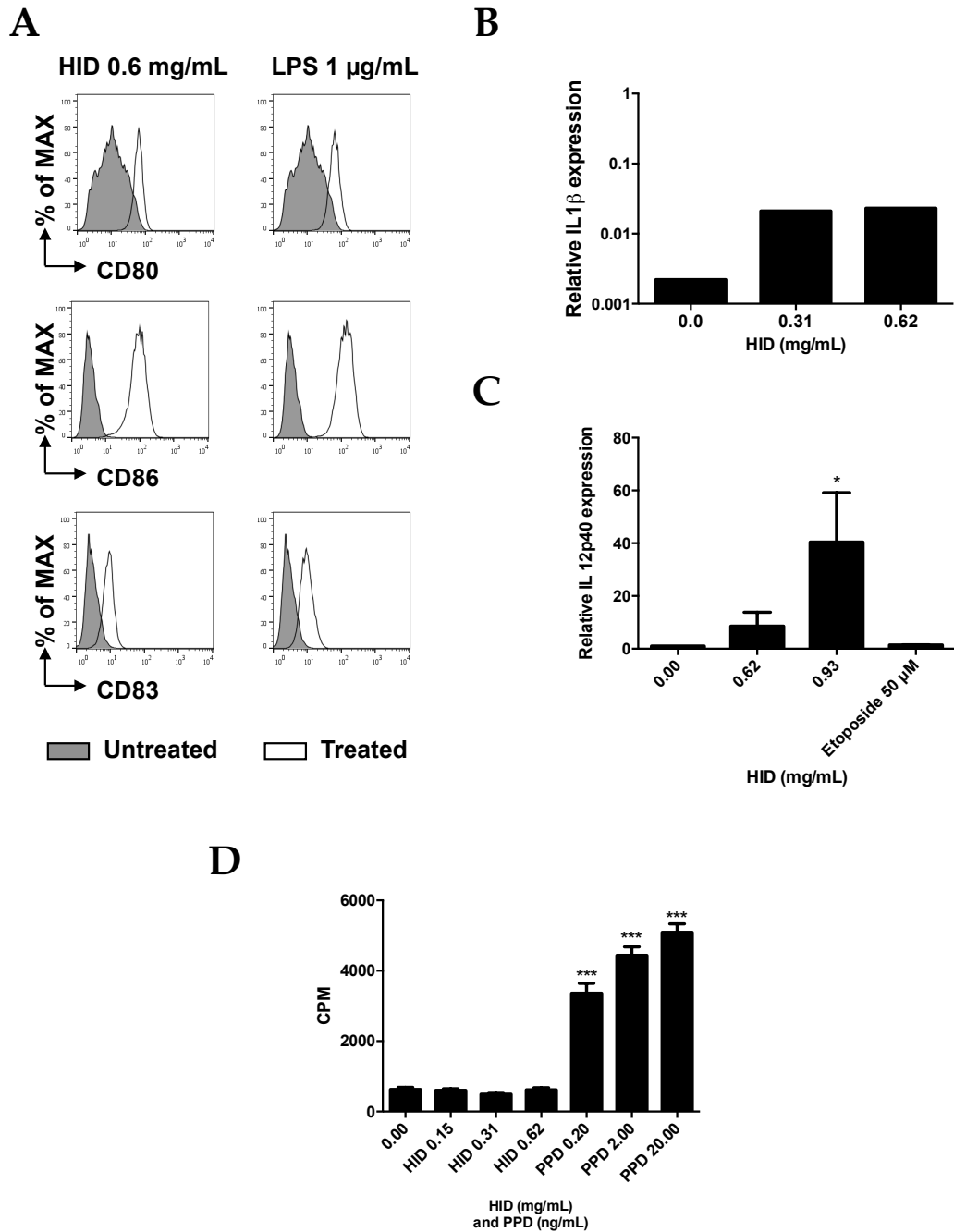
Figure 3.7 CD80, CD86 and CD83 expression in DC from a representative donor, untreated or following 48 h treatment with dld1 supernatant obtained after HID treatment. LPS-treated cells were used as positive control (A). Example of IL1β expression in one donor, representative of three different experiments, performed with similar results. GAPDH gene expression was used as control (B). IL12p40 expression on DCs incubated for 48 h with supernatant of HID-treated cells, normalized on untreated cells (mean of 3 experiments). GAPDH was used as control housekeeping gene (C). CD8+ T Cell proliferation (CPM) induced by HID and tubercolin PPD, positive control, as assessed by ^{3}H-Thymidine incorporation.

3.4. Conclusions

During the last year of my PhD I extensively characterized the HID profile as ICD inducer on human colon cancer cells. After assessing the apoptotic potential of HID, I demonstrated its ability to trigger both ER and oxidative stress with the same kinetics and I correlated those two events with the cytotoxic potential of HID. I discovered that the immunogenicity of HID-mediated cell death is governed by the preapoptotic mobilization on the outer cellular membrane and secretion of CLR and ATP, respectively, coupled with HSP70 translocation during the early phases of apoptosis and the late release of HMGB1. The interaction of immature DCs with immunogenic tumor dying cells led to an increase in the expression of maturation-associated markers on DCs and the secretion of inflammatory IL1β and IL12p40. Furthermore, I confirmed that the stimulation of the immune system was elicit by the HID-treated dying cancer cells and not by HID itself, since HID didn't exert any direct effect on T-cells. At this point, to confirm HID factual endogenous vaccine-like potential, it would be interesting translating these results into a murine cell line in order to be able to perform *in vivo* studies.

This was the first report where the ability of a botanical drug to trigger all hallmarks of ICD, comprised DCs activation and maturation, was demonstrated. Different synthetic chemotherapeutic drugs induce ICD and were characterized in detail [5]. In contrast, there is a paucity of data regarding natural products of potential clinical relevance [6]. A variety of natural anticancer compounds have been successfully characterized [7, 8]. However, their immunogenic potential has not been analyzed in comparable detail [9]. Furthermore, toxicity seems not to be an issue related to HID use. Indeed, neither lethality nor conspicuous alteration in mice behavior was noticed after root powder suspension was administered to test acute toxicity on Swiss

albino mice [121]. Furthermore, the LD$_{50}$ (the amount of a toxic sufficient to kill 50 percent of a population) measured for liver and kidney is at least 130 times higher than the concentrations used in this study [117]. An ethanolic root extract of HI prevented cytogenetic damage triggered by cisplatin on lymphocytes [144]. The impact of my studies could be enormous in the view of HID as adjuvant of other traditional antitumor agents. HID have synergistic antileukemia potential with 6-thioguanine, cytarabine and methotrexate, and interesting could be to try to increase HID immunological stimulation in a combination therapy with a pure ER stressor. The latter agent could increase the entity of HID immune response potentially reaching the effect of a type II ICD inducer. Otherwise HID could be used with the aim of increasing responsiveness to other immunological anticancer therapy, such as the use of monoclonal antibodies that target immunological checkpoints.

On the whole, the antitumor profile of HID that emerges from this study provides a clear rationale for the design of *in vivo* experiments and rightfully paved the way for pilot clinical trials.

3.5. Material and Methods

3.5.1. Plant Decoction and Extract Preparation

HI (voucher #MAPL/20/178) was collected from Ram Bagh (Rajasthan, India), and authenticated by Dr. MR Uniyal, Maharishi Ayurveda Product Ltd., Noida, India. The plant decoction was prepared according to the method described in the Ayurvedic Pharmacopoeia of India [145]. Briefly, 10 g of grinded roots of *HI* were mixed with 300 mL of boiling water, allowing the volume of water to reach 75 mL. The decoction was filtered, lyophilized, aliquoted and stored at room temperature. Immediately before the assays, the samples were resuspended in water in a 31 g: 1000 mL ratio and centrifuged at 4000 rpm for 5 minutes to discard any insoluble material. Eventually,

samples were sterile-filtered when necessary. The experiments and the HPLC analysis were performed using this stock solution of 31 mg/mL.

3.5.2. HPLC Analysis and Validation:

HID was subjected to HPLC analysis to quantify its main phytomarkers, namely 2- hydroxy-4-methoxybenzaldehyde (2H4MBAL), 3-hydroxy-4-methoxybenzaldehyde (3H4MBAL) and acid 2- hydroxy-4-methoxybenzoic (2H4MBAC127). The reference compounds (all obtained from Sigma Aldrich) were used as external standards to set up and calculate appropriate calibration curves. The analyses were performed using a Jasco modular HPLC (Tokyo, Japan, model PU 2089) coupled to a diode array apparatus (MD 2010 Plus) linked to an injection valve with a 20 mL sampler loop. The column used was a Tracer Extrasil ODS2 (2560.46 cm, i.d., 5 mm) with a flow rate of 1.0 mL/minutes. The mobile phase consisted of solvent solution B (methanol) and A (water/formic acid = 95:5). The gradient system adopted was characterized by five steps: 1, isocratic, B/30 for 15 minutes; 2, B raised progressively from 30% to 40% at 20 minutes; 3, B then raised to 60% at 50 minutes; 4, B achieved 80% at 55 minutes and 5, 100% at 60 minutes. Injection volume was 40.0 mL. Following chromatogram recording, peaks from HI samples were identified by comparing their UV spectra and retention time with those from the pure standards. The identity was also confirmed by 1H NMR on the enriched fraction of the compounds obtained by soxhlet extraction in CHCl3/EtOH 1:1. Dedicated Borwin software (Borwin ver. 1.22, JMBS Developments, Grenoble, France) was used to calculate peak area by integration.

Individual stock solutions of 2H4MBAL, 3H4MBAL and 2H4MBAC were prepared in water. Six different calibration levels were prepared within the following range: 2–20 mg/mL for 2H4MBAL, 1.5–40.0 mg/mL for 3H4MBAL, and 1–100 mg/mL for 2H4MBAC. Each calibration solution was

injected into HPLC in triplicate. The calibration graphs were provided by the regression analysis of peak area of the analytes versus the related concentrations. The analysis of HI (31 mg/mL) was performed under the same experimental conditions. The obtained calibration graphs allowed the determination of the concentration of the three components. Three different batches of HI were tested.

3.5.3. Cell Cultures and Treatments

Authenticated human colon adenocarcinoma cell line MMR-deficient, dld1, was purchased from ATCC. Dld1 were propagated in adhesion and cultured in RPMI 1640 supplemented with 10% inactivated Fetal Bovine Serum (FBS), 1% GlutaMAX-I, and 1% kanamycin (all purchased by Gibco-Life Technologies), at 37°C and 5% CO_2. All cultures were tested by PCR and proven to be mycoplasma free prior to experimental investigations.

PBMCs from healthy donors (Blood donor center of the University Hospital of Basel) were obtained by gradient centrifugation. Both CD14+ monocytes and CD8+ T cells were magnetically isolated from PBMCs by using antibody-coated beads (Milteny Biotech) and cultured in RPMI 1640 supplemented with 1% GlutaMAX-I, 1% non-essential amino acids (NEAA), 1% sodium pyruvate, HEPES, 1% Kanamycin sulfate and 10% FBS (all purchased by Gibco-Life Technologies) for CD14+ monocytes and 5% pooled human AB serum for co-culture of myeloid and T cells. DC were generated in presence of GM-CSF and IL4, as previously described [146].

10,000 cells were seeded in 200 μL of complete medum, 58000 in 500 μL or $1.7 \times 10^6 / 7$ mL respectively in 96, 24 wells plates or 10 cm dishes. Cell lines cultured were treated with HID, oxaliplatin or etoposide at the indicated concentrations. To rule out a role of contaminating endotoxin in the elicitation

of the effects of HI polimixin B (Calbiochem) was added at 10 μg/mL to all cultures during cell treatment with HID.

For ER stress-related experiments dld-1 cells were pretreated with sodium tauroursodeoxycholate (TUDCA) 1 mM (Sigma Aldrich) or AMGPERK44 (Tocris Bioscience) 5 μM for 1 h and then co-incubated with increasing concentrations HID for 24 h, then viability was assessed using 4-methylumbelliferyl heptanoate (MUH, Sigma Aldrich) that becomes highly fluorescent after hydrolysis of the ester linkage and, thus, measures lipase and esterase activity [147]. After treatment with ER stress inhibitors and HID, cells were washed with PBS and incubated with MUH 1 mg/mL. After 30 minutes of incubation at 37°C and 5% CO_2, absorption at 460 nm was measured using a microplate reader (Tecan).

3.5.4. Analysis of Cell Viability and Induction of Apoptosis

The acid phosphatase (APH) assay was used to determine dld-1 viability. 405 nm absorbance is directly proportional to numbers of viable cells present in monolayers. After 48 h, cells were washed twice with PBS and then resuspended in 100 μL of the assay buffer [0.1 M sodium acetate, 0.1% Triton-X-100, supplemented with 4-nitrophenyl phosphate disodium salt hexahydrate (N9389, Sigma Aldrich)] were added to each well. After 90 minutes incubation at 37°, 10 μL NaOH 1 N was added to each well and the absorption at 405 nm was measured within 10 minutes on a microplate analyzer.

To discriminate regulated form of cell death, Guava Nexin Reagent (Merck Millipore) was used. Through the use of 7-AAD and annexin V-phycoerythrin, the assay allows the discrimination of apoptotic and necrotic events. Cells were incubated with the reagent for 20 minutes at room temperature in the dark and then analyzed via flow cytometry. Dld-1 cells

were first detached with TrypLE™ Express Enzyme (Thermofisher Scientific), washed twice with PBS and then incubated with the reagent.

3.5.5. Proliferation Assay

Proliferation of PBMCs obtained by healthy donors was evaluated by ^{3}H-thymidyne incorporation. PBMCs cells were cultured for 5 days after treatment with HI 0.6 mg/mL-4.8 μg/mL. Cells were treated with 1 μCi/200 μL ^{3}H-thymidine (Amerchem) for 18h and harvested on paper filters. ^{3}H-thymidine uptake from PBMCs was measured in a liquid scintillation counter. Tubercolin PPD (Staten Serum Institute) was used as positive control for ^{3}H-thymidine incorporation.

3.5.6. Detection of ROS Levels

ROS levels were determined after 1, 3, 6, 18 or 24 h of WSE treatment by using the probe 2′,7′-Dichlorofluorescin diacetate (DCFDA), which was added during the last 20 minutes of incubation. Hydrogen peroxide was used as positive control. Dld-1 cells were detached with TrypLE™ Express Enzyme after the reagent was added. After three washing in PBS, cellular fluorescence was imaged using a Leica DMLB/DFC300F fluorescence microscope (Leica Microsystems) equipped with an Olympus ColorviewIIIu CCD camera (Polyphoto). Fluorescence images (100 cells per sample from randomly selected fields) were digitally acquired and processed for fluorescence determination at the single cell level on a personal computer using the public domain program, Image J. Mean fluorescence values were determined by averaging the fluorescence of at least 100 cells/treatment condition/experiment.

3.5.7. Analysis of Calreticulin, HSP70 and HSP90 Expression, and ATP and HMGB1 Release

After treatment, cells were collected with TrypLE Express (Life Technologies), washed with PBS and with Flow Cytometry buffer (FCB) (2% FBS, 1% BSA in PBS), incubated for 1 hour at 4°C with primary antibodies, washed, and incubated for 1 hour at 4°C with secondary antibodies, if neecessary. After final washes, cells were incubated in FC buffer including 1 nmol/L Sytox Red (Thermo Fisher Scientific) or Propidium iodide (PI) 0.5 µg/mL for 15 minutes and analyzed on Attune Flow Cytometer (Life Technologies). The permeabilized cells were excluded from the analysis due to intracellular staining, and the fold changes in the mean fluorescence intensity (MFI) for each DAMP were analyzed.

Fluorochrome-labeled monoclonal antibodies recognizing CD1a, CD8, CD14, CD16, CD83, CD80, CD86, HLA-DR were obtained from Becton Dickinson, PE-labeled calreticulin (1:100 dilution in FC) was obtained from abcam, while non-labelled Hsp70 from thermofisher (1:100 dilution in FC) and coupled with the Alexa Fluor 647 labelled-goat anti-mouse igg (H+L) cross-adsorbed secondary antibody (Thermofisher Scientific) (1:100 dilution in FC). The appropriate antibody and specific binding was evaluated by flow cytometry (FACScalibur, Becton Dickinson, or Guava EasyCyte 5HT, Merck Millipore).

The kit ATPLiteTM 1step (Perkin Elmer, Waltham, MA, USA) was used for the detection of ATP extracellular concentration. Jurkat cells were seeded and treated with WSE in Hank's Balanced Salt Solution (HBSS) or complete medium for 6 and 24 h, respectively. At the end of incubation, supernatants were collected and treated with 100 µL of ATPLite 1step reagent containing luciferase and D-luciferin. After shaking for 2 minutes at 700 rpm using the

orbital microplate shaker 711/+ (Asal srl, Florence, Italy), luminescence of the samples was measured in a 96-well black plate using the microplate reader Victor X3 (Perkin Elmer).

3.5.8. Immunofluorescence

Dld-1 cells were cultured in 8 well culture chambers slide (Falcon) and, after treatment with HID for 24 h, they were fixed with formalin 4%, permeabilized with methanol 90% and incubated with mouse monoclonal anti-HMGB1 specific antibodies (Abcam), followed by incubation with goat anti-mouse Alexa Fluor 546 secondary antibody (Invitrogen). Nuclei were counterstained with DAPI. Cells were examined under an Olympus BX61 fluorescence microscope (Olympus) and images were captured by a digital camera and Analysis Software (Soft Imaging System GmbH) with a 20X, 60X or 100x magnification.

3.5.9. Western Blot analysis

After incubation in 10 cm dishes with various concentrations of HID for 1, 3, 6 or 24 h cells were washed three times with cold PBS. Cells were subsequently scraped and collected in 1 mL of PBS and centrifuged twice, after which the pellet was lysed with 220 μL of Lysis buffer (NaCl 0.75 M, Triton X-100 1:20, Tris-Cl 0.25 M and leupeptin 2 μg/mL and PMFS 100 μg/mL added before use). Cells were then homogenized and allowed to stand at 4°C for 30 minutes. Cells were centrifuged at 14,000 g for 15 minutes at 4°C. Then, proteic lysates were collected and transferred to clean eppendorfs.

Samples (30 μg proteins) were separated on 10% SDS-polyacrylamyde gels (Bio-Rad, Hercules) and electroblotted onto 0.2 μm nitrocellulose membranes. Membranes were incubated overnight at 4 °C with primary antibodies recognizing either PERK (Abcam), pPERK (aAcam), EIF2α (Cell

Signaling) and pEIF2 α (Cell signaling). Membranes were washed with TBS-T (TBS + 0.05% Tween20), and then incubated with a horseradish peroxidase (POD) linked anti-rabbit secondary antibody (1:2000; GE Healthcare,). Immunoreactive bands were visualized by enhanced chemiluminescence (ECL; Pierce). The same membranes were stripped and reprobed with a β-actin antibody (1:1000; Sigma–Aldrich) for TH or total ERK1/2 (1:1000; Cell Signaling) for pERK1/2. Data were analyzed by densitometry, using Quantity One software (Bio-Rad). Values were expressed as fold increase versus respective contralateral intact site.

3.5.10. Gene Expression Analysis

Total cellular RNA was extracted from tumor cells, CD14+ or DCs cells using the RNeasyVR Mini Kit (Qiagen) and reverse transcribed using M-MLV reverse transcriptase (Invitrogen-Life Technologies, Lucerne, Switzerland) according to manufacturer's protocol. Human IL12p40, IL1β gene expression was analyzed by quantitative real-time PCR using Taqman assay (Applied Biosystems-Life Technologies) and ABI Prism 7300 (Applied Biosystems). Gene expression was quantified using Ct method upon normalization with GADPH expression, as reference housekeeping gene.

3.5.11. Statistical Analysis

All results are expressed as mean ± SEM of at least three independent experiments. Differences between treatments were assessed by t test or one-way ANOVA and Dunnet or Bonferroni was used as post-tests. All statistical analyses were performed using GraphPad InStat 6.0 version (GraphPad Prism). $P < 0.05$ was considered significant.

Conclusive Remarks

The immune system is the best natural resource that organisms could deploy against cancer. Potentially it should recognize and eradicate transformed cells before they form a full-blown neoplasm. However, the complexity, the heterogeneity and the ability of tumor cells to constantly acquire new mutations make them able to escape immunosurveillance. This problem, also representing a hallmark of cancer [11], can be overcome thanks to the activity of some chemotherapeutic drugs that are able to break tumor tolerance while trigging an immunostimulant version of RCD. This particular type of agents, together with tumor eradication, initiates an intrinsic mechanism through which demising tumor cells trigger the immune system, create a proper lymphocyte T- induced memory, and act as an endogenous vaccine [133]. ICD has been discovered barely more than ten years ago and its huge potential has now been understood. Many chemotherapeutic drugs, commonly used in clinical settings induce ICD. Doxorubicin and oxaliplatin are the more common examples, but many others such as epirubicin, idarubicin, mitoxantrone, bortezomib, bleomycin, and cyclophosphamide induce ICD [148]. To understand the impact that ICD inducer could have on cancer treatment, it's interesting noticing that so far (November 2017) 6525 clinical studies involve at least one above-cited molecule [149]. Furthermore, the idea of combinatorial treatment between conventional antitumor drugs or other types of immune therapy with ICD inducers is rapidly entrenching. The aim of coupling ICD inducers to different anticancer strategy is to add or boost an immunomodulatory effect that renders therapy more efficient and avoids relapses [148]. Good evidence of this interest is the 8 clinical studies that investigate the additive effect of ICD inducers and checkpoint inhibitors, the 151 clinical reports that combine ICD inducers with antitumor vaccine

therapies, and the 527 clinical analysis about the activity of ICD inducers combined with targeted antitumor therapy based on monoclonal antibodies [149].

In this context, natural products are perfect candidates for combinatorial therapeutic strategy. Usually they are characterized by low toxicity and interesting pharmacological properties [55]. Indeed, talking about botanical drugs, their strength is exactly their complex nature that makes them a library of biological active compounds able to target several pathways simultaneously. This same strength could be considered a pitfall from the point of view of product standardization [123]. However, in the case of both botanical drugs investigated in this thesis, phytochemicals analysis clearly demonstrated the presence of specific phytomarkers, which can be conveniently used as fingerprints.

During the three years of my PhD, I provided a comprehensive preclinical, *in vitro* study of cell death mechanisms and immunologic characteristics of two botanical drugs, *Withania somnifera* and *Hemidesmus indicus*, and one ITC derivative synthesized *ad hoc* in order to reach the ER, MG28.

The least promising agent in terms of ICD induction was the latter mentioned MG28. Assuming that concurrent ER and oxidative stress are the *sine qua non* characteristics needed to trigger ICD, MG28 was synthesized with the rationale of directly bring a very active chemical moiety (ITC) to the ER and there, to induce oxidative stress. The result would have been a type II ICD inducer, such as Hyp-PDT, the most efficient ICD inducer so far. MG28 did not exert significant apoptosis on the murine colon cancer CT26 cell line. However, since ICD induction is tumor-specific [127], we tested MG28 on leukemia cells (Jurkat), as well. In this case, MG28 triggered apoptosis through both

intrinsic and extrinsic pathway but the data we obtained suggested a non-implication of ROS in its mechanism of action letting us desisting from further studies.

The DMSO extract of the root of *Withania somnifera* showed an interesting cytostatic and proapoptotic potential, accompanied by increased ROS levels and $_i[Ca^{2+}]$ mobilization, that could suggest ER stress. The extract induces DAMPs trafficking, including CLR and HSP70 and 90 exposure, and ATP release. However, we demonstrated, as well, its aptitude to induce DNA damage. The profile here described pave the way for further studies to deepen the immunogenic profile and exclude mutagenic properties of the extract.

The most promising and characterized botanical drug during the course of my studies was the aqueous decoction of *Hemidesmus indicus* root. I tested the decoction on the human colon cancer dld1 cell line. I assessed its ability to trigger apoptosis that resulted driven mainly by oxidative and ER stress. This evidence paved the way on DAMP's trafficking studies that showed the ability of the decoction to trigger the mobilization of CLR, HSP70, ATP, and HMGB1, following the accepted spatiotemporal order necessary to trigger ICD [128]. Hence, we demonstrated that *Hemidesmus*-mediated demising cells stimulate DCs maturation and activation and that this activity is not elicited by *Hemidesmus* itself, but from the danger signaling that it triggers into cells through its cytotoxic activity. These very promising results pave the way for the design of clinical studies to understand its antitumor and immunostimolant potential, alone or in combination with other agents.

On the whole, the knowledge of the ability of natural compounds to provoke ICD suggests that they could serve as new tools for therapeutic interventions both alone or in combination with traditional antineoplastic agents, and for increasing the efficacy of anticancer drugs and at the same

time stimulating an immune response.

References

1 Smith EL, Zamarin D, Lesokhin AM (2014) Harnessing the immune system for cancer therapy. *Current opinion in oncology* 26:600-607

2 Zitvogel L, Apetoh L, Ghiringhelli F, et al. (2008) The anticancer immune response: indispensable for therapeutic success? *The Journal of clinical investigation* 118:1991

3 Zitvogel L, Kepp O, Kroemer G (2011) Immune parameters affecting the efficacy of chemotherapeutic regimens. *Nature reviews Clinical oncology* 8:151-160

4 Krysko DV, Garg AD, Kaczmarek A, et al. (2012) Immunogenic cell death and DAMPs in cancer therapy. *Nature Reviews Cancer* 12:860-875

5 Kepp O, Senovilla L, Vitale I, et al. (2014) Consensus guidelines for the detection of immunogenic cell death. *Oncoimmunology* 3:e955691

6 Chen H-M, Wang P-H, Chen S-S, et al. (2012) Shikonin induces immunogenic cell death in tumor cells and enhances dendritic cell-based cancer vaccine. *Cancer Immunology, Immunotherapy* 61:1989-2002

7 Qurishi Y, Hamid A, Majeed R, et al. (2011) Interaction of natural products with cell survival and signaling pathways in the biochemical elucidation of drug targets in cancer. *Future Oncology* 7:1007-1021

8 Rasool M, Malik A, Naseer MI, et al. (2015) The role of epigenetics in personalized medicine: challenges and opportunities. *BMC medical genomics* 8:S5

9 Hostanska K, Hajto T, Spagnoli G, et al. (1995) A plant lectin derived from Viscum album induces cytokine gene expression and protein production in cultures of human peripheral blood mononuclear cells. *Natural immunity* 14:295-304

10 Ferlay J, Soerjomataram I, Dikshit R, et al. (2015) Cancer incidence and mortality worldwide: sources, methods and major patterns in GLOBOCAN 2012. *International journal of cancer* 136:

11 Hanahan D, Weinberg RA (2011) Hallmarks of cancer: the next generation. *cell* 144:646-674

12 Gilman A (1963) The initial clinical trial of nitrogen mustard. *The American Journal of Surgery* 105:574-578

13 https://www.cancer.org/cancer/cancer-basics/history-of-cancer/cancer-treatment-chemo.html.

14 Jemal A, Siegel R, Ward E, et al. (2007) Cancer statistics, 2007. *CA: a cancer journal for clinicians* 57:43-66

15 Zitvogel L, Tesniere A, Kroemer G (2006) Cancer despite immunosurveillance: immunoselection and immunosubversion. *Nature Reviews Immunology* 6:715-727

16 Tesniere A, Panaretakis T, Kepp O, et al. (2008) Molecular characteristics of immunogenic cancer cell death. *Cell Death & Differentiation* 15:3-12

17 Harvey AL (2008) Natural products in drug discovery. *Drug discovery today* 13:894-901

18 Garg AD, Agostinis P (2017) Cell death and immunity in cancer: From danger signals to mimicry of pathogen defense responses. *Immunological Reviews* 280:126-148

19 Matzinger P (2002) The danger model: a renewed sense of self. *Science* 296:301-305

20 Medzhitov R, Janeway CA (2002) Decoding the patterns of self and nonself by the innate immune system. *Science* 296:298-300

21 Green DR, Ferguson T, Zitvogel L, et al. (2009) Immunogenic and tolerogenic cell death. *Nature Reviews Immunology* 9:353-363

22 Matzinger P (1994) Tolerance, danger, and the extended family. *Annual review of immunology* 12:991-1045

23 Galluzzi L, Buqué A, Kepp O, et al. (2017) Immunogenic cell death in cancer and infectious disease. *Nature Reviews Immunology* 17:97-111

24 Garg AD, Romano E, Rufo N, et al. (2016) Immunogenic versus tolerogenic phagocytosis during anticancer therapy: mechanisms and clinical translation. *Cell Death & Differentiation* 23:938-951

25 Kroemer G, Galluzzi L, Kepp O, et al. (2013) Immunogenic cell death in cancer therapy. *Annual review of immunology* 31:51-72

26 Garg AD, Galluzzi L, Apetoh L, et al. (2015) Molecular and translational classifications of DAMPs in immunogenic cell death. *Frontiers in immunology* 6:

27 Rock KL, Kono H (2008) The inflammatory response to cell death. *Annu. Rev. pathmechdis. Mech. Dis.* 3:99-126

28 Kearney CJ, Martin SJ (2017) An Inflammatory Perspective on Necroptosis. *Molecular Cell*

65:965-973

29 Garg AD, Dudek AM, Agostinis P (2013) Cancer immunogenicity, danger signals, and DAMPs: what, when, and how? *Biofactors* 39:355-367

30 Tabas I, Ron D (2011) Integrating the mechanisms of apoptosis induced by endoplasmic reticulum stress. *Nature cell biology* 13:184-190

31 Rufo N, Garg AD, Agostinis P (2017) The Unfolded Protein Response in Immunogenic Cell Death and Cancer Immunotherapy. *Trends in Cancer* 3:643-658

32 Ghiringhelli F, Apetoh L, Tesniere A, et al. (2009) Activation of the NLRP3 inflammasome in dendritic cells induces IL-1 *β* –dependent adaptive immunity against tumors. *Nature medicine* 15:1170-1178

33 Fulda S, Debatin K-M (2006) Extrinsic versus intrinsic apoptosis pathways in anticancer chemotherapy. *Oncogene* 25:4798-4811

34 Vanden Berghe T, Kaiser WJ, Bertrand MJ, et al. (2015) Molecular crosstalk between apoptosis, necroptosis, and survival signaling. *Molecular & cellular oncology* 2:e975093

35 Obeid M, Tesniere A, Ghiringhelli F, et al. (2007) Calreticulin exposure dictates the immunogenicity of cancer cell death. *Nature medicine* 13:54-61

36 Garg A, Martin S, Golab J, et al. (2014) Danger signalling during cancer cell death: origins, plasticity and regulation. *Cell Death & Differentiation* 21:26-38

37 Apetoh L, Ghiringhelli F, Tesniere A, et al. (2007) Toll-like receptor 4–dependent contribution of the immune system to anticancer chemotherapy and radiotherapy. *Nature medicine* 13:1050-1059

38 Goldszmid RS, Idoyaga J, Bravo AI, et al. (2003) Dendritic cells charged with apoptotic tumor cells induce long-lived protective CD4+ and CD8+ T cell immunity against B16 melanoma. *The Journal of Immunology* 171:5940-5947

39 Aaes TL, Kaczmarek A, Delvaeye T, et al. (2016) Vaccination with necroptotic cancer cells induces efficient anti-tumor immunity. *Cell reports* 15:274-287

40 Yang H, Ma Y, Chen G, et al. (2016) Contribution of RIP3 and MLKL to immunogenic cell death signaling in cancer chemotherapy. *Oncoimmunology* 5:e1149673

41 Kepp O, Tesniere A, Schlemmer F, et al. (2009) Immunogenic cell death modalities and their impact on cancer treatment. *Apoptosis* 14:364-375

42 Michaud M, Martins I, Sukkurwala AQ, et al. (2011) Autophagy-dependent anticancer

immune responses induced by chemotherapeutic agents in mice. *Science* 334:1573-1577

43 Garg AD, Krysko DV, Vandenabeele P, et al. (2012) The emergence of phox-ER stress induced immunogenic apoptosis. *Oncoimmunology* 1:786-788

44 Dudek AM, Garg AD, Krysko DV, et al. (2013) Inducers of immunogenic cancer cell death. *Cytokine & growth factor reviews* 24:319-333

45 Tsai C-F, Yeh W-L, Huang SM, et al. (2012) Wogonin induces reactive oxygen species production and cell apoptosis in human glioma cancer cells. *International journal of molecular sciences* 13:9877-9892

46 Verfaillie T, Rubio N, Garg A, et al. (2012) PERK is required at the ER-mitochondrial contact sites to convey apoptosis after ROS-based ER stress. *Cell Death & Differentiation* 19:1880-1891

47 Garg AD, Krysko DV, Vandenabeele P, et al. (2011) DAMPs and PDT-mediated photo-oxidative stress: exploring the unknown. *Photochemical & Photobiological Sciences* 10:670-680

48 Garg AD, Krysko DV, Verfaillie T, et al. (2012) A novel pathway combining calreticulin exposure and ATP secretion in immunogenic cancer cell death. *The EMBO journal* 31:1062-1079

49 Koks CA, Garg AD, Ehrhardt M, et al. (2015) Newcastle disease virotherapy induces long‐term survival and tumor‐specific immune memory in orthotopic glioma through the induction of immunogenic cell death. *International journal of cancer* 136:

50 Miyamoto S, Inoue H, Nakamura T, et al. (2012) Coxsackievirus B3 is an oncolytic virus with immunostimulatory properties that is active against lung adenocarcinoma. *Cancer research* 72:2609-2621

51 Wong DYQ, Ong WWF, Ang WH (2015) Induction of immunogenic cell death by chemotherapeutic platinum complexes. *Angewandte Chemie* 127:6583-6587

52 Garg AD, Vandenberk L, Fang S, et al. (2017) Pathogen response-like recruitment and activation of neutrophils by sterile immunogenic dying cells drives neutrophil-mediated residual cell killing. *Cell Death & Differentiation* 24:832-843

53 Tesniere A, Schlemmer F, Boige V, et al. (2010) Immunogenic death of colon cancer cells treated with oxaliplatin. *Oncogene* 29:482-491

54 Menger L, Vacchelli E, Adjemian S, et al. (2012) Cardiac glycosides exert anticancer effects by inducing immunogenic cell death. *Science translational medicine* 4:143ra199-143ra199

55 Du J, Tang XL (2014) Natural products against cancer: A comprehensive bibliometric study of the research projects, publications, patents and drugs. *Journal of cancer research and*

therapeutics 10:27

56 Swinney DC, Anthony J (2011) How were new medicines discovered? *Nature reviews Drug discovery* 10:507-519

57 fda.gov.

58 Surh Y-J (2003) Cancer chemoprevention with dietary phytochemicals. *Nature Reviews Cancer* 3:768-780

59 Chen ST, Dou J, Temple R, et al. (2008) New therapies from old medicines. *Nature biotechnology* 26:1077-1083

60 Govindaraju B, Rao SR, Venugopal R, et al. (2003) High frequency plant regeneration in Ashwagandha (Withania somnifera (L.) Dunal): An important medicinal plant. *Plant Cell Biotechnol. Mol. Biol* 4:49-56

61 Mirjalili HM, Fakhr‐Tabatabaei SM, Bonfill M, et al. (2009) Morphology and withanolide production of Withania coagulans hairy root cultures. *Engineering in Life Sciences* 9:197-204

62 Davis L, Kuttan G (2000) Immunomodulatory activity of Withania somnifera. *Journal of Ethnopharmacology* 71:193-200

63 Umadevi M, Rajeswari R, Rahale CS, et al. (2012) Traditional and medicinal uses of Withania somnifera. *The Pharma Innovation* 1:102

64 Kaur K, Rani G, Widodo N, et al. (2004) Evaluation of the anti-proliferative and anti-oxidative activities of leaf extract from in vivo and in vitro raised Ashwagandha. *Food and chemical toxicology* 42:2015-2020

65 Christina A, Joseph DG, Packialakshmi M, et al. (2004) Anticarcinogenic activity of Withania somnifera Dunal against Dalton's ascitic lymphoma. *Journal of ethnopharmacology* 93:359-361

66 Davis L, Kuttan G (2001) Effect of Withania somnifera on DMBA induced carcinogenesis. *Journal of ethnopharmacology* 75:165-168

67 Padmavathi B, Rath PC, Rao AR, et al. (2005) Roots of Withania somnifera inhibit forestomach and skin carcinogenesis in mice. *Evidence-based complementary and alternative medicine* 2:99-105

68 Singh D, Dey C, Bhutani K (2001) Downregulation of p34cdc2 expression with aqueous fraction from Withania somnifera for a possible molecular mechanism of anti-tumor and other pharmacological effects. *Phytomedicine* 8:492-494

69 Mathur R, Gupta SK, Singh N, et al. (2006) Evaluation of the effect of Withania somnifera

root extracts on cell cycle and angiogenesis. *Journal of ethnopharmacology* 105:336-341

70 Dhuley J (1997) Effect of some Indian herbs on macrophage functions in ochratoxin A treated mice. *Journal of Ethnopharmacology* 58:15-20

71 Davis L, Kuttan G (2002) Effect of Withania somnifera on cell mediated immune responses in mice. *Journal of experimental & clinical cancer research: CR* 21:585-590

72 Vyas AR, Singh SV (2014) Molecular targets and mechanisms of cancer prevention and treatment by withaferin a, a naturally occurring steroidal lactone. *The AAPS journal* 16:1-10

73 Cohen SM, Mukerji R, Timmermann BN, et al. (2012) A novel combination of withaferin A and sorafenib shows synergistic efficacy against both papillary and anaplastic thyroid cancers. *The American Journal of Surgery* 204:895-901

74 Choudhary MI, Yousuf S (2013) Withanolides: Chemistry and Antitumor Activity. In: (ed) Natural Products, Springer,

75 Ichikawa H, Takada Y, Shishodia S, et al. (2006) Withanolides potentiate apoptosis, inhibit invasion, and abolish osteoclastogenesis through suppression of nuclear factor- κ B (NF- κ B) activation and NF- κ B–regulated gene expression. *Molecular cancer therapeutics* 5:1434-1445

76 Senthil V, Ramadevi S, Venkatakrishnan V, et al. (2007) Withanolide induces apoptosis in HL-60 leukemia cells via mitochondria mediated cytochrome c release and caspase activation. *Chemico-biological interactions* 167:19-30

77 Trump BF, Berezesky IK (1992) The role of cytosolic Ca2+ in cell injury, necrosis and apoptosis. *Current opinion in cell biology* 4:227-232

78 Xu C, Bailly-Maitre B, Reed JC (2005) Endoplasmic reticulum stress: cell life and death decisions. *Journal of Clinical Investigation* 115:2656

79 Malik F, Kumar A, Bhushan S, et al. (2007) Reactive oxygen species generation and mitochondrial dysfunction in the apoptotic cell death of human myeloid leukemia HL-60 cells by a dietary compound withaferin A with concomitant protection by N-acetyl cysteine. *Apoptosis* 12:2115-2133

80 Yu S-M, Kim S-J (2014) Withaferin A-caused production of intracellular reactive oxygen species modulates apoptosis via PI3K/Akt and JNKinase in rabbit articular chondrocytes. *Journal of Korean medical science* 29:1042-1053

81 Lee YY, Hong SH, Lee YJ, et al. (2010) Tauroursodeoxycholate (TUDCA), chemical chaperone, enhances function of islets by reducing ER stress. *Biochemical and biophysical research communications* 397:735-739

82 Choi MJ, Park EJ, Min KJ, et al. (2011) Endoplasmic reticulum stress mediates withaferin

A-induced apoptosis in human renal carcinoma cells. *Toxicology in Vitro* 25:692-698

83 Sharma A, Singh K, Almasan A (2012) Histone H2AX phosphorylation: a marker for DNA damage. *DNA repair protocols* 613-626

84 Panjamurthy K, Manoharan S, Balakrishnan S, et al. (2009) Protective effect of Withaferin-A on micronucleus frequency and detoxication agents during experimental oral carcinogenesis. *African Journal of Traditional, Complementary and Alternative Medicines* 6:

85 Panjamurthy K, Manoharan S, Menon VP, et al. (2008) Protective role of withaferin‐A on 7, 12‐dimethylbenz (a) anthracene‐induced genotoxicity in bone marrow of Syrian golden hamsters. *Journal of biochemical and molecular toxicology* 22:251-258

86 Fimognari C, Ferruzzi L, Turrini E, et al. (2012) Metabolic and toxicological considerations of botanicals in anticancer therapy. *Expert opinion on drug metabolism & toxicology* 8:819-832

87 Ahmad MK, Mahdi AA, Shukla KK, et al. (2010) Withania somnifera improves semen quality by regulating reproductive hormone levels and oxidative stress in seminal plasma of infertile males. *Fertility and sterility* 94:989-996

88 Cooley K, Szczurko O, Perri D, et al. (2009) Naturopathic care for anxiety: a randomized controlled trial ISRCTN78958974. *PLoS One* 4:e6628

89 Chopra A, Lavin P, Patwardhan B, et al. (2004) A 32-week randomized, placebo-controlled clinical evaluation of RA-11, an Ayurvedic drug, on osteoarthritis of the knees. *JCR: Journal of Clinical Rheumatology* 10:236-245

90 Chaurasiya ND, Uniyal GC, Lal P, et al. (2008) Analysis of withanolides in root and leaf of Withania somnifera by HPLC with photodiode array and evaporative light scattering detection. *Phytochemical analysis* 19:148-154

91 Verrière V, Higgins G, Al-Alawi M, et al. (2012) Lipoxin A4 stimulates calcium-activated chloride currents and increases airway surface liquid height in normal and cystic fibrosis airway epithelia. *PloS one* 7:e37746

92 Royall JA, Ischiropoulos H (1993) Evaluation of 2′, 7′-dichlorofluorescin and dihydrorhodamine 123 as fluorescent probes for intracellular H2O2 in cultured endothelial cells. *Archives of biochemistry and biophysics* 302:348-355

93 Wu X, Zhou Q-h, Xu K (2009) Are isothiocyanates potential anti-cancer drugs? *Acta Pharmacologica Sinica* 30:501-512

94 Lam TK, Gallicchio L, Lindsley K, et al. (2009) Cruciferous vegetable consumption and lung cancer risk: a systematic review. *Cancer Epidemiology and Prevention Biomarkers* 18:184-195

95 Catanzaro E, Fimognari C (2017) Antileukemic Activity of Sulforaphane. *Glucosinolates*

301-317

96 Choi WY, Choi BT, Lee WH, et al. (2008) Sulforaphane generates reactive oxygen species leading to mitochondrial perturbation for apoptosis in human leukemia U937 cells. *Biomedicine & Pharmacotherapy* 62:637-644

97 Miao Z, Yu F, Ren Y, et al. (2017) D, L-Sulforaphane Induces ROS-Dependent Apoptosis in Human Gliomablastoma Cells by Inactivating STAT3 Signaling Pathway. *International journal of molecular sciences* 18:72

98 Singh SV, Srivastava SK, Choi S, et al. (2005) Sulforaphane-induced cell death in human prostate cancer cells is initiated by reactive oxygen species. *Journal of Biological Chemistry* 280:19911-19924

99 Hakamata W, Tamura S, Hirano T, et al. (2014) Multicolor imaging of endoplasmic reticulum-located esterase as a prodrug activation enzyme. *ACS medicinal chemistry letters* 5:321-325

100 Matsuura K, Canfield K, Feng W, et al. (2016) Chapter Two-Metabolic Regulation of Apoptosis in Cancer. *International review of cell and molecular biology* 327:43-87

101 Fulda S, Debatin K (2006) Extrinsic versus intrinsic apoptosis pathways in anticancer chemotherapy. *Oncogene* 25:4798-4811

102 Thomas E, Gopalakrishnan V, Somasagara RR, et al. (2016) Extract of vernonia condensata, inhibits tumor progression and improves survival of tumor-allograft bearing mouse. *Scientific reports* 6:23255

103 Liu B, Zhang B, Guo R, et al. (2014) Enhancement in efferocytosis of oxidized low-density lipoprotein-induced apoptotic RAW264. 7 cells through Sirt1-mediated autophagy. *International journal of molecular medicine* 33:523-533

104 Lee YM, Shin JW, Lee EH, et al. (2012) Protective effects of propofol against hydrogen peroxide-induced oxidative stress in human kidney proximal tubular cells. *Korean journal of anesthesiology* 63:441-446

105 Khan N, Afaq F, Mukhtar H (2007) Apoptosis by dietary factors: the suicide solution for delaying cancer growth. *Carcinogenesis* 28:233-239

106 Gura T (1997) Systems for identifying new drugs are often faulty.

107 Shanks N, Greek R, Greek J (2009) Are animal models predictive for humans? *Philosophy, ethics, and humanities in medicine* 4:2

108 Trachootham D, Zhou Y, Zhang H, et al. (2006) Selective killing of oncogenically transformed cells through a ROS-mediated mechanism by β-phenylethyl isothiocyanate.

Cancer cell 10:241-252

109 Xu K, Thornalley PJ (2001) Involvement of glutathione metabolism in the cytotoxicity of the phenethyl isothiocyanate and its cysteine conjugate to human leukaemia cells in vitro. *Biochemical pharmacology* 61:165-177

110 Higgins LG, Kelleher MO, Eggleston IM, et al. (2009) Transcription factor Nrf2 mediates an adaptive response to sulforaphane that protects fibroblasts in vitro against the cytotoxic effects of electrophiles, peroxides and redox-cycling agents. *Toxicology and applied pharmacology* 237:267-280

111 Zhang Y (2011) The molecular basis that unifies the metabolism, cellular uptake and chemopreventive activities of dietary isothiocyanates. *Carcinogenesis* 33:2-9

112 Buytaert E, Callewaert G, Hendrickx N, et al. (2006) Role of endoplasmic reticulum depletion and multidomain proapoptotic BAX and BAK proteins in shaping cell death after hypericin-mediated photodynamic therapy. *The FASEB journal* 20:756-758

113 Bradford MM (1976) A rapid and sensitive method for the quantitation of microgram quantities of protein utilizing the principle of protein-dye binding. *Analytical biochemistry* 72:248-254

114 Sedlak J, Lindsay RH (1968) Estimation of total, protein-bound, and nonprotein sulfhydryl groups in tissue with Ellman's reagent. *Analytical biochemistry* 25:192-205

115 Nayar T, Rasiya Beegam A, Mohanan N, et al. (2006) Flowering plants of Kerala. A handbook. *Thiruvananthapuram: Tropical Botanic Garden and Research Institute 1069p. ISBN 8190039768 En Geog* 6:

116 George S, Tushar K, Urmikrishnan K, et al. (2008) Henúdesmus indicus (L.) R. Br. A Review. *Journal of Plant Sciences* 3:146-156

117 Das S, Singh Bisht S (2013) The bioactive and therapeutic potential of Hemidesmus indicus R. Br.(Indian Sarsaparilla) root. *Phytotherapy Research* 27:791-801

118 Das P, Joshi P, MANDAL S, et al. (1992) NEW COUMARINO-LIGNOIDS FROM HEMIDESMUS INDICUS R. BR. *Indian journal of chemistry. Sect. B: Organic chemistry, including medical chemistry* 31:342-345

119 Zhao Z, Matsunami K, Otsuka H, et al. (2013) A condensed phenylpropanoid glucoside and pregnane saponins from the roots of Hemidesmus indicus. *Journal of natural medicines* 67:137-142

120 Austin A, Herbals R (2008) A review on Indian sarsaparilla, Hemidesmus indicus (L.) R. Br. *Journal of biological sciences* 8:1-12

121 Evans D, Rajasekharan S, Subramoniam A (2004) Enhancement in the absorption of water and electrolytes from rat intestine by Hemidesmus indicus R. Br. root (water extract). *Phytotherapy Research* 18:511-515

122 Das S, Dash S, Padhy S (2003) Ethno-medicinal information from Orissa state, India, A review. *J. Hum. Ecol* 14:165-227

123 Fimognari C, Lenzi M, Ferruzzi L, et al. (2011) Mitochondrial pathway mediates the antileukemic effects of Hemidesmus indicus, a promising botanical drug. *PLoS One* 6:e21544

124 Ferruzzi L, Turrini E, Burattini S, et al. (2013) Hemidesmus indicus induces apoptosis as well as differentiation in a human promyelocytic leukemic cell line. *Journal of ethnopharmacology* 147:84-91

125 Panaretakis T, Kepp O, Brockmeier U, et al. (2009) Mechanisms of pre‐apoptotic calreticulin exposure in immunogenic cell death. *The EMBO journal* 28:578-590

126 Martins I, Kepp O, Schlemmer F, et al. (2011) Restoration of the immunogenicity of cisplatin-induced cancer cell death by endoplasmic reticulum stress. *Oncogene* 30:1147-1158

127 Zitvogel L, Kepp O, Senovilla L, et al. (2010) Immunogenic tumor cell death for optimal anticancer therapy: the calreticulin exposure pathway. *Clinical Cancer Research* 16:3100-3104

128 Kepp O, Galluzzi L, Martins I, et al. (2011) Molecular determinants of immunogenic cell death elicited by anticancer chemotherapy. *Cancer and Metastasis Reviews* 30:61-69

129 Zitvogel L, Kepp O, Kroemer G (2010) Decoding cell death signals in inflammation and immunity. *Cell* 140:798-804

130 Spisek R, Charalambous A, Mazumder A, et al. (2007) Bortezomib enhances dendritic cell (DC)–mediated induction of immunity to human myeloma via exposure of cell surface heat shock protein 90 on dying tumor cells: therapeutic implications. *Blood* 109:4839-4845

131 Castelli C, Ciupitu A-MT, Rini F, et al. (2001) Human heat shock protein 70 peptide complexes specifically activate antimelanoma T cells. *Cancer Research* 61:222-227

132 Fucikova J, Kralikova P, Fialova A, et al. (2011) Human tumor cells killed by anthracyclines induce a tumor-specific immune response. *Cancer research* 71:4821-4833

133 Garg AD, Nowis D, Golab J, et al. (2010) Immunogenic cell death, DAMPs and anticancer therapeutics: an emerging amalgamation. *Biochimica et Biophysica Acta (BBA)-Reviews on Cancer* 1805:53-71

134 Chen J, Xie J, Jiang Z, et al. (2011) Shikonin and its analogs inhibit cancer cell glycolysis by targeting tumor pyruvate kinase-M2. *Oncogene* 30:4297-4306

135 Gardai SJ, McPhillips KA, Frasch SC, et al. (2005) Cell-surface calreticulin initiates clearance of viable or apoptotic cells through trans-activation of LRP on the phagocyte. *Cell* 123:321-334

136 Garg AD, Krysko DV, Vandenabeele P, et al. (2012) Hypericin-based photodynamic therapy induces surface exposure of damage-associated molecular patterns like HSP70 and calreticulin. *Cancer Immunology, Immunotherapy* 61:215-221

137 van Eden W, Spiering R, Broere F, et al. (2012) A case of mistaken identity: HSPs are no DAMPs but DAMPERs. *Cell Stress and Chaperones* 17:281-292

138 Kazama H, Ricci J-E, Herndon JM, et al. (2008) Induction of immunological tolerance by apoptotic cells requires caspase-dependent oxidation of high-mobility group box-1 protein. *Immunity* 29:21-32

139 Thorburn J, Horita H, Redzic J, et al. (2009) Autophagy regulates selective HMGB1 release in tumor cells that are destined to die. *Cell Death & Differentiation* 16:175-183

140 Chiba S, Baghdadi M, Akiba H, et al. (2012) Tumor-infiltrating DCs suppress nucleic acid-mediated innate immune responses through interactions between the receptor TIM-3 and the alarmin HMGB1. *Nature immunology* 13:832-842

141 Semino C, Angelini G, Poggi A, et al. (2005) NK/iDC interaction results in IL-18 secretion by DCs at the synaptic cleft followed by NK cell activation and release of the DC maturation factor HMGB1. *Blood* 106:609-616

142 Banchereau J, Briere F, Caux C, et al. (2000) Immunobiology of dendritic cells. *Annual review of immunology* 18:767-811

143 Nace G, Evankovich J, Eid R, et al. (2012) Dendritic cells and damage-associated molecular patterns: endogenous danger signals linking innate and adaptive immunity. *Journal of innate immunity* 4:6-15

144 Ananthi R, Chandra N, Santhiya S, et al. (2010) Genotoxic and antigenotoxic effects of Hemidesmus indicus R. Br. root extract in cultured lymphocytes. *Journal of ethnopharmacology* 127:558-560

145 Pharmacopoeia I (2007) Government of India. *Ministry of health and family welfare* 2:1020-1021

146 Bracci L, Schumacher R, Provenzano M, et al. (2008) Efficient Stimulation of T Cell Responses by Human IFN-α–induced Dendritic Cells Does Not Require Toll-like Receptor Triggering. *Journal of immunotherapy* 31:466-474

147 Dolinsky VW, Douglas DN, Lehner R, et al. (2004) Regulation of the enzymes of hepatic microsomal triacylglycerol lipolysis and re-esterification by the glucocorticoid

dexamethasone. *Biochemical Journal* 378:967-974

148 Pol J, Vacchelli E, Aranda F, et al. (2015) Trial Watch: Immunogenic cell death inducers for anticancer chemotherapy. *Oncoimmunology* 4:e1008866

149 ClinicalTrials.gov.